Stability assessment of tugs in escort operations using time domain simulations

Dynamic behaviour after impact loads

R.M.Marijnissen

A thesis presented for the degree of
Master of Science
In Marine Technology

DAMEN

TU Delft

Stability assessment of tugs in escort operations using time domain simulations

Dynamic behaviour after impact loads

by

Renske Maria Marijnissen

to obtain the degree of Master of Science
at the Delft University of Technology,
to be defended publicly on Wednesday November 13, 2019 at 13:00 AM.

Student number:	4379780	
Project duration:	March 20, 2019 – November 13, 2019	
Thesis committee:	Dr. ir. P.R. Wellens,	TU Delft, chair
	Dr. ir. H.J. de Koning Gans,	TU Delft, supervisor
	Dr. ir. A. Vrijdag,	TU Delft
	Ir. S. Rooijakkers,	Damen Shipyards
	Ir. N. Teeuwen,	STC group

An electronic version of this thesis is available at `http://repository.tudelft.nl/`.

Abstract

In the past decade several high performance tugs were involved in serious accidents. This encouraged the discussion about the current regulation for tugs, which are nowadays equipped with large power installations. Those regulations, set by class societies, distinguish thee types of stability, namely: tow-tripping, self-tripping and escort stability. The latter is analysed in this research.
Class societies Bureau Veritas and ABS have set the following requirement to simulations tools used to predict the safety of escort tugs:

"The numerical simulation tool should be able to analyse the dynamic effects before a steady state is reached."

To fulfil this requirement, the existing performance prediction tool TugSim is extended to a four degrees of freedom time domain simulation tool. This tool is able to simulate the dynamic behaviour of tugs in escort operations. The challenge is to find accurate expressions for the hydrodynamic forces in this simulation tool, especially for the roll motion. To obtain these forces, a combination of several methods is used. So are the steady state force contributions, being the damping terms as a result of a pure sway velocity, obtained with TugSim. The pure roll damping is obtained using the results of some free decay tests together with the method of Ikeda, which accounts for the additional lift induced roll damping when sailing with forward speed. The remaining terms, coherent with the yaw velocity, are obtained using a combination of the semi-empirical method developed by V. Ankudinov and some turning cycle tests.

The developed simulation tool has been used to perform a sensitivity analysis. In this sensitivity analysis it is investigated whether the impact of inaccurate approximations of the hydrodynamic force contributions would significantly influence the calculated heeling angle. Three reference values has been introduced, which all indicate the ease with which the tug starts to roll after three different types of impact loads. For this analysis it is assumed that the easier the tug starts to roll, the more dangerous the situation will become.
From the sensitivity analyses it can be concluded that there is a strong coupling between roll and yaw. Because the dominating roll moment contribution, being the roll moment as a result of a pure sway velocity (K_v), is strongly dependent on the drift angle. Tugs in escort operations are facing a high flow velocity, due to the velocity of the assisted vessel. This facing flow velocity causes the drift angle to be almost similar to the heading angle. Which means that whenever the heading angle increases, the drift angle increases as well. An increasing drift angle results in a higher hydrodynamic roll moment and so a higher heeling angle. So a variation of the yaw damping terms inherently results in a change of the heeling angle.

The sensitivity analysis also points out that many of the, from manoeuvring theory arising, hydrodynamic force contributions barely influence the dynamic behaviour of tugs in escort operations. Besides, an inaccurate prediction of the added mass terms would not result in significant errors in the calculated heeling angle.

In addition to the sensitivity analysis, time domain simulations are used to analyse the dynamic behaviour during specific manoeuvres and after impact loads. Multiple relevant dynamic scenarios are simulated and it is investigated whether the safety margin set by class is sufficient to resist arising heeling angle peaks. Here it is assumed that limit of safety is reached whenever the heeling angle exceeds the heeling angle at which the tug's deck starts to immerse. The dynamic scenarios include the following events: Towline failure, engine failure, turning cycle, zigzag manoeuvre and transitioning from steering to port side to steering to starboard side.
The time domain simulations have shown that, apart from during the transition from steering to port side to steering to starboard side, no heeling angle peaks will arise that exceed the angle of deck immersion and so the safety margin set by class is sufficient. However, it is concluded that the risk of capsizing during the transition from steering to port side to steering to starboard side is high.

Acknowledgement

After five years my student career comes to an end, five years of hard work and lots of pleasure. I am grateful that I got the opportunity to finish this period with an internship at Damen Shipyards in Gorichem. It gave me a sneak preview of the working life that awaits me and offered me the opportunity to study the most interesting subject, hydrodynamics. I am willing to solve problems which seems to be unsolvable. But with the help from colleagues and professors, they are solvable.

A special thanks to Siebe Rooijakkers, my daily supervisor at Damen Shipyards. Thanks for the many brainstorm sessions we had and your critical eye. Thanks to Frans Sas and Jochem de Jong, who made time for me as well. Every input is welcome and yours was very useful. It is nice to notice that you had such an interest in the subject I investigated. A special thanks to professors Henk de Koning Gans and Peter Wellens as well, for being my supervisor and committee chairman. Not only a thanks for the help during my graduation period, but also for the help during my bachelor and master itself. Due to you, my knowledge and especially interest in hydrodynamic has increased a lot since I started my master. At last I would like to thank Niek Teeuwen and Wim Sinke for guiding me during a visit at the STC group and showing all the simulator, it has been an interesting day.

Contents

Nomenclature

Roman symbols

$\dot{p}$	Roll accelerations	$[rad/s^2]$
$\dot{r}$	Yaw accelerations	$[rad/s^2]$
$\dot{u}$	Surge accelerations	$[m/s^2]$
$\dot{v}$	Sway accelerations	$[m/s^2]$
$\vec{F}_{centrifugal}$	Centrifugal force	$[N]$
$\vec{F}_{centripetal}$	Centripetal force	$[N]$
$\overrightarrow{x_a}$	distance to point of attachment of force	$[m]$
$\overrightarrow{x_G}$	Distance to centre of gravity	$[m]$
$\overrightarrow{X_O}$	Position of body fixed frame expressed in reference frame Q(U,V,Z)	$[m]$
$\overrightarrow{x_p}$	Distance from origin of body fixed frame to towlines point of attachment	$[m]$
A_∞	Infinite frequency added mass matrix	$[kg]$
a_{ij}	Added mass coefficient	$[kg]$
$A_{lateral}$	Lateral area	$[m^2]$
AR_e	Effective aspect ratio	$[-]$
B_{44APP}	Additional roll damping due to appendages	$[Nms]$
B_{44E}	Eddy contribution to roll damping	$[Nms]$
B_{44F}	Skin friction induced roll damping	$[Nms]$
B_{44L}	Lift induced roll damping	$[Nms]$
B_{44}	Total roll damping	$[Nms]$
b_f	Span length of a fin	$[m]$
B_{wl}	Waterline breath	$[m]$
BL	Towline breaking load	$[N]$
C_d	Dimensionless drag coefficient	[-]
C_f	Frictional resistance coefficient	[-]
c_f	Chord length of a fin	$[m]$
C_L	Dimensionless lift coefficient	[-]
C_{RB}	Rigid body Coriolis, centripetal and centrifugal matrix	
GM	Geometric metacentre height	$[m]$
GZ	Hydrostatic righting lever	$[m]$
I_{ij}	Area moment of inertia	$[m^4]$
K_D	Total roll damping as defined in [42]	$[Ns]$

K_{HD}	Hydrodynamic moment contribution around x-axis	$[Nm]$
k_{ii}	Radii of inertia	$[m]$
K_m	Roll moment contribution due to side force as a result of the sway velocity	$[Ns]$
k_{tow}	Towline stiffness	$[N/m]$
K_z	Roll moment contribution due to vertical force as a result of the sway velocity	$[Ns]$
KG	Vertical distance between keel and centre of gravity	$[m]$
l_0	Unstretched towline length	$[m]$
L_{oa}	Overall ship length	$[m]$
L_{pp}	Length between perpendiculars	$[m]$
L_{wl}	Waterline length	$[m]$
LCB	Longitudinal centre of buoyancy	$[m]$
m	Mass	$[kg]$
M_A	Added mass matrix	$[kg]$
M_{RB}	Rigid body mass matrix	$[kg]$
N_{HD}	Hydrodynamic moment contribution around z-axis	$[Nm]$
S_{tow}	Towline force	$[N]$
T_a	Draught at aft perpendicular	$[m]$
T_f	Draught at front perpendicular	$[m]$
T_{mean}	Mean draught	$[m]$
U_0	Velocity of assisted ship	$[m/s]$
v_a	Inflow velocity facing the vessel	$[m/s]$
v_Q	The velocity of reference frame Q(U,V,Z)	$[m/s]$
v_s	Ship velocity relative to the assisted vessel	$[m/s]$
X_{HD}	Hydrodynamic force contribution in local x-direction	$[N]$
Y_{HD}	Hydrodynamic force contribution in local y-direction	$[N]$
K	Moment around x-axis	$[Nm]$
k	Form factor	[-]
L	Lift	$[N]$
M	Moment around y-axis	$[Nm]$
N	Moment around z-axis	$[Nm]$
p	Roll velocity	$[rad/s]$
q	Pitch velocity	$[rad/s]$
r	Yaw velocity	$[rad/s]$

S	Wetted surface	$[m^2]$
T	Draught	$[m]$
u	Surge velocity	$[m/s]$
v	Sway velocity	$[m/s]$
w	Heave velocity	$[m/s]$
X	Force in x-direction	$[N]$
Y	Force in y-direction	$[N]$
Z	Force in z-direction	$[N]$

Greek symbols

β	Drift angle	[°]
∇	Vessel volume	$[m^3]$
Ψ	Heading angle	[°]
ρ	Water density	$[kg/m^3]$
σ	Steering angle	[°]
τ	Trim quantity (positive for trim by stern)	[m]
τ_{hd}	Hydrodynamic force	$[N]$
τ_{prop}	Propeller force	$[N]$
τ_{rudder}	Rudder force	$[N]$
τ_{tow}	Towline force	$[N]$
φ	Heeling angle	[°]

Hydrodynamic derivatives

$K_{\dot{p}}$	Roll added mass contribution due to roll velocity	$[Ns^2m]$
$K_{\dot{r}}$	Roll added mass contribution due to yaw velocity	$[Ns^2m]$
$K_{\dot{v}}$	Roll added mass contribution due to sway velocity	$[Ns^2]$
K_p	Roll damping contribution due to roll velocity	$[Nms]$
K_r	Roll damping contribution due to yaw velocity	$[Nms]$
K_v	Roll damping contribution due to sway velocity	$[Ns]$
$N_{\dot{r}}$	Yaw added mass contribution due to sway velocity	$[Nms^2]$
$N_{\dot{v}}$	Yaw added mass contribution due to sway velocity	$[Ns^2]$
N_{rr}	Non linear yaw damping contribution due to yaw velocity	$[Nms^2]$
N_{rv}	Non linear yaw damping contribution due to coupled yaw and sway velocity	$[Ns^2]$
N_r	Linear yaw damping contribution due to yaw velocity	$[Nms]$
N_{vv}	Non linear yaw damping contribution due to sway velocity	$[Ns^2/m]$

N_v	Linear yaw damping contribution due to sway velocity	$[Ns]$
$X_{\dot{u}}$	Surge added mass contribution due to surge velocity	$[Ns^2/m]$
X_{rr}	Lift induced drag coefficient	$[Ns^2/m^2]$
X_{uu}	Non linear surge damping contribution due to surge velocity	$[Ns/m]$
X_u	Linear surge damping contribution due to surge velocity	$[Ns/m]$
X_{vr}	Lift induced drag coefficient	$[Ns^2/m]$
X_{vv}	Lift induced drag coefficient	$[Ns^2]$
X_v	Linear surge damping contribution due to sway velocity	$[Ns/m]$
$Y_{\dot{r}}$	Sway added mass contribution due to yaw velocity	$[Ns^2]$
$Y_{\dot{v}}$	Sway added mass contribution due to sway velocity	$[Ns^2/m]$
Y_{rr}	Non linear sway damping contribution due to yaw velocity	$[Ns^2]$
Y_{rv}	Non linear sway damping contribution due to coupled yaw and sway velocity	$[Ns^2/m]$
Y_r	Linear sway damping contribution due to yaw velocity	$[Ns]$
Y_{vv}	Non linear sway damping contribution due to sway velocity	$[Ns^2/m^2]$
Y_v	Linear sway damping contribution due to sway velocity	$[Ns/m]$

1 Introduction

1.1 Problem definition

The size of ships has been growing significantly over the past years. Between 1996 and 2015 the average dead weight of container ships has increased with 90%. Cruise and passenger ship sizes have increased with around 30% and the average dead weight of the bulk carriers has increased with 55% over the same period [33]. Those growing ship sizes have resulted in the desire to scale up the power of tugs as well. Where in 1970 there were still many single and twin screw tugs performing ship-assist work with a maximum bollard pull of 54 tonnes, nowadays a tug of 50 or less tonnes bollard pull is rare [3].
Even though the installed power at tugs has increased significantly since 1970, the stability and safety regulations did not change much since then. Regulations encourage owners to build tugs under 24 meter to avoid loadline rules or under 500grt in order to avoid SOLAS. This has resulted in tugs with relatively flat and short hulls, equipped with large power installations [3]. This kind of tugs were frequently involved in serious accidents in the past decade. An example of such an accident is the capsizing of the, in 2014 new built, 30-metre-long JMS Delta in China in 2015. Here the tug has been capsized at the start of a turning cycle [19]. 22 people lost their lives [6].

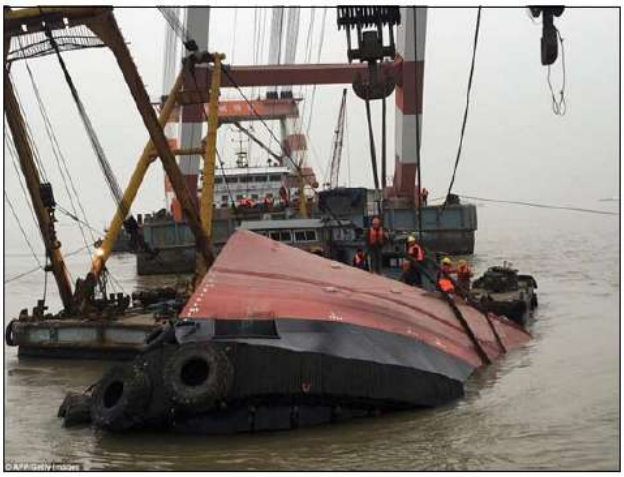

Figure 1.1: Capsizing of JMS Delta [6]

In response to this accident Robert Allen stated the following in an article for WorkBoat: "Regardless of the rules, we as naval architects must clearly define the boundaries of safe operation" [35]. In the run-up to International Tug and Salvage Convention and Exhibition (ITS) in Boston in 2016, Robert Allan again pronounced his concerns about the limitations of the present regulations. Those concerns have broad support and Damen feels responsible to contribute to the improvement of the current regulations as well. It can be concluded that today's tugs are able to generate high steering forces, but the question remains whether they are able to balances those with sufficient stability.

To guarantee the safety of tugs, a few changes in the regulations are made in the last years. So has class society Bureau Veritas, in cooperation with Damen, developed their *Safety Guidelines for Design, Construction and Operation of Tugs* and published it at the ITS in 2014. Thereafter in 2016, the IMO adopted the Intact Stability code and included those safety guidelines [8]. In those guidelines three types of tug stability are distinguished, namely tow-tripping stability, self-tripping stability and escort stability. This research will focus on the latter only.
Each type of stability is assessed using an application of the so called "classical approach". This approach uses

a stability diagram to obtain the maximum allowable heeling angle where tug has sufficient up-righting energy left to get back in its up-right position. Damen has developed a numerical simulation tool which is able to find each static equilibrium in which the tug complies the current regulations. Even though such a tool is accepted by class, it has one major disadvantage, namely: it is not able to analyse the dynamic behaviour of the tugs.

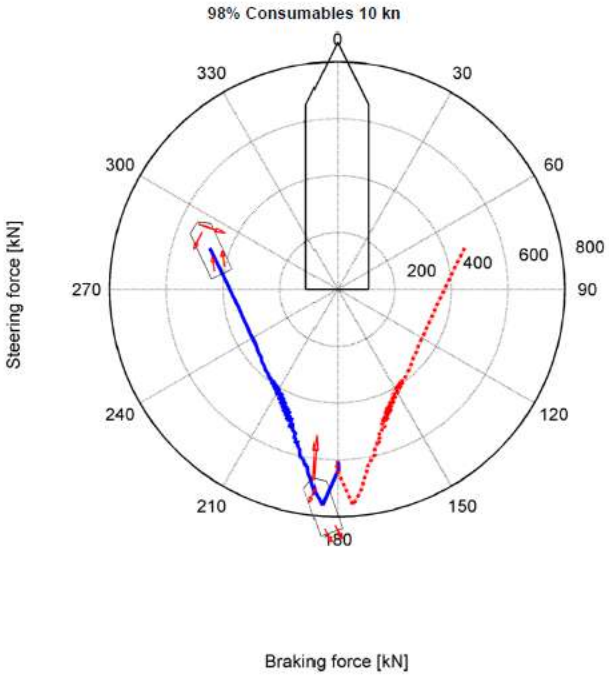

Figure 1.2: Example of TugSims output

The developed numerical tool is named TugSim, an example its output is provided in figure 1.2. The dots in this polar diagram are all representing possible static equilibria meeting the regulations concern escort tugs. As it was initially developed being a design tool, able to predict the tugs towing performance, the dynamics of the tug where not required.
Nowadays TugSim is used and accepted for evaluating the escort stability of a tug, even though it does not meet all the requirements set by class. One of those requirements to be met is defined as follows [8]:

"The numerical simulation tool should be able to analyse the dynamic effects before a steady state is reached."

The lacking ability to analyse and predict the dynamic effects, means that it is currently unknown whether the tug is able to sail from one static equilibrium to another without exceeding its maximum allowable heeling angle. Addition of the dynamic effects should help to define the limits of safe operation.

In the current industry a method to derive those limits of safe operation is desired, as stated in [8]. As nowadays a traffic light based colour coding is used to define the "operational", "cautionary" and "stop work" zones, which cover a certain range of heeling angles. In figure 1.3 an example of an inclinometer indicating the different zones is given. The "stop work" zone often covers all heeling angles exceeding the down flooding angle. However, the range of heeling angles covering the "cautionary" zone is hard to define. Whether operating with a certain heeling angle is safe or not, depends on multiple factors. For example, sailing under a 14° heeling with a forward velocity of 8 knots may be safe, but sailing

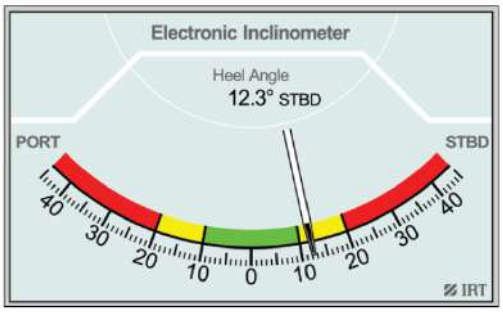

Figure 1.3: Illustration of inclinometer indicating different zones

with the same heeling angle and a higher velocity could be dangerous. Besides the velocity, many other parameters or ship characteristics may influence the safety. To find the limits of safe operation for tugs in escort operations, knowledge should be gained about the dynamic behaviour of the tugs while operating. This knowledge could, in future work, be used to extend TugSim to a captain advisory system on board of a tug. In this research a suitable method will be developed to analyse this dynamic behaviour. The corresponding main goal reads as follows:

"Develop a numerical time domain simulation tool, considering four degrees of freedom, being able to analyse and predict the dynamic behaviour of tugs in escort operations"

1.2 Research objectives

To achieve the formulated main goal of this research, several sub-objectives are formulated. These are as follows:

1. *Provide an accurate formulation of the roll moment valid for tugs*
2. *Identify the tug-tow system's sensitivity to variations of, from manoeuvring theory arising, hydrodynamic force contributions.*
3. *Identify what manoeuvres or impact loads could possibly result in hazardous situations*
4. *Evaluate the current regulations concern escort tugs*

1.3 State of the art

In the past years multiple performance prediction tools has been developed. One of those tug's performance prediction tools has been elaborated in [15], here the hydrodynamic forces are calculated using a combination of CFD and semi-empirical methods. The method is validated using data obtained from [34]. Another tug's performance prediction tool using CFD is elaborated in [1], here the same validation data is used as in [15]. In [48] a verification and validation study on the results of CFD calculations of a DAMEN tug has shown that this method deals with large uncertainties. Apart from the uncertainties arising when using CFD, the performance prediction tools have another disadvantage: They are not able to simulate the dynamic behaviour of the tugs. To include the dynamic behaviour, a combination of performance prediction methods and manoeuvring methods could be used. In [38] such a combination of potential flow theory, semi-empirical methods and strip theory is applied and used to simulate the non-linear dynamic interaction between tethered ship and tug during escort. However, this method has not yet been validated. Another method considering the dynamic interaction between the tethered ship and the tug is provided in [42]. In this method the focus is on the dynamic behaviour of the tethered ship instead of the tug itself. It uses a 3-DOF manoeuvring method derived from [28] and added the fourth degree of freedom, the roll motion, using mainly damping and added mass terms obtained with potential flow methods. The manoeuvring method described in [28] is well applicable to large merchant ships, as yields for most developed manoeuvring methods ([21], [27], [4]). The tethered ship mostly meets the requirements set by those manoeuvring methods, however most tug does not. A tug has a significantly different geometry, which requires different hydrodynamic derivatives. Besides, the roll moment does not seem to be a result of the side force only, as described in [42], but a moment contribution as a result of a vertical force should be considered as well [48]. The only literature that considers the dynamic behaviour of tugs and includes a validation study, is provided in [2]. However, the paper shows only the results of a time domain simulation of an escorting tug, but the applied numerical method is omitted.

The challenge of this research is to develop a numerical simulation tool being able to simulate the dynamic behaviour of tugs in escort operations. Including a validation of the tool and a sensitivity analysis, to show what hydrodynamic force contributions are worth it to be investigated more extensively in future work. The implementation of the roll moment, being essential for escorting tugs, should be as accurate as possible and should also contribute for the moment as a result of the resulting vertical force.

1.4 Research methodology

In the past decades, several methods to simulate a manoeuvring vessel has been developed [24], all having their pros and cons. In this research the pros of each method will be combined in one simulation model applicable for tugs in escort operations. The literature used to achieve this, is mainly based on classic manoeuvring theory as described in i.a. [21], [28] and [14]. However, this theory often considers only three degrees of freedom, namely:

surge, sway and yaw. As the heeling angle plays a major role for tugs in escort operations, a method to include the roll motion should be found. A literature review would result in a basic formulation of the roll motion during manoeuvring, which could later be extended.

With the knowledge gained from an extensive literature review, a numerical method will be developed. During the development of this numerical method, it will become clear what additional force contributions and calculation steps should be considered to transform the quasi-static TugSim into a time domain simulation tool. A formulating of those, in TugSim lacking, hydrodynamic force contribution will be obtained. These formulations will be based on literature and adjusted if required.

Before the written method suitable to simulate tugs in escort behaviour could actually be used to analyse the dynamic behaviour of tugs in escort operations, the method should be validated. This will be done using data retrieved from experiments at model scale and full scale. After validation, focus will be on the sensitivity of the tug-tow-system. To obtain an overview of influential input parameters, a sensitivity analysis has been performed. The results from this analysis enables to evaluate the simulation method itself and the current regulations concern escort stability. The research will be finalised with the simulation of some case studies, to quantify the heeling angle behaviour during different dynamic scenarios.

To conclude: To analyse the dynamic behaviour of tugs in escort operations and the impact of changing input parameters, a time domain simulation tool will be used. This simulation tool will be developed using Matlab and Simulink. The use of Simulink, combined with application of object-oriented programming, contributes to the desire to make the simulation tool general applicable. Within Damen, object-oriented programming is used as a tool to make the complete design process of ships more modular.

1.5 Report outline

The outline of the report is as follows: In chapter 2 an extensive literature review is provided, in which the focus is on the derivation of the hydrodynamic forces using existing manoeuvring methods. This literature is used to develop the numerical method applied to obtain the simulation tool, this method is elaborated in chapter 3. After the numerical method is provided, this method will be validated in chapter 4. In chapter 5 the sensitivity of the tug-tow-system to multiple input parameters is evaluated. In chapter 6 multiple case studies are simulated to show the absolute impact of changing input parameters and to evaluate the dynamic behaviour after impact loads. At last, in chapter 7 conclusions are drawn and recommendations are provided.

2

Literature review

As mentioned in the introduction, a manoeuvring model will be used as a tool to analyse the dynamic effects of a tug during escort operations. Manoeuvring models are nowadays used in simulators or to predict the safety of manoeuvring operations in harbours or restricted waterways. In the past decades, from around 1960, several manoeuvring models are developed and most of them are based on the following equations of motion, given as matrix formulation [44]:

$$\underline{\underline{M}}\vec{\dot{V}} + \vec{C}(V) = \overrightarrow{F_0} \tag{1}$$

Here M is the inertial matrix, V is the vector containing the velocities in every considered degree of freedom, C contains the centripetal and centrifugal inertial forces and $\overrightarrow{F_0}$ contains the external forces applied to the ship. $\overrightarrow{F_0}$ is a vector and can be written as $(X, Y, Z, K, M, N)^T$. The total external force can be written as a superposition of several force components such as the propulsion force, forces induced by wind or waves, rudder forces, etc. However all forces are significant, this research focuses on the prediction of the hydrodynamic forces only. The remaining forces will be derived using a method previously developed at Damen. How these hydrodynamic forces can be derived is a part of this chapter. Besides, in this chapter more general and detailed background will be given about manoeuvring theory. The outline of the chapter will be as follows:

In the first section the rigid body dynamics, which are included in the left hand side of equation 1 are elaborated. This includes the derivation of Newton's equations of motion for only three degrees of freedom, namely: surge, sway and yaw. In section 2.2 the formulation of the manoeuvring equations in these directions are provided. The derivation of the hydrodynamic force contributions, again in three degrees of freedom, will be elaborated in sections 2.3 and 2.4. Where section 2.3 focuses on the available methods developed to obtain the hydrodynamic forces and section 2.4 will elaborated the corresponding physical background. At last, in section 2.5 it is explained how the fourth degree of freedom, namely the roll motion, could be added according to the found literature.

2.1 Rigid body dynamics

Before Newton's equations of motion can be derived, the sign convention and the definition of the different frames of reference should be known, these are provided in the first subsection 2.1.1. Thereafter, in the subsection 2.1.2, Newton's equations of motion are derived.

2.1.1 Sign convention

In most manoeuvring models use is made of two frames of reference, namely an earth fixed/inertial frame of reference and a body fixed frame of reference. In this research an additional frame of reference is required, this frame should be fixed to the assisted ship. The simulation of the escorting tug may be considered as a tug sailing while facing a current, with a velocity equal to the velocity of the assisted ship. Here it is assumed that the current velocity is uniform and irrotational.
The point of interest will be the position of the tug relative to the assisted ship such that the towline force can be calculated and the risk of collision of the tug and ship can be estimated. Whenever it is assumed that the escort operations take place in calm deep water, the position of the tug relative to an earth fixed point does not contribute to the ability to analyse the safety of the escort operation. So where an earth fixed frame is commonly used to describe the tugs position, in this research the tugs position will only be calculated relative to the assisted ship. This reference frame is indicated with $Q_{(U,V,Z)}$ in figure 2.1.

The body fixed frame has it's origin in point O. In this research the location of O is defined as follows: $(\frac{L_{wl}}{2}, 0, T_{mean})$, where $\frac{L_{wl}}{2}$ is measured from the aft of the vessel. Besides, the distance from O to the centre of gravity is indicated with (x_G, y_G, z_G). The distance from the centre of gravity to the towing point is

indicated with (x_P, y_P, z_P).

The velocity vector for a 6 DOF system can be described as follows:

$$\vec{v} = (u, v, w, p, q, r)^T \tag{2}$$

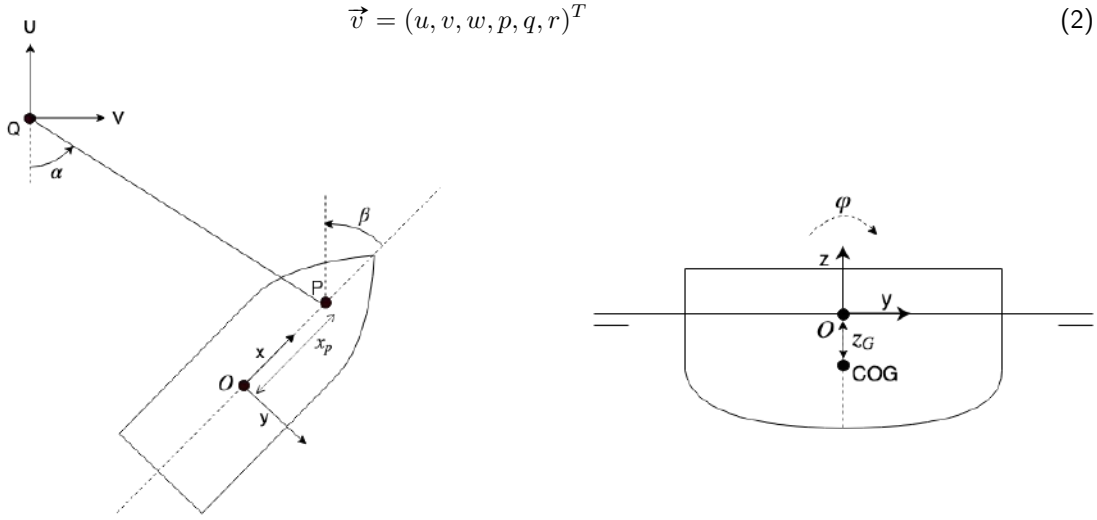

Figure 2.1: Illustration of reference systems

2.1.2 Equations of motion

In the introduction of this research it is mentioned that the fourth degree of freedom, which is the roll motion, may not be neglected when simulating the behaviour of a tug in escort operations. This causes the classical manoeuvring models, as described in i.a. [21] and [28], to be unsuitable in their original form, as those classic models only consider three degrees of freedom. The implementation of the fourth degree of freedom is one of the objectives in this research. However, first Newton's equations of motion will be elaborated for the usual three degrees of freedom only, namely surge, sway and yaw. Thereafter, in section 2.5, the fourth degree of freedom will be added.

In equation 1 the rigid body dynamics are included in the left hand side and the superposition of all external forces is included in the right hand side. In the following sections information related to the external forces will be provided while this section focuses on the rigid body dynamics only.
When separating the rigid body dynamics from the external forces, equation 1 can be rewritten into:

$$\underline{\underline{M_{RB}}}\,\dot{\vec{v}} + \overrightarrow{C_{RB}}(\vec{v}) = \tau_{hd} + \tau_{prop} + \tau_{rudder} + \tau_{tow} \tag{3}$$

$$\tau_{hd} = -\underline{\underline{M_A}}\,\dot{\vec{v}} - \underline{\underline{D}}\,\vec{v} \tag{4}$$

Where M_{RB} and C_{RB} for a 3DOF system can be written as:

$$\underline{\underline{M_{RB}}} = \begin{bmatrix} m & 0 & 0 \\ 0 & m & mx_G \\ 0 & -mx_G & I_{zz} \end{bmatrix} \quad \overrightarrow{C_{RB}} = \begin{bmatrix} -mvr - mx_G r^2 \\ mur \\ mx_G ur \end{bmatrix}$$

Here I_{zz} is the second moment of inertia around the z-axis which actually represents the inertia force required to turn the rigid body around it's own z-axis. The matrices above are a result of the standard formulation for a moving rigid body in a non-inertial frame of reference, including the centripetal and centrifugal forces. This is formulated as follows:

$$m \cdot (\dot{\vec{u}} + \dot{\vec{\omega}} \times \vec{u} + \dot{\vec{\omega}} \times \overrightarrow{x_G} + \vec{\omega} \times (\vec{\omega} \times \overrightarrow{x_G})) = \vec{F}_{external} \tag{5}$$

Where $\vec{u} = (u, v, w)^T$ and $\vec{\omega} = (p, q, r)^T$.

2.2 Formulation of hydrodynamic forces

Now the rigid body dynamics are derived, more detailed information can be given about the external forces included in the right hand side of equation 3. In this research the focus will be on the derivation of the hydrodynamic forces, the derivation of the remaining external forces required for simulation is provided in chapter 3. Note that in this section only three degrees of freedom will be considered.

2.2.1 Regression method

The hydrodynamic forces are usually formulated using a Taylor expansion of which the order depends on the required accuracy. In equation 6 a Taylor expansion of property F depending on a single variable (x) is provided.

$$F(x) = F(x_0) + (x - x_0)\frac{dF}{dx} + (x - x_0)^2\frac{1}{2!}\frac{d^2F}{dx^2} + (x - x_0)^3\frac{1}{3!}\frac{d^3F}{dx^3} + ... \tag{6}$$

For simplicity reasons the derivatives are rewritten as follows:

$$\frac{dF}{dx} = F_x, \quad \frac{1}{2!}\frac{d^2F}{dx^2} = F_{xx}, \quad \frac{1}{3!}\frac{d^3F}{dx^3} = F_{xxx}$$

In manoeuvring theory, those terms are usually referred as "*Hydrodynamic derivatives*".
In case of a 3DOF manoeuvring model, the hydrodynamic forces X, Y and N are all a function of 6 variables, namely $f(u, v, r, \dot{u}, \dot{v}, \dot{r})$. For a property depending on multiple variables the Taylor expansion can be written as in equation 7. Here the Taylor expansion is given for every force component up to the first order.

$$\begin{aligned}
X_{HD} &= X_0 + (u - u_0)X_u + (v - v_0)X_v + (r - r_0)X_r + (\dot{u} - \dot{u_0})X_{\dot{u}} + (\dot{v} - \dot{v_0})X_{\dot{v}} + (\dot{r} - \dot{r_0})X_{\dot{r}} \\
Y_{HD} &= Y_0 + (u - u_0)Y_u + (v - v_0)Y_v + (r - r_0)Y_r + (\dot{u} - \dot{u_0})Y_{\dot{u}} + (\dot{v} - \dot{v_0})Y_{\dot{v}} + (\dot{r} - \dot{r_0})Y_{\dot{r}} \\
N_{HD} &= N_0 + (u - u_0)N_u + (v - v_0)N_v + (r - r_0)N_r + (\dot{u} - \dot{u_0})N_{\dot{u}} + (\dot{v} - \dot{v_0})N_{\dot{v}} + (\dot{r} - \dot{r_0})N_{\dot{r}}
\end{aligned} \tag{7}$$

Since most vessels are symmetric in the xz-plane, no transverse force will act on the vessel during a straight-line motion at constant speed and zero drift angle. This indicates that Y_u and N_u are both zero, the pressure distribution shown in figure 2.2 confirms this assumption to be valid. Besides, the cross-coupled derivatives X_v, $X_{\dot{v}}$, X_r and $X_{\dot{r}}$, just like $Y_{\dot{u}}$ and $N_{\dot{u}}$, are zero because of symmetry about the xz-plane [32].

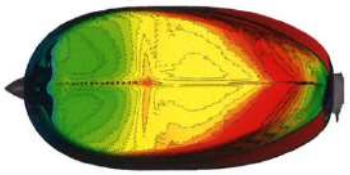

Figure 2.2: Pressure distribution for $\beta = 0°$

With these simplifications and the assumptions that the initial values of all force contributions are zero, equation 7 can be reduced to:

$$\begin{aligned}
X_{HD} &= X_u u + X_{\dot{u}}\dot{u} \\
Y_{HD} &= Y_v v + Y_r r + Y_{\dot{v}}\dot{v} + Y_{\dot{r}}\dot{r} \\
N_{HD} &= N_v v + N_r r + N_{\dot{v}}\dot{v} + N_{\dot{r}}\dot{r}
\end{aligned} \tag{8}$$

These results can be filled in equation 3 resulting in a set of equations given in (9). Here it can be seen that $X_{\dot{u}}, Y_{\dot{v}}, Y_{\dot{r}}, N_{\dot{v}}$ and $N_{\dot{r}}$ are multiplied with an acceleration term and by definition those terms represent added masses. The terms which will be multiplied by velocity terms, being X_u, Y_v, Y_r, N_v and N_r, are usually referred as 'damping terms'.

$$\begin{aligned}
(m - X_{\dot{u}})\dot{u} - (v - x_G r)mr &= X_u \\
(m - Y_{\dot{v}})\dot{v} + (mx_G - Y_{\dot{r}})\dot{r} + mur &= Y_v v + Y_r r \\
-(mx_G + N_{\dot{v}})\dot{v} + (I_{zz} - N_{\dot{r}})\dot{r} + mx_G ur &= N_v v + N_r r
\end{aligned} \tag{9}$$

Note that those damping terms are not similar to the damping terms in seakeeping theory while they have a different origin. In seakeeping theory the damping terms are usually a summation of the potential damping and the viscous damping which are frequency dependent. The oscillations of manoeuvring vessels in surge, sway and yaw directions will generally be at very low frequencies, where the potential damping coefficients tend to zero. For free sailing vessels the natural frequency of roll is usually the dominating frequency, so in this case the potential roll damping should be included. The effect of potential damping in time domain simulations is referred as *'fluid memory effect'* and will be explained later in subsection 2.4. Besides the contribution of this frequency dependent damping coefficient, multiple other hydrodynamic force contributions are elaborated in the section 2.4.

2.2.2 Second order terms

In equation 9 the hydrodynamic forces are written as a Taylor expansion up to the first order, which means that the hydrodynamic derivatives are assumed to be linear dependent on the velocity and acceleration. A first order Taylor approximation is assumed to be valid for small changes of the variables $u, v, r, \dot{u}, \dot{v}$ and $\dot{r}$. However, a suitable approximation is desired for larger changes as well. For example, in figure 2.3 the blue line represents the force in y-direction resulting from a straight line captive model test (subsection 2.3.2). The red dashed line is a first order linear approximation this force. Seen the behaviour of the force in the y-direction it can be concluded that a first order linear approximation is not able to predict the hydrodynamic force accurately and at least some second order terms are required.

Whenever the Taylor expansion will be up to the second order, the second order derivatives with respect to the acceleration will arise, indicated as: $X_{\dot{u}\dot{u}}, Y_{\dot{v}\dot{v}}, Y_{\dot{r}\dot{r}}, ...$ It is unnecessary to consider those terms. As mentioned previously the derivatives with respect to the accelerations represent the added mass coefficients. The theoretical way to calculate the added mass terms, which will be described in subsection 2.4.1, is already nonlinear and is assumed to be accurate enough. So no extra higher order terms are required.
Besides the second derivatives with respect to the accelerations, coupling terms between the accelerations and velocities arise as well. Those are indicated as: $X_{u\dot{u}}, Y_{v\dot{v}}, Y_{r\dot{r}}, ...$ As described in [14] those terms may be neglected, as they do not have a physical meaning. So the only coupling terms that should be taken into account are the coupling terms between the velocities.

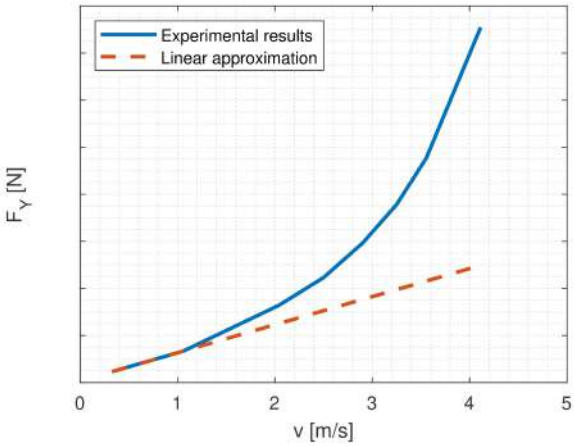

Figure 2.3: Linear approximation of F_Y

That mentioned, enables us to write the regression of the hydrodynamic forces up to the second order. To make sure the forces are acting in the good direction, the quadratic velocity terms are replaced by a multiplication of a the velocity by its absolute magnitude. The regression of the hydrodynamic forces than becomes as follows:

$$\begin{aligned} X_{HD} &= X_{\dot{u}}\dot{u} + X_u + X_{uu}u|u| \\ Y_{HD} &= Y_{\dot{v}}\dot{v} + Y_{\dot{r}}\dot{r} + Y_v v + Y_r r + Y_{vv}v|v| + Y_{rr}r|r| + Y_{rv}r|v| + Y_{vr}v|r| \\ N_{HD} &= N_{\dot{r}}\dot{r} + N_{\dot{v}}\dot{v} + N_v v + N_r r + N_{vv}v|v| + N_{rr}r|r| + N_{rv}r|v| + N_{vr}v|r| \end{aligned} \tag{10}$$

Note that it is still assumed Y and N are decoupled from X, as described in subsection 2.2.1.
In the Taylor expansion up to the second order hydrodynamic derivatives Y_{rv}, Y_{vr}, N_{rv} and N_{vr} arise. Those terms represent a contribution to the combined sway-yaw damping. However, in most existing manoeuvring methods only Y_{rv} and N_{rv} are considered. Here it is assumed that Y_{vr} and N_{vr} are similar to Y_{rv} and N_{rv}.
To obtain the damping force and moment, Y_{rv} and N_{rv} should be multiplied by r|v|. Which means that the negatively defined damping terms will, regardless of the sway direction, always counteract the yaw motion. Inclusion of $N_{vr}v|r|$ and $Y_{vr}v|r|$ will be mathematically correct, however it is nowadays unknown whether those force contributions should be included from a physical point of view. For this reason, those contributions will be left out in the scope of this research.

2.2.3 Lift induced drag

In subsection 2.2.1 it is mentioned that in many existing manoeuvring methods Y and N are decoupled from X. However this assumption seems disputable, since significant differences in the formulation of the X-force arise between the existing semi-empirical methods. So is X in [21] only dependent on u and $\dot{u}$, in contrast to the methods described in [15] and [5] where X depends on v as well.

The results of some captive model tests and CFD simulations, performed with a DAMEN tug [48], has shown that the x-force during a pure sway motion has a small non-zero value. Theory written in [32] and [25] confirm this finding. Figure 2.4a shows the asymmetric pressure distribution resulting in a nonzero x-force and figure 2.4b shows an indicative relation between X and v.

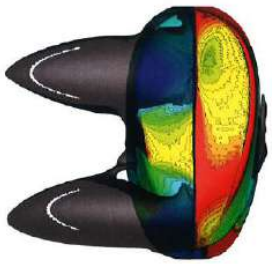

(a) Pressure distribution for 90° drift

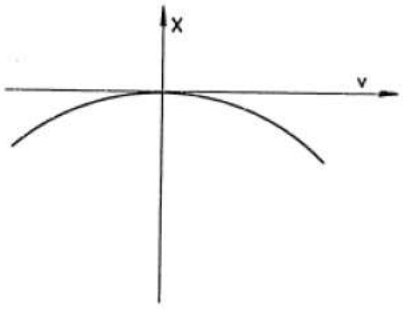

(b) Indicative relation between X and v [25]

Figure 2.4: Illustration of x-force during pure sway motion

The presence of this x-force is due to a phenomena named: Lift induced drag. An increasing surge velocity results in an increasing lift coefficient, according to the Lanchester-Prandtl theory this results in an additional drag coefficient. Equation 11 can be used to formulate the additional drag [11].

$$c_{d_i} = C_L^2 \frac{L}{\pi T} \tag{11}$$

In appendix B the full derivation of the hydrodynamic derivatives arising from lift induced drag is provided. Contributing for the lift induced drag results in three additional hydrodynamic derivatives, referred as: X_{vv}, X_{vr} and X_{rr}. The in figure 2.4b indicated relation between X and v seems to be quadratic, which confirms that the lift induced drag could be formulated as:

$$c_{d_i} = X_{vv}v^2 + X_{vr}vr + X_{rr}r^2$$

Accounting for the lift induced drag and omitting Y_{vr} and N_{vr} results in the final formulations of the hydrodynamic forces in surge, sway and yaw direction:

$$\begin{aligned} X_{HD} &= X_{\dot{u}}\dot{u} + X_u + X_{uu}u|u| + X_{vv}v^2 + X_{vr}vr + X_{rr}r^2 \\ Y_{HD} &= Y_{\dot{v}}\dot{v} + Y_{\dot{r}}\dot{r} + Y_v v + Y_r r + Y_{vv}v|v| + Y_{rr}r|r| + Y_{rv}r|v| \\ N_{HD} &= N_{\dot{r}}\dot{r} + N_{\dot{v}}\dot{v} + N_v v + N_r r + N_{vv}v|v| + N_{rr}r|r| + N_{rv}r|v| \end{aligned} \tag{12}$$

2.2.4 Non-dimensionalisation of hydrodynamic derivatives

When using hydrodynamic derivatives it is often convenient to non-dimensionalise the force components such that they can be treated as constants with respect to the instantaneous speed. The commonly used method of dimensionalisation is the *prime system* of SNAME [14]. In this method forces and moments are non-dimensionalised using the multiplications given in table 2.1.

Table 2.1: Non-dimensionalisation according to prime system

Unit	Prime system II
Time	$\frac{L}{U}$
Mass	$\frac{1}{2}\rho L^2 T$
Length	L
Force	$\frac{1}{2}\rho U^2 LT$
Moment	$\frac{1}{2}\rho U^2 L^2 T$
Linear velocity	U
Angular velocity	$\frac{U}{L}$
Linear acceleration	$\frac{U^2}{L}$
Angular acceleration	$\frac{U^2}{L^2}$

The use of LT is inspired by the wing theory (section 2.4.2), where $A_{lateral} = L \cdot T$. An example of the non-dimensionalisation of the parameters, is as follows:

To calculate the Y-force contribution due to a yaw velocity, Y_r should be multiplied by r:

$$Y = Y_r \cdot r \tag{13}$$

The dimensions of the properties in equation 13 are as follows:

$$[\frac{kgm}{s^2}] = [unkown] \cdot [\frac{1}{s}] \longrightarrow [unknown] = [\frac{kgm}{s}]$$

When using the properties given in table 2.1, Y_r' can be derived as follows:

$$Y_r' = \frac{Y_r}{\frac{[\frac{1}{2}\rho L^2 T][L]}{[L/U]}} = \frac{1}{\frac{1}{2}\rho L^2 TU} Y_r$$

An overview of all dimensionless hydrodynamic derivatives is provided in appendix A.

2.3 Methods to derive the hydrodynamic derivatives

In section 2.2 the formulation of the hydrodynamic forces using a second order Taylor expansion is derived. This has resulted in an expression given in equation 12. In this section the existing methods to predict those hydrodynamic derivatives are elaborated. In [39] the current status of manoeuvring prediction methods is described and here several types of manoeuvring models are distinguished based on their source of estimation of the hydrodynamic forces. In figure 2.5 those types are arranged based on their complexity and reliability of results. Not all of the methods mentioned in figure 2.5 require the formulation of the hydrodynamic forces using hydrodynamic derivatives, as derived in section 2.2. Those methods which do not require the formulation are marked in blue, in the following subsections the reason why is provided.

2.3.1 Database and semi-empirical methods

As can be seen in figure 2.5 the database and semi-empirical methods are the least reliable methods, however they are relatively cheap and less complex compared to other methods. They are suitable to use in the first stage of the design process. In the database method, the hydrodynamic forces are based on previously retrieved data only. An example of such a method can be found in [27]. In database methods the so called hydrodynamic derivatives found in section 2.2 will not be used and the forces are calculated using coefficients obtained from fitting experimental data. In semi-empirical methods, the hydrodynamic coefficients are calculated using a combination of data and simplified methods such as the slender body theory and the cross flow drag theory. In section 2.4 a more detailed explanation about this way to determine the hydrodynamic forces will provided.

Most semi-empirical methods are based on data retrieved from common merchant ships, which are typically single-screw slow/medium speed vessels. For example in [27] the data is retrieved from 21 different vessel types, including container ships, bulk carriers, LNG carriers, RoRo vessels, etc. The same yields for other widely used prediction

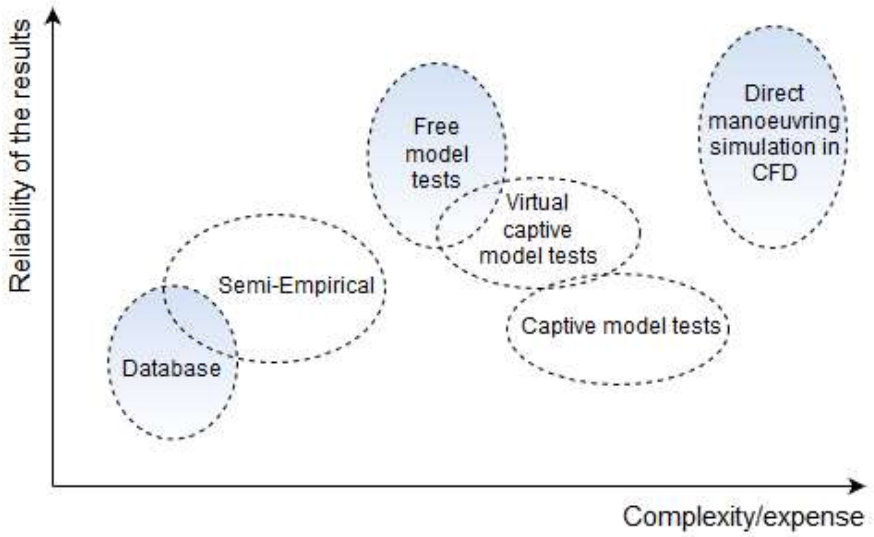

Figure 2.5: Complexity versus accuracy for hydrodynamic force estimation methods [39]

methods such as [21] and [28]. Another characteristic of this group of methods is that most of them consider only three degrees of freedom, namely: surge, sway and yaw. There are some methods considering the fourth degree of freedom, such as written in [15] and [5]. However those methods are usually referred as *performance prediction methods* for tugs specific and are not able to calculate the dynamic manoeuvring behaviour. Those performance prediction methods often use classical semi-empirical methods to predict the hydrodynamic forces. Like in [15] and [5] where the in 1985 developed method by Ankudinov [4] is used. In this method as well the roll moment is calculated as well, being a result of the lateral force. It is described as $K = F_Y \cdot z_p$, where z_p is the vertical distance to the centre of pressure. Whether this method is suitable for simulation purposes, will be evaluated in sections 2.5 and 3.9.

2.3.2 Model tests

Besides database and semi-empirical manoeuvring models, model tests are a commonly used methodology to arrive at manoeuvring characteristics. There are two different ways to perform model tests, namely: free model tests and captive model tests. Free model tests is the most complete way of performing manoeuvres since, except from scaling effects, no presumptions are made. In free model tests the IMO manoeuvring criteria [46] are directly obtained and so the hydrodynamic derivatives are not calculated explicitly. The main disadvantage of this method is the fact that it is only applicable for a single design, which makes it an expensive method too. To make model test results more efficient and generally applicable, captive model tests are introduced. Captive model tests results offer the very practical advantage of generalising free manoeuvring problems. The ITTC distinguished several types of captive model tests, namely: Straight line tests, harmonic tests and steady circular motion tests. Each model test is used to obtain one or more of the hydrodynamic derivatives as obtained in section 2.2.

Straight line tests

The most simple variant of captive model tests, where a straight line towing is performed for a range of drift angles. Eventually with rudder deflection and/or propeller variations. In figure 2.6a a picture of a straight line captive model tests with the DAMEN RSD 2513 tug can be seen. All motions relative to the carriage are restricted.

(a) Straight line captive model test for RSD 2513

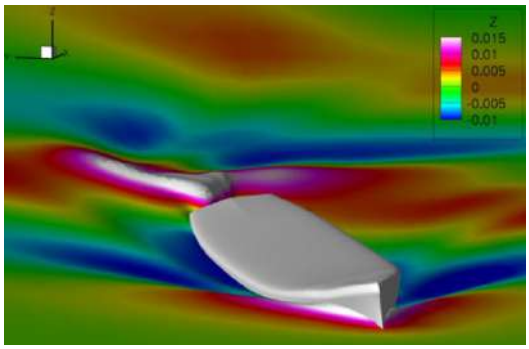

(b) Illustration of direct CFD [7]

Figure 2.6: Examples of methods to derive the hydrodynamic forces

Harmonic tests
Planar Motion Mechanism (PMM), which generates sinusoidal motions in sway, surge, roll and yaw, can be used to calculate hydrodynamic forces. Besides the pure sway, surge, roll and yaw motions, combinations can be made. Such as say-yaw and yaw-drift combinations, eventually with rudder deflection. Following the method described in [26] enables to calculate the added mass and damping terms and with that to determine the hydrodynamic derivatives. The big advantage of harmonic tests is that it may be used to evaluate the coupled damping terms as well.

Steady circular motion tests
By using a PMM or a rotating arm, pure yaw or combined yaw-drift motions can be performed. And like for the other types of captive model tests, rudder deflections could be considered as well. With this method forces coherent to the yaw motion could directly be obtained.

2.3.3 Modelling in CFD

The applicability of CFD in ship hydrodynamics has been growing over the past years. Even in ship manoeuvring CFD is used to determine the hydrodynamic forces. There are two ways to apply CFD to derive those hydrodynamic forces, namely: Direct CFD and Virtual captive model tests. The latter uses the same approach as the straight line captive model tests mentioned in subsection 2.3.2. This approach has been applied to tugs in [48] and [5] and to a container vessel in [47]. Those researchers show that the hydrodynamic forces obtained in CFD are in good agreement with those obtained in model tests, however with a relatively large uncertainty.
Direct manoeuvring simulation in CFD is the most expensive and complex method to derive the forces, but it has the highest reliability of all methods. In direct CFD simulations the equations of motion are directly coupled to the calculated pressures. This approach has been applied in [7] and it turned out that those methods are able to simulate the manoeuvring behaviour accurately. Though, this method is nowadays extremely time consuming and expensive to use it in a commercial way, it may offer opportunities for future development. An example of applied direct CFD can be seen in figure 2.6b.

2.4 Background of hydrodynamic derivatives

In section 2.2 a general formulation for the hydrodynamic forces is derived using a second order Taylor expansion. This section is followed up by section 2.3 in which several ways to derive the hydrodynamic forces are elaborated. Despite the relatively high reliability of results coming from direct manoeuvring in CFD or free model tests (figure 2.5), a general applicable and fast method to derive the hydrodynamic forces is often desired and so semi-empirical methods are commonly used. Therefore more knowledge about the physical background behind these methods is provided in this section.

In the Taylor expansion (12) first and second order terms can be distinguished which are also known as linear and non linear terms respectively. Besides, distinction can be made between the so called hydrodynamic derivatives which will be multiplied with one or two velocity components and the derivatives to be multiplied with an acceleration term. In subsection 2.2.1 it is mentioned that those derivatives are named damping and added mass

coefficients respectively. This results in the following distinction:

$$\begin{aligned} \text{Added mass terms :} \quad & X_{\dot{u}}, Y_{\dot{r}}, Y_{\dot{v}}, N_{\dot{r}}, N_{\dot{v}} \\ \text{Linear damping terms :} \quad & X_u, X_v, Y_v, Y_r, N_r, N_v \\ \text{Non linear damping terms :} \quad & X_{uu}, X_{vv}, X_{vr}, X_{rr}, Y_{vv}, Y_{rr}, Y_{rv}, N_{vv}, N_{rr}, N_{rv} \end{aligned}$$

Although the added mass terms are similar to the added mass terms in seakeeping theory, the damping terms are not. Multiple methods to derive the linear and non linear damping coefficients are developed in the past. Within these methods several phenomena are described that contribute to the hydrodynamic damping forces on the manoeuvring vessel. In table 2.2 the different contributions to the hydrodynamic forces are listed and a distinction between linearity and non linearity is made. Those methods and phenomena will be described and related to the linear and non linear damping coefficients found in equation 12. But first, the derivation of the added mass is described in subsection 2.4.1.

Table 2.2: Separation of linear and non-linear damping

Linear damping	**Non-linear damping**
Fluid memory effects	Skin friction
Skin friction	Viscous shedding
Lift due to linear circulation	Cross-flow drag

Note that the physical background of hydrodynamic derivatives X_{vv}, X_{vr} and X_{rr} is already provided in 2.2.3. Those terms will not be covered in this section.

2.4.1 Added mass

To simulate the manoeuvring behaviour of a tug in 3 degrees of freedom, five added mass terms should be calculated. As mentioned before, those added mass coefficients are similar to those derived in seakeeping theory. The following similarities are valid:

$$M_A = \begin{bmatrix} a_{11} & 0 & 0 \\ 0 & a_{22} & a_{26} \\ 0 & a_{62} & a_{66} \end{bmatrix} = \begin{bmatrix} -X_{\dot{u}} & 0 & 0 \\ 0 & -Y_{\dot{v}} & -Y_{\dot{r}} \\ 0 & -N_{\dot{v}} & -N_{\dot{r}} \end{bmatrix}, \quad a_{26} = a_{62} = -Y_{\dot{r}} = -N_{\dot{v}}$$

Knowing that the notation for degrees of freedom in seakeeping theory is as follows: 1=surge, 2=sway, 3=heave, 4=roll, 5=pitch and 6=yaw.

The added mass can be calculated using *Strip Theory Method* [45]. Here a ship is split into a finite number of transversal 2D slices. For each slice, with it's specific geometry, the added mass can easily be calculated. The total added mass of the ship is obtained by integration of the 2D values over the length of the hull.
This results in the following expressions for the total added mass coefficients:

$$\begin{aligned} a_{22} &= \int_{L_1}^{L_2} a_{22}(x)dx \\ a_{26} &= \int_{L_1}^{L_2} a_{22}(x)xdx \end{aligned} \tag{14}$$

Where a_{ij} is the 2D added mass of the cross section at location x. To determine the 2D added mass of a section with a specific shape, a Lewis transformation can be used. Here the added mass terms are expressed as a function of some geometrical parameters. Those expressions may be found in [45].

Note that the strip theory cannot be used to determine the surge added mass (m_{11}). To calculate this the *Method of Equivalent Ellipsoid* may be applied. Here the ship can be relatively assumed as a 3D body, which is, in case of a ship, mostly an elongated ellipsoid. a_{11} Can be described as:

$$a_{11} = mk_{11}, \quad \text{with} \quad k_{11} = \frac{A_0}{2 - A_0}, \quad \text{and} \quad A_0 = \frac{2(1-e^2)}{e^3}\Big[\frac{1}{2}ln\Big(\frac{1+e}{1-e}\Big) - 2\Big] \tag{15}$$

2.4.2 Low Aspect-ratio Wing Theory

In manoeuvring theory the *Low Aspect-ratio Wing theory* is often used to predict the side force and yaw moment for a ship under a steady drift angle. Here the ship is represented by a wing with a very low aspect ratio and the lift and drag are linear dependent on the inflow velocity. A few similarities can be made between the classic wing theory and the wing theory applied to manoeuvring ships, those are illustrated in figure 2.7.

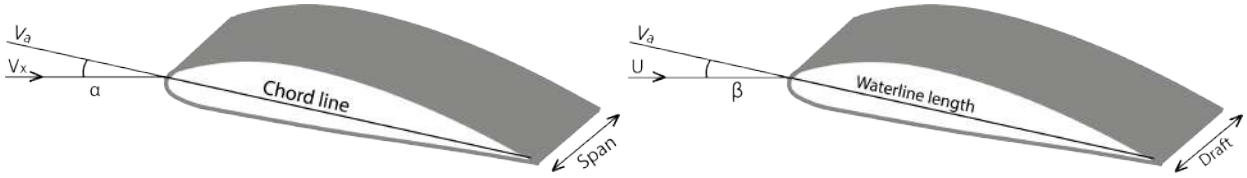

(a) Classic wing geometry

(b) Geometry of wing representing a ship

Figure 2.7: Similarities between geometries of classic wing and ship hull

The effective aspect ratio of the wing can be calculated using equation 16.

$$AR_e = \frac{2 \cdot \text{Span}}{\text{Chord line length}} = \frac{2T}{L_{wl}} \tag{16}$$

Of all possibilities for constructing non linear models of small aspect-ratio wings only one found wide use in ship manoeuvring: this is the model based on separation of linear and non linear parts of the load. The linear part can be estimated by use of the linear lift theory and the non linear part is described with the *cross-flow drag model*.

Lift due to linear circulation

The linear circulation along a surface generates a lift component. One of the methods used to derive this lift component is the in 1924 developed Munk Method [36]. This method was originally developed to calculate the aerodynamic loads on airships. After 1924 several attempts are made to improve the accuracy of the method, those are described in [44]. The aim of this method is to derive the lift forces on a wing as a function of the angle of attack, α. Due to a certain angle of attack, pressure differences between both sides of the wing will arise which will result in a lift force.

The applicability of this theory rests on the validity of the Kutta condition at the ship's stern, which is illustrated in figure 2.8. The Kutta condition implies that the flow at the stern leaves the trailing edge smoothly, as viscosity effects are neglected. As opposed to the expectation of a growing boundary layer and separation of the flow due to viscosity, especially at larger drift angles.

The main idea behind the method is the application of the potential flow theory to the fluid surrounding a hull strip with further integration of obtained 2D inertial loads along the ship's length.

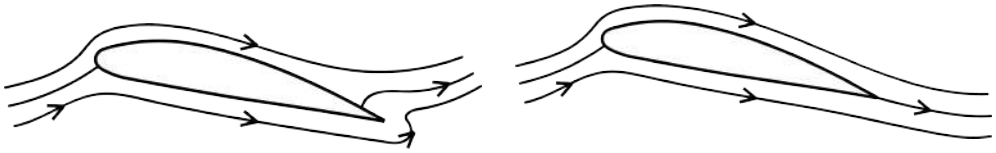

(a) Irrotational flow around airfoil

(b) Rotational flow around airfoil with Kutta condition at stern

Figure 2.8: Flow around airfoil

Previous research has turned out that flow separation for tugs sailing with large drift angles plays a significant role, especially at the aft ship [48]. This makes the applicability of the low aspect-ratio wing theory disputable. Nevertheless, the theory may be used to predict the linear lift forces for small drift angles up till the so called stall angle. The stall angle is defined as the drift angle at which flow separation starts to take place.

The total lift, and with that the induced moment, is a function of the 2D added mass which should accelerated. This results in the following formulations [37]:

$$L = Y_v = -v^2\beta \int_{-\frac{L}{2}}^{\frac{L}{2}} \frac{dm(x)}{dx} dx$$
$$N_v = -v^2\beta \int_{-\frac{L}{2}}^{\frac{L}{2}} x \frac{dm(x)}{dx} dx \tag{17}$$

So N_v represents the yaw moment as a result of a sway velocity, this moment is also known as the *Munk moment*. In manoeuvring theory, this moment is important as it mostly destabilises the manoeuvring. If the vessel sails under a (small) drift angle and so it has a transverse velocity component, force is acting along the side. Those forces generate a moment, whenever the moment generated at the bow is larger than the moment generated at the stern, the drift angle becomes even larger. This is illustrated in figure 2.9.

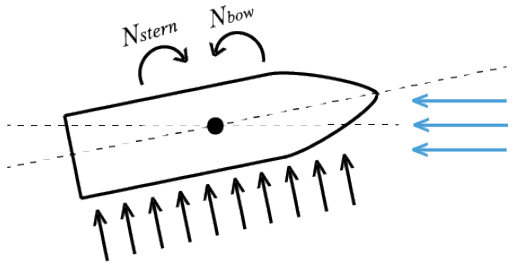

Figure 2.9: Illustration of the Munk Moment (N_v)

Now a method to derive the hydrodynamic derivatives N_v and Y_v is provided, N_r and Y_r can be obtained as well. This can be done in the same way, using a 2D strip approach given in equation 17. However, instead of the velocity component 'v' the rotational velocity component 'r' should be used. For every section at position x, the rotational velocity acts like an (extra) vertical velocity component equal to the rotational velocity times the distance in x-direction from the section to the centre of rotation ($r \cdot x_r$).

Cross-flow drag

Lifting forces arise from two physical mechanisms, namely the linear part due to flow circulation around the hull, calculated using the Munk method and the non linear part. The cross-flow drag has a significant contribution to the non linear part of the forces and moments acting on the hull. At higher drift angles the cross-flow drag becomes even the dominant viscous effect. In figure 2.10 an illustration of the cross flow phenomena acting along a hull and a keel can be seen.

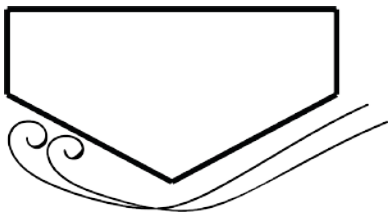

(a) Cross-flow around the hull

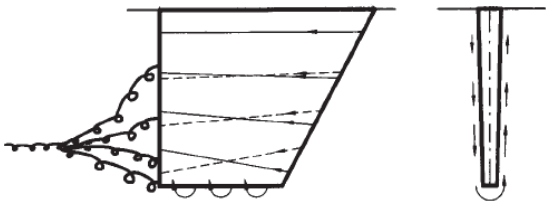

(b) Cross-flow phenomena along keel [29]

Figure 2.10: Illustration of cross-flow phenomena

A link could be made between the cross-flow acting around the free edge of a keel and the cross flow along the ship's hull. Because in both cases there is nothing to prevent the flow on the high pressure side to escape to the low pressure side, a cross-flow around the tip is generated. Cross-flow induces an additional lift force that is assumed to be dependent on the rotational and transverse velocity only and is acting in the opposite direction to

the transverse velocity component. The forces generated by this phenomena can be calculated using a 2D strip theory approach given in equations 18 and 19 [14].

$$Y = -\frac{\rho}{2}\int_{-\frac{L_{wl}}{2}}^{\frac{L_{wl}}{2}} T(x)C_d^{2D}(x)|v + xr|(v + xr)dx \tag{18}$$

$$N = -\frac{\rho}{2}\int_{-\frac{L_{wl}}{2}}^{\frac{L_{wl}}{2}} T(x)C_d^{2D}x(x)|v + xr|(v + xr)dx \tag{19}$$

Here C_d^{2D} is the 2D drag coefficient which can be calculated using Hoerner's curves [41]. This constant is dependent on the instantaneous waterline breadth of the section and it's draft, which both depend on the heeling angle. Whether the section shape more closely resembles an ellipse or a rectangle with round corners influences C_d^{2D} as well [17].

From equations 18 and 19 it can be seen that there is a coupling between the yaw rate and transverse velocity. Those coupling terms could, in terms of hydrodynamic derivatives, be expressed as follows [14] :

$$\begin{aligned} Y &= -Y_{vv}v|v| - Y_{vr}v|r| - Y_{rr}r|r| \\ N &= -N_{vv}v|v| - N_{vr}v|r| - N_{rr}r|r| \end{aligned} \tag{20}$$

2.4.3 Fluid memory effects

Although classical manoeuvring methods neglect the fluid memory effects by relying on a zero frequency assumption, the fluid memory effects may play a role in manoeuvring forces for surface vessels. The phenomena is well known in seakeeping theory and it can be defined as: The affect on ship motions of waves generated in the free surface due to previous ship motions. It can be interpreted as filtered potential damping forces.
As already mentioned in subsection 2.2.1 the dominating oscillation frequency of the surge, sway and yaw motions are generally very low, where the potential damping tends to zero. In contrast to the roll motion for free sailing vessels, where the natural frequency is often the dominating frequency. For this reason the frequency dependent potential damping is often considered in 4DOF manoeuvring models using Cummin's equation.

The Cummin's equation is used to transfer the equation of motion from frequency domain (seakeeping) to time domain (manoeuvring). Cummins found out that the potential could be separated into two parts, one valid during the duration of a given impulse and the other valid after the impulse. By expressing the pressure as a function of these potentials and integrating it over the wetted surface, a time dependent function is obtained:

$$(M_{RB} + A_\infty)\ddot{\eta} + \int_0^\infty K(t-\tau)\dot{\eta}(\tau)d\tau + C\eta = F_{external} \tag{21}$$

in which:

$$\begin{aligned} A_\infty &= \text{infinite frequency added mass matrix} \\ K &= \text{retardation function matrix} \\ F(t) &= \text{external excitation force} \end{aligned}$$

The retardation function is one that takes the fluid memory effects into account and can be formulated as follows:

$$K(t) = \frac{2}{\pi}\int_0^\infty B(\omega)cos(\omega t)d\omega \tag{22}$$

The frequency dependent damping $B(\omega)$ can be obtained using a 3D-panel method, this approach enables to include quadratic viscous terms as well. A more detailed explanation of the transformation from frequency domain to time domain is described in [10].

For tugs in tow operations, the natural roll motion will probably not be the dominating frequency as the tug will not be free to roll due to the restriction by the towline. Nevertheless, it is still desired to include the frequency dependent potential and viscous roll damping to be able to simulate situations such as towline release or loss of propulsion. Which both enables to analyse the safety of the vessel and determine the limits of safety.

2.4.4 Skin friction

Damping is caused by generated waves which dissipate energy (potential damping) as well as by viscous effects such as skin friction. In most cases viscous effects are neglected in seakeeping calculations for the sway, heave, pitch and yaw motions of ships, as the potential damping is dominating the viscous damping [29].
In most manoeuvring models only the surge and roll non linear viscous damping are taken into account. For surge yields that the non linear force acts in the direction opposite to the forward velocity and so is expressed, in terms of hydrodynamic derivatives, as $X_{u|u|}$. To calculated this force the ITTC resistance prediction method [22] may be used. Here the frictional resistance is can be determined using equation 23.

$$X_{uu} = -\frac{1}{2}\rho S(1+k)C_f \tag{23}$$

This approach is based on the frictional resistance of a flat plat in a 2D flow. The effects of longitudinal pressure gradients, lateral streamline convergence and lateral pressure gradients are not considered. Nevertheless, it is claimed that this approach includes some effects of the 3D shape and viscous resistance [29].

In the previous subsection (2.4.3), the so called fluid memory effects are elaborated. Here it is mentioned that the roll damping may play a part, as it is required to simulate the tugs behaviour after a towline release or loss of propulsion. The total roll damping is a superposition of the potential damping and viscous damping. The skin friction during roll motion is part of the viscous damping and is usually calculated using work published in 1984 by Ikeda [18]. It may be included using the Cummin's equation (21).

2.5 Roll moment

In the previous sections background information has been provided about different ways to derive the hydrodynamic forces of a manoeuvring vessel. However, most of the discussed methods are suitable for relatively large merchant ships and consider only three degrees of freedom. The question remains whether these methods are applicable to tugs in escort operations. In chapter 1 it is already concluded that for simulating an escorting tug, the roll motion should be included. In literature only a few manoeuvring models that consider this fourth degree of freedom can be found. One of those methods is described in [42]. The principle of deriving the hydrodynamic roll moment used in this method, will be the basis of the method described in chapter 3.

2.5.1 Rigid body dynamics for a 4DOF system

Besides the necessity of calculating the hydrodynamic roll moment, Eulers equations of motion should be extended with the fourth degree of freedom. In equation 24 the additional terms are marked in blue, here it is assumed that the centre of gravity is located at the centerline of the tug such that y_G equals zero.

$$\begin{aligned}
(m - X_{\dot{u}})\dot{u} - (v - x_G r)mr + z_G \cdot p \cdot r &= X_u u + X_v v + X_{uu} u|u| + X_{vv} v^2 + X_{rr} r^2 + X_{vr} vr \\
(m - Y_{\dot{v}})\dot{v} + (mx_G - Y_{\dot{r}})\dot{r} + mur - z_G \cdot \dot{p} &= Y_v v + Y_r r + Y_{vv} v|v| + Y_{rr} r|r| + Y_{rv} r|v| + Y_{vr} v|r| \\
-(mx_G + N_{\dot{v}})\dot{v} + (I_{zz} - N_{\dot{r}})\dot{r} + mx_G ur - (I_{zx} \cdot \dot{p} + I_{yx} \cdot p^2 + I_{yz} \cdot p \cdot r) &= \\
N_v v + N_r r + N_{vv} v^2 + N_{rr} r^2 + N_{rv} rv + N_{vr} vr &
\end{aligned} \tag{24}$$

An additional equation of motion is introduced, which is defined in equation 25 [42].

$$(I_{xx} \cdot \dot{p} - I_{xz} \cdot \dot{r}) + (I_{yx} \cdot p \cdot r + I_{yz} \cdot r^2) - m \cdot z_G \cdot (\dot{v} + u \cdot r) = K_{HD} - \Delta \cdot GZ_0(\varphi) \tag{25}$$

The inclusion of the roll motion means that the restoring moment due to buoyancy and gravity must me included, which may be expressed as $\Delta \cdot GZ_0(\varphi)$. I_{yx} and I_{yz} are assumed to be zero for bodies being symmetric in the xz-plane [14]. This reduces equations 24 and 25 to the following final equations of motion:

$$
\begin{aligned}
(m - X_{\dot{u}})\dot{u} - (v - x_G r)mr + z_G \cdot p \cdot r &= X_u u + X_v v + X_{uu} u|u| + X_{vv} v^2 + X_{rr} r^2 + X_{vr} vr \\
(m - Y_{\dot{v}})\dot{v} + (mx_G - Y_{\dot{r}})\dot{r} + mur - z_G \cdot \dot{p} &= Y_v v + Y_r r + Y_{vv} v|v| + Y_{rr} r|r| + Y_{rv} r|v| \\
(mx_G - N_{\dot{v}})\dot{v} + (I_{zz} - N_{\dot{r}})\dot{r} + mx_G ur - I_{zx} \cdot \dot{p} &= N_v v + N_r r + N_{vv} v|v| + N_{rr} r|r| + N_{rv} r|v| \\
I_{xx} \cdot \dot{p} - I_{xz} \cdot \dot{r} - mz_G(\dot{v} + u \cdot r) &= K_{HD} - \Delta \cdot GZ_0(\varphi)
\end{aligned}
\tag{26}
$$

2.5.2 Formulation of hydrodynamic roll moment

As mentioned before the theory written in [42] will be the basis of the method used in this research. Therefore, this theory will be elaborated in this section. Note that this will not directly be used in the numerical method.

Just as the sway and yaw motions, the roll motion is assumed to be decoupled from the surge velocity. The first order Taylor expansion for the roll motion is as follows:

$$K_{HD} = K_{\dot{p}}\dot{p} + K_p p + K_{\dot{r}}\dot{r} + K_r r + K_{\dot{v}}\dot{v} + K_v v \tag{27}$$

As mentioned in the introduction of this section, the method to include the roll motion is based on the theory written in [42]. Here the total hydrodynamic roll moment is expressed as:

$$K_{HD} = K_M - a_{42} \cdot \dot{v} - a_{44} \cdot \dot{p} - a_{46} \cdot \dot{r} + K_D \tag{28}$$

In which K_M is similar to K_v, being the moment resulting from the force acting on the side of the tug, but corrected for the actual heeling angle. To calculate this force the strip theory in vertical direction is used. The strip theory may be expressed as done in equation 29.

$$K_v = \int_{-T}^{0} y_{3DOF}(u, v, \varphi) \cdot z dz \tag{29}$$

Here $y_{3DOF}(u, v, \varphi)$ is the side force per unit length in vertical direction when considering four degrees of freedom. So the tugs instantaneous draught is divided into horizontal slices each with height dz and the force acting on each slice is multiplied with their moment lever. Vertical variation of the force may be neglected, as described in [42].

K_D in equation 28 represents the damping term, being a function of the roll velocity only. It accounts for the linear, quadratic and cubic contributions of the damping. This term may be represented by K_p and a possible quadratic term K_{pp} as well. It should be noted that some roll damping is already included in K_v. Therefore the K_p is used for tuning purposes in [42].

From subsection 2.4.1 it can be concluded that a_{42}, a_{44} and a_{46} in equation 28 represent respectively $K_{\dot{v}}, K_{\dot{p}}$ and $K_{\dot{r}}$. So the only missing term in equation 28 seems to be the coupled yaw-roll damping, expressed as K_r. In section 3.9 this roll damping contribution will be evaluated. Besides it will be explained how the contributions can be obtained an whether all force contributions in equation 27 should be considered.

3

Numerical method

In this chapter it is explained how the manoeuvring model is numerically implemented. In chapter 1 it is already mentioned that DAMEN has developed a simulation tool able to evaluate the performance of an escort tug, named TugSim. This tool is a quasi-static tool which should preferably be translated into a dynamic model which could be used to determine the limits of safety during escort operations. Some parts of the manoeuvring model are partly copied from the existing TugSim tool and adapted if required. The development of those parts in the simulation tool does not fall within the scope of this research, hence those parts may be seen as "black boxes". Those "black boxes" are illustrated in the integration scheme provided in figure 3.1.

The output parameters from the black boxes are not directly suitable to use in a time domain simulation, some additional calculations should be made to include the dynamics of the tug. Those additional calculations and the principles of the methods applied in the black boxes are described in this chapter.
As mentioned in the introduction written in chapter 1, the focus of this research will be on the derivation of the hydrodynamic forces. This derivation has been elaborated in sections 3.4, 3.5 and 3.9. Here the first two sections consider only three degrees of freedom. The addition of the fourth degree of freedom, namely the roll motion, is elaborated in section 3.9. In table 3.1 an overview of the methods used to derive of each hydrodynamic force contribution is provided. Besides, an indication of the uncertainty level is included. In the corresponding sections it is explained how these uncertainty levels are established.

Table 3.1: Overview of applied methods including indication of uncertainty level

Method	**Level of uncertainty**	**Obtained hydrodynamic force contributions**
TugSim	Low	$X_u, X_{uu}, Y_v, Y_{vv}, K_v, N_v, N_{vv}$
Semi-empirical	High	$X_{rv}, X_{rr}, Y_r, Y_{rr}$, Y_{rv},N_r, N_{rr}, N_{rv}
Free decay tests	Low	K_p
Ikeda	High	K_p
Potential flow method	Moderate	$X_{\dot{u}}, Y_{\dot{v}}, Y_{\dot{r}}, N_{\dot{v}}, N_{\dot{r}}$

The outline of this chapter follows the steps to be taken to obtain the dynamic behaviour of the tug, in the same order as illustrated in figure 3.1. All steps are listed in table 3.2 together with their in- and outputs and the corresponding section.

Table 3.2: Overview of calculation steps and corresponding in- and output parameters

Step	**Input**	**Output**	**Section(s)**
Velocities and orientation	$\dot{u}, \dot{v}, \dot{p}, \dot{r}$, X, Y, φ, Ψ u, v, p, r	X, Y, φ, Ψ u, v, p, r	3.1
Drift angle calculation	u, v, Ψ, U_0	β, v_a	3.2
Centripetal and Centrifugal forces	u, v, p, r	X, Y, K, N	3.3
Hydrodynamic forces	$\beta, \varphi, \sigma, v_a$	X, Y, K, N	3.4, 3.5, 3.9
Towline force	X, Y, φ, Ψ	X, Y, K, N	3.6
Propulsion force	Thrust Percentage, $\varphi, \sigma, v_a, \beta$	X, Y, K, N	3.7
Accelerations	$\sum X, \sum Y, \sum K, \sum N$, Added mass coefficients	$\dot{u}, \dot{v}, \dot{p}, \dot{r}$	3.8

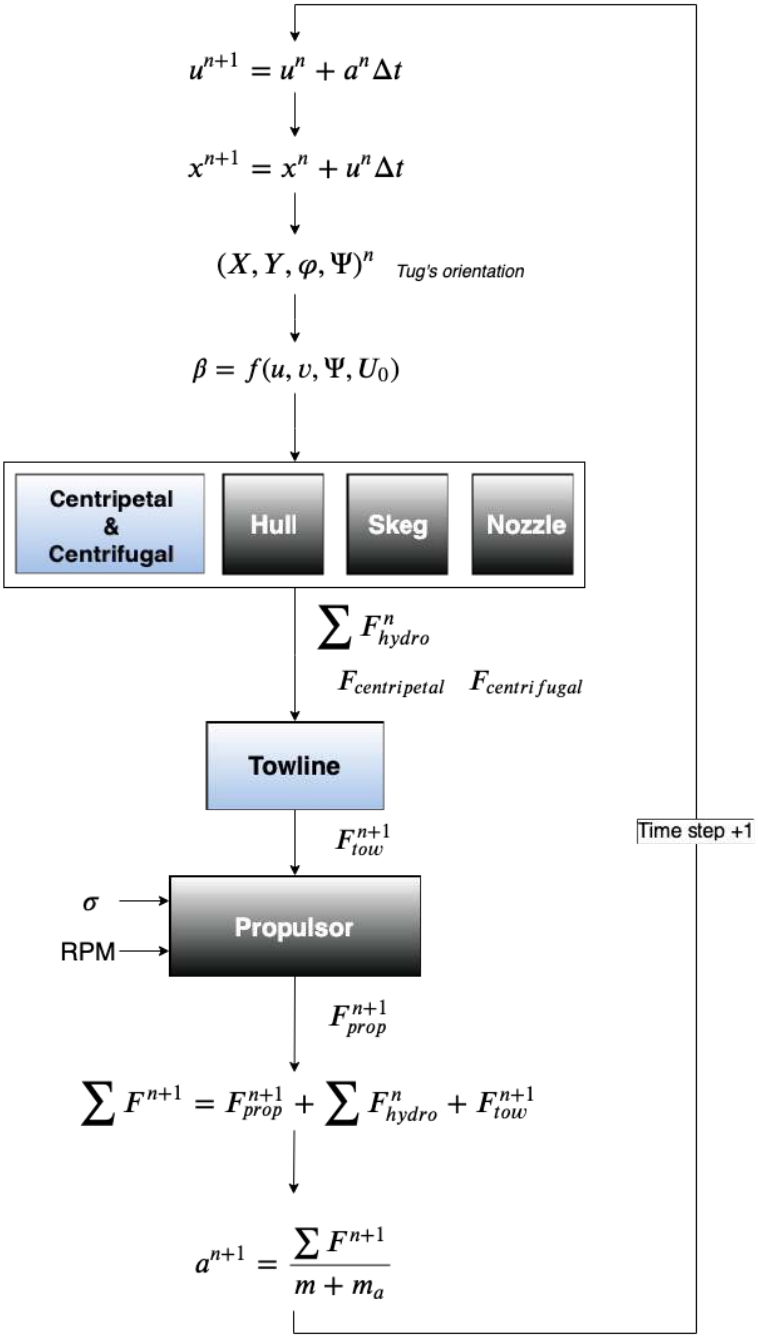

Figure 3.1: Forward Euler integration scheme

3.1 Velocities and orientation

As can be seen in equation 26 the motion equations are first-order differential equations. To solve those differential equations numerically a Forward Euler integration scheme can be used, as illustrated in figure 3.1.

In subsection 2.1 the used frames of reference has been elaborated. Due to the use of a reference frame fixed to the assisted vessel, instead of an earth-fixed reference frame, distinction should be made between the relative velocity and the actual velocity of the vessel. The actual velocity will be used to calculate the hydrodynamic forces acting on the vessel and the relative velocity is used to calculate the position with respect to the assisted vessel. The latter is required to obtain the towline force (section 3.6).

The actual velocity may be considered as the inflow velocity facing the vessel and is formulated as follows:

$$v_a = v_s - v_Q \tag{30}$$

Where:
$v_a =$ the inflow velocity facing the vessel
$v_s =$ the ship velocity relative to the assisted vessel
$v_Q =$ the velocity of reference frame $Q(U, V, Z)$, i.e. the velocity of the assisted vessel

When assuming that the inflow velocity v_a is uniform and irrotational, equation 30 can be written in vector form as follows:

$$\vec{v_a} = \vec{v_s} - \vec{v_Q} + = \begin{pmatrix} u_s \\ v_s \end{pmatrix} - \begin{pmatrix} -U_0 \cdot cos(\Psi) \\ U_0 \cdot sin(\Psi) \end{pmatrix} = \begin{pmatrix} u_s + U_0 \cdot cos(\Psi) \\ v_s - U_0 \cdot sin(\Psi) \end{pmatrix}$$

In the integration scheme the velocity components (u_s, v_s, p, r) and accelerations $(\dot{u_s}, \dot{v_s}, \dot{p}, \dot{r})$ are defined in the body fixed frame. Those properties are used to calculate the tugs position defined in reference frame Q. The global position (X_Q, Y_Q) together with the heading angle (Ψ) and the heeling angle (φ) define the tugs orientation. The orientation is obtained as follows:

$$\begin{aligned} X_O^{n+1} &= X_O^n + \Delta t(u_s \cdot cos(\Psi) - v_s \cdot sin(\Psi)) \\ Y_O^{n+1} &= Y_O^n + \Delta t(u_s \cdot cos(\Psi) + v_s \cdot cos(\Psi)) \\ \Psi^{n+1} &= \Psi^n + \Delta t \cdot r \\ \varphi^{n+1} &= \varphi^n + \Delta t \cdot p \end{aligned} \tag{31}$$

3.2 Drift angle calculation

After the displacements in the considered degrees of freedom and the tug's orientation are calculated, the drift angle 'β' can be obtained. The calculation of the drift angle is essential as the hydrodynamic forces, as well as the propulsion forces, are strongly dependent on it. The way this drift angle is calculated in a dynamic manoeuvring model differs from the method used in the quasi-static TugSim. Note that for a tug in escort operations the forward velocity of the assisted ship may be seen as a current with a velocity equal, but opposite, to the velocity of the assisted vessel (U_0). In the quasi-static TugSim it is assumed that the tugs velocity component in the direction of the forward displacement of the assisted vessel, so in the global x-direction, is always equal to U_0. Which implies that the inflow velocity v_a equals U_0 and that β is always the angle between the local and global x-axis (Ψ).
A manoeuvring model enables to analyse the dynamic behaviour of a tug before a steady state is reached, preferably without restrictions of velocity components. This means that v_a does not have to be equal to U_0. In figure 3.2 the differences between the situations are indicated. In figure 3.2a the definition used in TugSim is illustrated and in figure 3.2b the situation in the manoeuvring model can be seen. Notice that the heading angle Ψ now differs from β, that v_a is not directed in parallel to the global x-axis and that the magnitude of v_a does not necessarily equal U_0. In figure 3.2c the vector summation is provided.

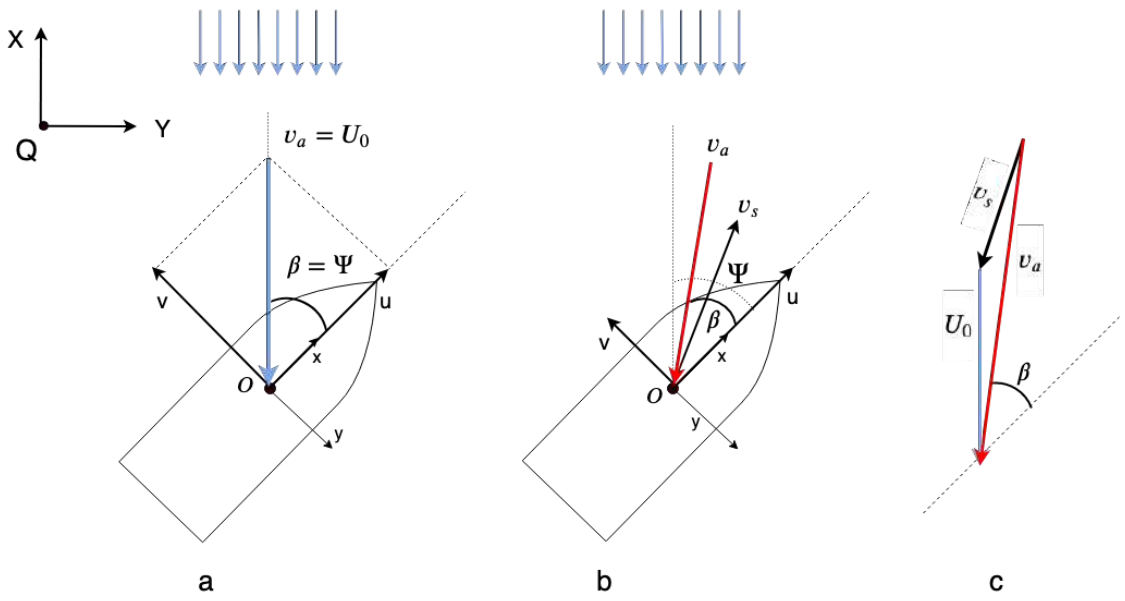

Figure 3.2: Illustration of the drift angle

From figure 3.2 it can be concluded that the drift angle β can be derived using the decomposition of velocity vectors $\vec{v_s}$ and $\vec{v_Q}$, of which the letter is represented by U_0 in figure 3.2.
Besides the magnitude of β, the direction is important as well, this is illustrated in figure 3.3. Here two vectors representing the inflow velocity are illustrated both with, in absolute sense, the same angle with respect to the local x-axis. However the direction of the angle determines the direction of the force acting on the hull, for this reason the so-called "quadrant" of the angle should be considered as well. This may be done using the four-quadrant inverse tangent function.

The four-quadrant inverse tangent is defined as follows:

$$atan2(b,a) = \begin{cases} arctan(\frac{b}{a}) & \text{if} \quad a > 0 \\ arctan(\frac{b}{a}) + \pi & \text{if} \quad a < 0 \quad \text{and} \quad b \geq 0 \\ arctan(\frac{b}{a}) - \pi & \text{if} \quad a < 0 \quad \text{and} \quad b < 0 \\ +\frac{\pi}{2} & \text{if} \quad a = 0 \quad \text{and} \quad b > 0 \\ -\frac{\pi}{2} & \text{if} \quad a = 0 \quad \text{and} \quad b < 0 \\ \text{undefined} & \text{if} \quad a = 0 \quad \text{and} \quad b = 0 \end{cases}$$

Where a and b are the coordinates of the coordinates of the end-point of vector v_a expressed in the local coordinates system. To conclude, the drift angle between the local x-axis and the inflow velocity can be defined as follows:

$$\beta = atan2(b,a) \tag{32}$$

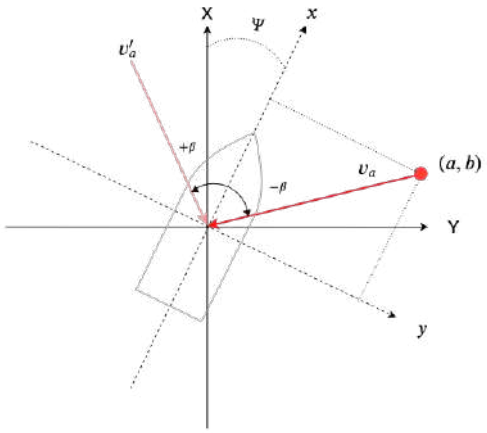

Figure 3.3: Illustration of the importance of the drift angle's quadrant

3.3 Centripetal and Centrifugal forces

If the centre tug is rotating around reference frame $Q(U,V,Z)$, it will experience centripetal and centrifugal forces. They can be calculated using the following set of equations:

$$\begin{aligned} X_{centripetal} + X_{centrifugal} &= m \cdot r \cdot (v + x_G \cdot r) - z_G \cdot p \cdot r \\ Y_{centripetal} + Y_{centrifugal} &= -m \cdot u \cdot r \\ K_{centrifugal} + K_{centrifugal} &= m \cdot z_G \cdot u \cdot r \\ N_{centrifugal} + N_{centrifugal} &= -m \cdot x_G \cdot u \cdot r \end{aligned} \tag{33}$$

In equation 1 those forces are included in $\vec{C}$.

3.4 Steady state forces

Free sailing tugs as well as tugs performing an escort operation, will once reach a static equilibrium. For tugs in escort operations, static equilibrium is obtained whenever the tug does not move in any direction relative to the assisted vessel. The forces acting on the vessel being in static equilibrium, i.e. being in steady state, are referred as the steady state forces. Distinction has been made between the steady state forces and the dynamic forces. The latter concern the forces acting on the tug before steady state is reached, those will later on be elaborated in section 3.5.

In DAMEN TugSim a method to find all static equilibria has been developed. TugSim uses multiple simplified methods, such as the low aspect ratio wing theory and many correction terms, to capture the captive model test results. The calculations are well validated for the Damen RSD 2513 at a speed of 8 knots (section 4.2), however a certain level of uncertainty should be considered due to the complexity of flow around the tugs [48].
Direct implementation of the captive model test results would be more accurate, but is not desired. Those results will only be valid for one specific speed and one design. TugSim is developed being a general applicable performance prediction tool, in which the total hydrodynamic force is a summation of the forces acting on several components. Following this method, the forces acting on multiple combinations of different skeg, nozzle and hull designs can be calculated.

In equation 34 the hydrodynamic forces, in terms of hydrodynamic derivatives, which may be calculated using DAMEN TugSim are marked in blue.

$$\begin{aligned} X_{HD} &= X_{\dot{u}}\dot{u} + X_u + X_v v + X_{uu}u|u| + X_{vv}v|v| + X_{vr}vr + X_{rr}r^2 \\ Y_{HD} &= Y_{\dot{v}}\dot{v} + Y_{\dot{r}}\dot{r} + Y_v v + Y_r r + Y_{vv}v|v| + Y_{rr}r|r| + Y_{vr}v|r| \\ N_{HD} &= N_{\dot{r}}\dot{r} + N_{\dot{v}}\dot{v} + N_v v + N_r r + N_{vv}v|v| + N_{rr}r|r| + N_{vr}v|r| \end{aligned} \tag{34}$$

Even though the tug does not move relative to the assisted vessel, it faces an non-zero incoming flow velocity, as explained in section 3.2. This incoming flow results in hydrodynamic forces acting on tug. The tug is divided in different components, namely: the hull, skegs and nozzles. For each component it is described how the hydrodynamic forces, while being in steady state, can be calculated.

3.4.1 Hull forces

The hull forces are one of the forces of which the calculation method is partly copied from TugSim. Although no full explanation will be provided, it should be noticed which principles are used and which hydrodynamic force components, as listed in section 2.4, are taken into account.

The hydrodynamic forces and moments are a function of the lift and drag, which are calculated using non-dimensional lift and drag coefficients:

$$Lift = C_L \cdot \frac{1}{2}\rho A_{lateral} v_a^2, \quad Drag = C_D \frac{1}{2}\rho A_{lateral} v_a^2 \tag{35}$$

Those lift and drag coefficients are summations of linear and non-linear contributions, all representing one of the hydrodynamic phenomena described in 2.4. The dimensionless lift coefficient for a bare hull is defined as follows:

$$C_L = C_{L,linear} + C_{L,nonlinear} \tag{36}$$

Here the linear lift coefficient represents the contribution of the linear circulation around the hull, based on the low aspect ratio wing theory as described in [41] and subsection 2.4.2 of this report. The non linear coefficient represents the cross flow drag, which is based on experimental results. In figure 3.4a both contributions are given as a function of the drift angle 'β'.

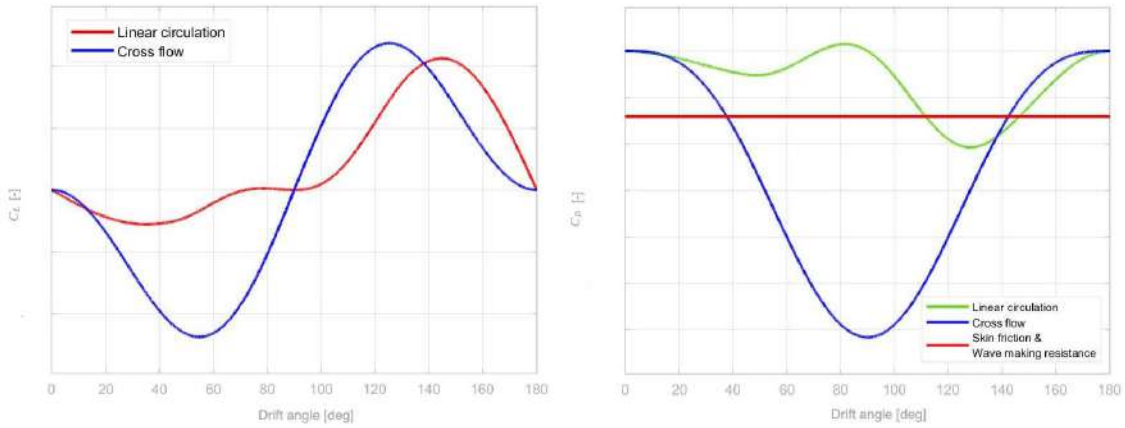

(a) C_L as a function of the drift angle

(b) C_D as a function of the drift angle

Figure 3.4: Lift and drag for a bare hull

The non-dimensional drag coefficient for a bare hull is defined as follows:

$$C_D = C_{D,linear} + C_{D,nonlinear} + C_{D0} \tag{37}$$

Just as for the lift coefficient, $C_{D,linear}$ and $C_{D,nonlinear}$ represent the contributions of the linear circulation and the cross flow drag respectively. C_{D0} is taken into account to contribute for the skin friction and the wave making resistance of the hull, it is defined as follows:

$$C_{D0} = \frac{R_T}{\frac{1}{2}\rho A_{lateral} v_a^2} \tag{38}$$

R_T is the total resistance of the vessel which is obtained using model tests and the scaling procedure described in [22]. In figure 3.4b the relative contributions of those hydrodynamic force contributions can be seen.

As mentioned before, the forces and moments acting on the bare hull are a function of the lift and drag coefficients, they can be expressed as follows:

$$\begin{aligned} F_X &= -Drag \cdot cos(\beta) + Lift \cdot sin(\beta) \\ F_Y &= Lift \cdot cos(\beta) + Drag \cdot sin(\beta) \\ M_X &= y_a \cdot F_Z - z_a \cdot F_Y \\ M_Z &= x_a \cdot F_Y \end{aligned} \tag{39}$$

In which x_a, y_a and z_a represent the distances from the origin of the local axis system to the point of attachment of the hydrodynamic forces. The longitudinal distance, x_a is derived using the manoeuvring theory described in [21]. x_a Is namely proportional to the ratio between the hydrodynamic derivatives N_v and Y_v.

3.4.2 Skeg forces

Just as for the calculation of the hydrodynamic forces acting on the hull, non dimensional lift and drag coefficients will be used to calculate the forces acting on the skegs. The lift and drag coefficients are defined in the same way as those for the hull (equations 36 and 37). Where the linear parts represent the contribution of the linear circulation, now derived using a wing theory valid for high aspect ratios as described in [12]. Here the generated lift and drag is dependent on the stall angle, defined as the drift angle at which the flow separation point is no longer the trailing edge of the profile anymore. This depends on the section profile of the skeg. In figure 3.5 the contributions to the lift and drag coefficients of a skeg can be seen. The black dotted line indicates the stall angle. The non linear contribution again represents the cross flow drag term and, like in equation 37, a factor C_{D0} is added to contribute for the frictional drag of the skegs.

The transverse and vertical distances between the origin of the local coordinate system and the point of attachment of skeg forces (y_a,z_a) are assumed to be constant. The longitudinal distance, x_a, shifts between 10% and 25% of the skegs length depending on the stall angle and the angle of attack of the skeg. A representative formulation of this distance is based on the results of captive model tests with different skegs.

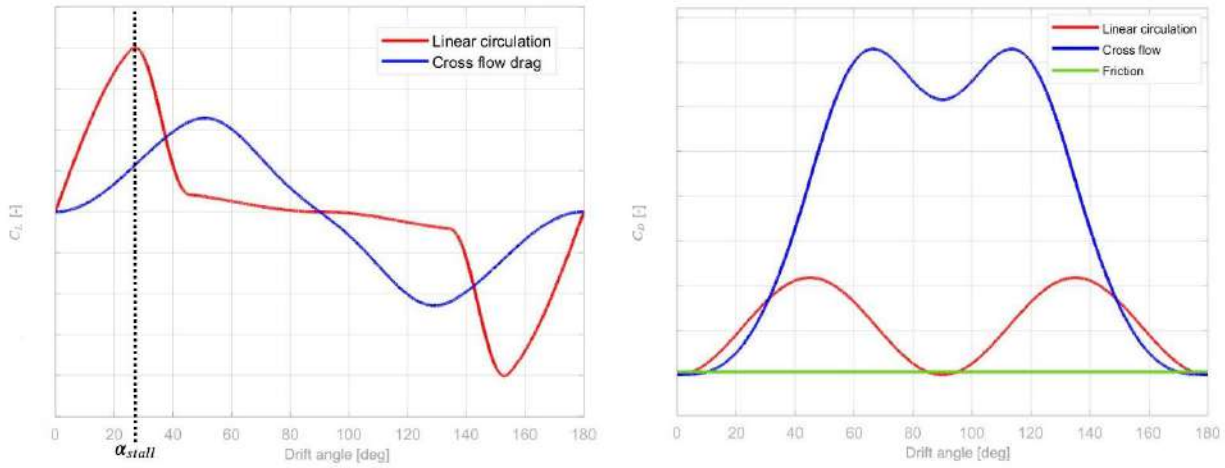

(a) C_L as a function of the drift angle

(b) C_D as a function of the drift angle

Figure 3.5: Lift and drag for skeg

3.4.3 Nozzle forces

The calculation of the nozzle force is based on the theory written by Whicker and Fehlner in 1958 [15], which is intentionally developed for calculating rudder forces. However, in the simulation model the nozzle is represented by a rudder with the same lateral area as the nozzle.

This theory claims that it includes, in addition to the linear lift and drag components, also a cross-flow drag component. However in the applied method those components are not decomposed explicitly. The method does not consider a frictional drag component, in contrast to the method applied to calculate the hull and skeg forces. It assumes that the frictional drag component is small compared to the cross-flow drag and the drag as a result of linear circulation. This may be confirmed by figure 3.5b.

Another disadvantage of the method is that it is only valid before stall. To be able to calculate the lift and drag after stall as well, the following assumptions are made:

After stall, the lift coefficient starts to decrease smoothly to zero and reaches it whenever the drift angle is 90°. The drag coefficient on the other hand starts to flatten its increase after stall and reaches its maximum whenever the drift angle is 90°. The calculated stall angle is a function of the effective aspect ratio of the nozzle. In figure 3.6 the lift and drag coefficients of the nozzle are illustrated.

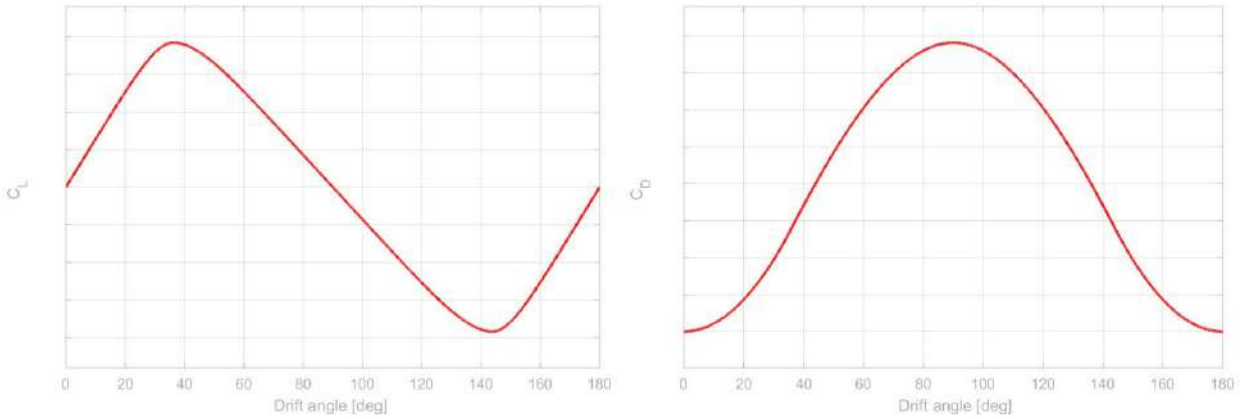

(a) C_L as a function of the drift angle

(b) C_D as a function of the drift angle

Figure 3.6: Lift and drag for a nozzle

The point of attachment of hydrodynamic force is assumed to collapse with the centre of gravity of the nozzle.

3.5 Dynamic forces

In section 3.4 the principals of the method used in DAMEN TugSim, to derive the steady state forces, are provided. Those forces are a function of the inflow velocity v_a and the drift angle β, which makes the method also suitable for calculating the x- and y-forces for variable surge and sway velocities. However in this method some essential terms, required to simulate the manoeuvring behaviour over time, are excluded. When referring to equation 34, it can be seen that terms coherent with the yaw velocity are excluded. Besides, the terms coherent with the accelerations are excluded, the derivation of the second group of terms is described in section 3.8. In this section it is explained why the terms coherent with the yaw velocity should be considered and how these can be derived.

3.5.1 Linear damping terms

In [14] the terms Y_r and N_r are referred as linear damping coefficients. Besides Y_v and N_v, those terms have a significant influence on the manoeuvring behaviour of the vessel. This has been illustrated in figure 3.7.
In figure 3.7a a vessel is illustrated which is moving in the negative y-direction. Besides a large force in the positive y-direction, it causes a moment around the z-axis. The asymmetry in the pressure distribution results in a differences between the moment generated by the y-force acting on the bow ($N_{v,bow}$) and the moment generated by the y-force at the stern ($N_{v,stern}$). The resulting moment is the sum of both moments. Because the directions of both moments are opposite, they partly compensate each other.
The same principal yields for the moment due to a yaw velocity (N_r). Here the total moment may again be seen as a summation of N_{bow} and N_{stern}. However, as illustrated in figure 3.7b, both moments act in the same direction and so they will reinforce each other. This contribution to the total moment around the z-axis counteracts the yaw motion generated by for example the propulsion force, whenever this contribution is assumed to be zero, the vessel will not stop rotating around it's own z-axis. This having said, it can be concluded that an expression for this yaw damping contribution should be included to make the method described in the previous sections suitable for simulating escorting tugs. According to figure 3.7 $Y_{r,bow}$ and $Y_{r,stern}$ counteract each other, what makes the total Y_r contribution smaller than Y_v. Nevertheless, it should be included in the calculation to make sure the forces are as accurate as possible.

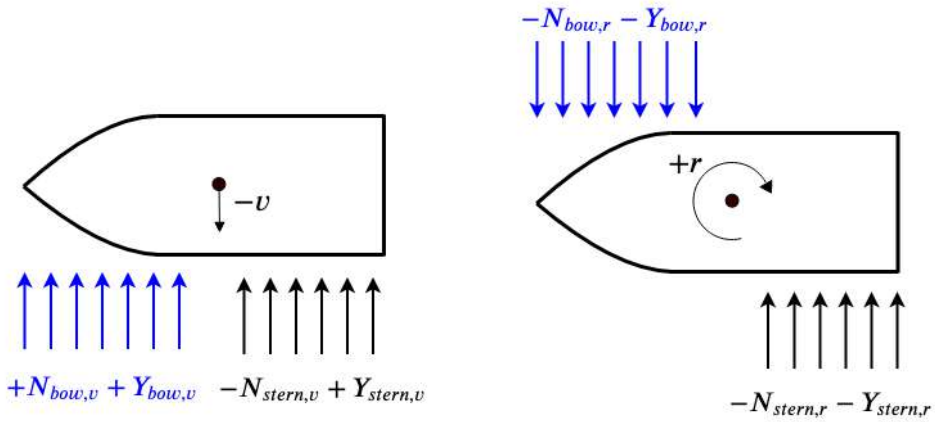

(a) N_v and Y_v

(b) N_r and Y_r

Figure 3.7: Illustration of yaw damping contributions

As those terms could not be calculated using the method described in section 3.4, an alternative method should be found. For those lacking hydrodynamic contributions (Y_r, N_r) an initial estimation can be made using one of the existing semi-empirical methods as described in subsection 2.3.1. For this purpose it is chosen to use the hydrodynamic derivatives provided in [4] as those terms are based on data retrieved from multiple twin screw vessels and the method is claimed to be valid for large drift angles. The dimensionless linear hydrodynamic derivatives are formulated as follows:

$$\begin{aligned} Y'_r &= 0.54 C_b p_{mx} + 0.25 C_b p_{my} \\ N'_r &= -0.25\pi p_{mx} - 0.175 C_b p_{my} \end{aligned} \tag{40}$$

In which:

$$\begin{aligned} p_{mx} &= \left(\frac{T}{L}\right)^2 \left(1 + 0.5 C_b \frac{T}{B}\right) \\ p_{my} &= \frac{BT}{L} \end{aligned}$$

The terms are made non-dimensional as presented in appendix A.

3.5.2 Cross-flow drag coefficients

In subsection 2.4.2 it is mentioned that the cross-flow drag may be seen as a non-linear damping contribution. This damping due to cross-flow drag is even dominating at higher speeds, where the linear damping tends to zero [14]. To prevent the simulated vessel from oscillating around its own z-axis at higher speeds and to improve the prediction of the hydrodynamic forces, the cross-flow drag should be considered as well.
This non-linear damping contribution could be expressed in terms of hydrodynamic derivatives as well, this can be done using the terms as marked in blue in the following equation:

$$\begin{aligned} Y_{HD} &= Y_{\dot{v}}\dot{v} + Y_{\dot{r}}\dot{r} + Y_v v + Y_r r + Y_{vv} v|v| + Y_{rr} r|r| + Y_{vr} v|r| \\ N_{HD} &= N_{\dot{r}}\dot{r} + N_{\dot{v}}\dot{v} + N_v v + N_r r + N_{vv} v|v| + N_{rr} r|r| + N_{vr} v|r| \end{aligned}$$

In equation 34 the terms which could be calculated using the method described in section 3.4 are also marked in blue, this includes hydrodynamic derivatives $Y_{vv}v|v|$ and $N_{vv}v|v|$. Those force contributions can be calculated using TugSim as well, so they should not necessarily be considered as "dynamic forces". As the calculated total steady state forces, including $Y_{vv}v|v|$ and $N_{vv}v|v|$, are well validated for Damen tugs (section 4.2) it is chosen to use the method described in 3.4 to calculate this non-linear contributions.

To account for the remaining non-linear force contributions, expressed as Y_{vr}, Y_{rr}, N_{rr} and N_{vr}, the semi-empirical method described in [4] will be applied. Those contributions can be calculated using the following expressions:

$$\begin{aligned} Y'_{rr} &= 0.25 N_{vv} \\ N'_{rr} &= -0.02 \cdot CD \frac{T}{2.5L} \\ Y'_{vr} &= 4 Y'_{rr} \\ N'_{vr} &= -\Big(0.1 + 0.03\Big(1.5 - C_b \frac{B}{T}\Big)\Big) \cdot \frac{T}{L} \end{aligned} \tag{41}$$

In which:

$$\begin{aligned} N'_{vv} &= -0.75 N_v \\ N'_v &= -0.25\pi p_{mx} - 0.41 p_{my} \\ CD &= 1.1 + 0.0045\frac{L}{T} - 0.1\frac{B}{T} + 0.016\Big(\frac{B}{T}\Big)^2 \end{aligned}$$

The terms are made non-dimensional as provided in appendix A as well.

3.5.3 Lift induced drag coefficients

In section 2.2.3 the second order lift induced drag coefficients are introduced. In appendix B the derivation of these hydrodynamic derivatives is provided, which results in the following expressions:

$$\begin{aligned} X_{vv} &= -\frac{Y_v^2}{0.5\rho U^2 \pi T} \\ X_{vr} &= -\frac{2 Y_v Y_r}{0.5\rho U^2 \pi T} \\ X_{rr} &= -\frac{Y_r^2}{0.5\rho U^2 \pi T} \end{aligned} \tag{42}$$

Whether those terms should be included in the simulation model for tugs in escort operations, will be evaluated in subsection 4.3.1.

3.5.4 Discussion

Previously developed semi-empirical manoeuvring models are generally developed for relatively large merchant ships and so is the method provided in [4]. The geometry of tugs differs significantly from these of merchant ships, which may lead to different contributions of i.a. cross-flow drag. Besides, the presence of appendages such as skegs and nozzles, may influence the hydrodynamic force contributions derived from semi-empirical models as well. In this discussion it is elaborated whether an in- or decrease of the hydrodynamic force contributions derived with [4] is expected when the method will be applied to tugs.

The linear moment N_r is expected to be higher for tugs compared to common merchant ships, particularly due to the presence of the skegs which generate additional lift. In figure 3.8 the Y_v term obtained using the method described in section 3.4 is given as a function of the drift angle, together with Y_v obtained from [4]. Distinction is made between the Y_v with and without skegs attached to the bare hull. It can be seen that whenever no skegs are attached, Ankudinov's approximation of $Y_v v + Y_{vv} v|v|$ is in good agreement with this obtained with the TugSim method, especially at smaller drift angles. However, when skegs are attached, the forces differ significantly.

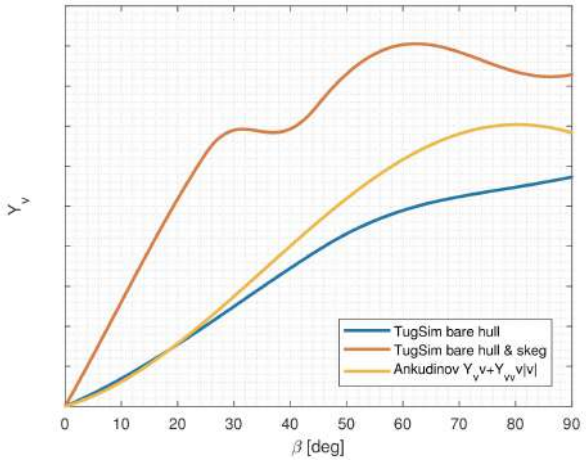

Figure 3.8: Comparison of Y_v terms obtained with TugSim calculations and semi-empirical method [4]

The differences in Y_v explain why a larger N_r is expected as well. Using figure 3.7, it can be concluded that an increase of $N_{bow,r}$ due to the presence of large skegs, results in a higher total N_r.
Due to the presence of skegs, Y_r is expected to be smaller or even opposite to the Y_r derived from [4]. Ankudinov's expression for $Y_r r$ is per definition positive if the yaw velocity is positive, which means that $Y_{r,stern}$ is always larger than $Y_{r,bow}$ (figure 3.7b). However, with the presence of large skegs this definition may be invalid. Figure 3.9a shows the side view of the tug being the validation case of this research (section 4.1). Besides, in figure 3.9b the velocity profile along a tug during a pure yaw motion is given, it shows that the part of the vessel having the largest distance to the centre of rotation faces the highest flow velocity. The force acting on the side of the vessel increases with the so called inflow velocity and the lateral area. As the skegs, having a large lateral area, are located relatively far ahead of the centre of rotation they could have a significant contribution to Y_r. This contribution will be opposite to the direction of rotation and may cause the total contribution to be significantly smaller as, or even opposite to, the original Y_r derived from [4].

(a) Visualisation of RSD 2513

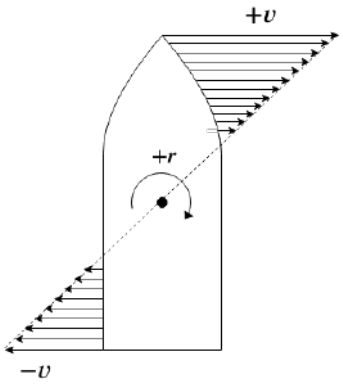

(b) Illustration of velocity profile during pure yaw motion

Figure 3.9: RSD 2513 side view and expected velocity profile

The same reasoning could be used for the cross-flow drag terms. The bow contribution of Y_{rr} and Y_{vr} are expected to be higher for tugs, just as N_{rr} and N_{vr}. Besides the presence of appendages brings multiple sharp edges and free ends, which cause additional viscous shedding. As illustrated in figure 2.10 trailing vortices appear along free ends, this loss of energy can be translated into additional non-linear damping.

To find out the ratio between the terms obtained with the method described in [4] and the terms valid for tugs sailing under large drift angles, they will be tuned using experimental data in section 4.3.1. Afterwards, the sensitivity of those terms will be analysed in chapter 5. In advance, it can stated that a relatively high level of uncertainty is expected when applying this method. The complex geometry, due to i.a. the presence of skegs, results in a complex flow pattern around the hull and appendages. This complexity is illustrated in [48]. To capture the pure and coupled yaw damping terms more accurately, additional experiments and research are required.

3.6 Towline force

After the hydrodynamic forces acting on the different components of the vessel are calculated, the towline force can be calculated. The towline force is dependent on the orientation of the vessel and the characteristics of the towline itself.

A commonly used way to predict the strain in an elastic towline is as follows [42]:

$$S_{tow}(L) = \begin{cases} 0 & \text{if} \quad L < l_0 \\ k \cdot (\frac{L-l_0}{l_0})^2 \cdot BL & \text{if} \quad L > l_0 \end{cases}$$

Here l_0 and L represent respectively the length of the unstretched towline and the distance between Q and P, as illustrated in figure 3.10. The towline characteristics k_{tow} and BL, representing the stiffness and breaking load respectively, are obtained from product information provided by towline manufacturer Bridon.

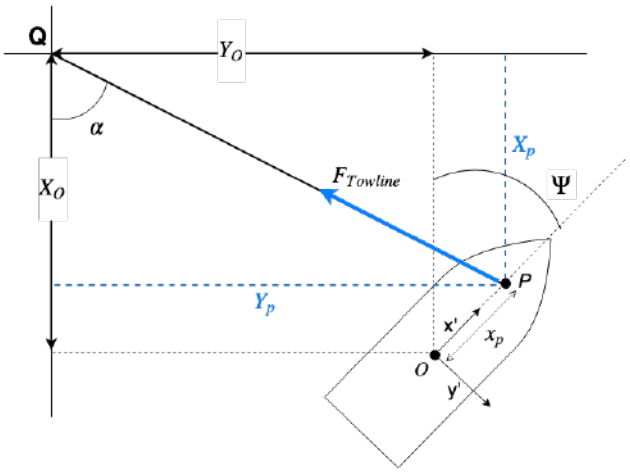

Figure 3.10: Illustration of position towing point

The position of the towing point in the global system depends on the position of the local coordinate system and the distance between its origin and the towing point of the vessel. To obtain the location of the towing point some corrections should be made, those are provided in equation 43.

$$\begin{aligned} X_p(\varphi, \beta) &= X_O + cos(\beta) \cdot x_p - sin(\varphi) \cdot z_p \cdot sin(\beta) \\ Y_p(\varphi, \beta) &= Y_O + sin(\beta) \cdot x_p + sin(\varphi) \cdot z_p \cdot cos(\beta) \\ \Delta z(\varphi) &= \Delta Z_O + |sin(\varphi) \cdot z_p \cdot tan(\varphi)| \end{aligned} \tag{43}$$

Here X_O and Y_O represent the location of point O and ΔZ_O is the initial vertical distance between the towing point and the point of attachment on the assisted ship. Vector (x_p, y_p, z_p) represents the location of the towing point relative to the body fixed frame.

3.7 Propulsion force

A change in thrust disturbs the obtained equilibrium and causes accelerations. The amount of thrust is depending on the steering angle (σ), the engine load percentage, the facing flow velocity (v_a) and the drift angle (β). In figure 3.11 a block diagram of the propulsion model is provided to illustrate the steps to be taken.

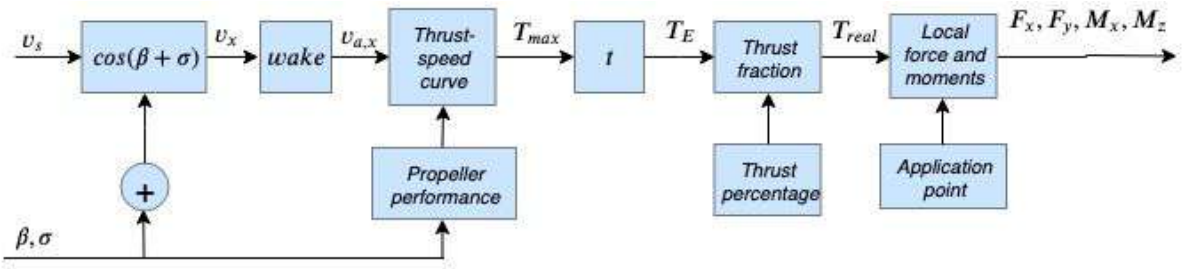

Figure 3.11: Propeller model block diagram [40]

As can be seen in the block model, a thrust-speed curve is used to obtain the thrust. This curve is given as an input and obtained using an external program named 'Propeller Performance'. This program is able to calculate the thrust based on the propeller, gearbox and engine characteristics. This thrust is corrected by a thrust deduction factor and a thrust percentage given as an input. Using the location of the thrusters expressed in the local coordinate systems, the local forces and moments can be calculated.

3.8 Determination of accelerations

The last step illustrated in figure 3.1 is to obtain the accelerations using Newtons second law. Which states that the acceleration in each direction equals the sum of the forces in that direction divided by the mass. For floating objects the added mass should be added to the mass of the object, this is described in subsection 3.8.2.
Because the motions in the different degrees of freedom are coupled, the following system of equations is used to solve the accelerations:

$$\underline{\underline{A}} \cdot \vec{v} = \vec{F} \quad \longrightarrow \quad \vec{v} = \underline{\underline{A}}^{-1}\vec{F} \tag{44}$$

Where for a 4DOF system:

$$\underline{\underline{A}} = \begin{bmatrix} m + a_{11} & 0 & 0 & 0 \\ 0 & m + a_{22} & -z_G & mx_G + a_{26} \\ 0 & -mz_G + a_{42} & I_{xx} + a_{44} & -I_{xz} + a_{46} \\ 0 & mx_G + a_{62} & -I_{zx} + a_{64} & I_{zz} + a_{66} \end{bmatrix}$$

and $\vec{F}$ is a vector containing the total forces in every degree of freedom. Note that it is assumed that the surge motion is uncoupled. The derivation of the properties used in $\underline{\underline{A}}$ will be elaborated in the following subsections.

3.8.1 Moments of inertia

I_{zz}, I_{xx} and I_{xz} are the moments of inertia. I_{xz} is zero whenever the floating object has two planes of symmetry. When there is only one plane of symmetry this term is non-zero, but small and so often neglected. The moments of inertia are often expressed in terms of the radii of inertia, which can be estimated using the following expressions [26] :

$$k_{xx} = 0.30 \cdot B \text{ to } 0.40 \cdot B, \quad k_{zz} = 0.22 \cdot L \text{ to } 0.28 \cdot L \tag{45}$$

The moments of inertia could be calculated using the following expression:

$$I_{ii} = k_{ii}^2 \cdot \rho\nabla \tag{46}$$

Note that it is assumed that I_{yz} and I_{xy} are zero, this assumption has already been justified in subsection 2.5.2.

3.8.2 Added mass and added moments of inertia

When a ship accelerates or decelerates on water, quantities of surrounding water moving together with the hull and increase the systems inertia terms. This phenomena can be described using added mass and inertia coefficients.

Later on in this report (section 5) a sensitivity analysis is performed to quantify the effect of a change is those added mass and added inertia terms. However, an initial estimation of those terms should be made first.

In [30] different analytical ways to derive the added mass coefficients are provided, such as the method of "equivalent ellipsoid" and the "strip theory". The body geometry dependent added mass terms can also be calculated using potential flow theory, which is applied to obtain the added mass of the bare hull in this research. However the presence of skegs and nozzles increases several added mass terms. Those contributions can be estimated using the formula for the added mass of a rectangular plate for accelerations perpendicular to the plate:

$$a_f = \frac{\rho \pi A R_e c_f A_{lateral}}{4\sqrt{AR_e^2 + 1}} \tag{47}$$

The effective aspect ratio, AR_e, can be calculated as follows:

$$AR_e = \frac{2b_f}{c_f} \tag{48}$$

Where b_f and c_f are respectively the span and chord length the fin, representing the skeg or nozzle. Using equation 47, the additional added mass coefficients can be calculated as follows:

$$\begin{aligned} a_{22f} &= a_f \\ a_{24f} &= -a_{22f} \cdot z_a \\ a_{26f} &= a_{22f} \cdot x_a \\ a_{44f} &= a_f \cdot z_a^2 \\ a_{66f} &= a_{22f} \cdot x_a^2 \end{aligned} \tag{49}$$

In which x_a and z_a are the coordinates of the centre of gravity of the fin. Note that the additional added mass due to surge is neglected, as the appendages are thin. Accounting for the added mass using the method described above, is the same as the adding $X_{\dot{u}}\dot{u}, Y_{\dot{v}}\dot{v}$,etc to the total hydrodynamic forces as done in equation 24.

A combination of potential flow theory and a simplified strip theory based method is expected to have a moderate level of uncertainty. The potential flow theory itself is assumed to predict the added mass of the bare hull accurately [14]. However, addition of the appendages will result in an increasing impact of viscosity effects. Besides, the simplified strip method as described above gives a rough approximation of the additional added mass, without considering the coupling between the degrees of freedom, the impact of viscosity due to the exact geometry of the fins.

3.9 Translation of a 3DOF into a 4DOF system

As mentioned in the introduction of this report, most manoeuvring models include only three degrees of freedom: surge, sway and yaw. For tugs in escort operations the roll motion may play a significant roll as it operates often under large heeling angles. Just as for the considered three degrees of freedom, the roll moment contributions may be split into two groups. In subsection 3.9.1 the principals of deriving the steady state forces are provided. Thereafter, in subsection 3.9.2, some notes are made about the contribution of dynamic forces. As no expression in terms of hydrodynamic derivatives can be found in existing literature, the first-order Taylor expansion for the total hydrodynamic roll moment is used, this is provided in equation 27. Here it is indicated which terms are derived using the method used in TugSim, these are marked in blue.

$$K_{HD} = K_{\dot{p}}\dot{p} + K_p p + K_{\dot{r}}\dot{r} + K_r r + K_{\dot{v}}\dot{v} + K_v v$$

As $K_{\dot{p}}, K_{\dot{v}}$ and $K_{\dot{r}}$ could be derived using the method described in subsection 3.8.2, this section focuses on the remaining terms being K_v, K_p and K_r.

3.9.1 Steady state forces

In subsection 2.5.2 the theory written in [42], which describes a way to include the roll motion in a manoeuvring model, is elaborated. This forms the basis of the method applied in the simulation tool. In this theory the moment

caused by the side force (equation 29) is corrected for the actual the heeling angle, using a strip theory. However, the side force itself is not corrected for the heeling angle. In the simulation tool for tugs in escort operations, this side force will be corrected for the heeling angle, namely due to a change of the lateral area. According to equation 35 a change in lateral area results in a change in lift and drag. In figure 3.12 the change of the lateral area as a result of a heeling angle is illustrated.

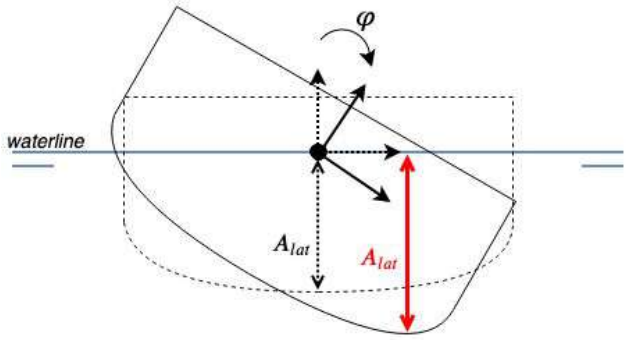

Figure 3.12: Differences between lateral area without heel (black) and with heel (red)

Besides a heeling angle, dynamic sinkage increases the lateral area as well. This effect is taken into account using an expression for the dynamic sinkage provided in [16].

So as given in equation 29 the roll moment is a result of the side force acting on the hull and appendages, however the resulting force acting in vertical direction (F_Z) contributes to the moment as well. An asymmetry in the pressure distribution on the hull, while sailing under a drift angle, is a result of the dynamic sinkage. In [48] a CFD analysis of the flow around the RSD 2513 tug, while sailing under a drift angle, is performed. In figure 3.13 some results of this study are given. It illustrates the asymmetry in the pressure distribution on the bottom of the bare hull for different drift angles. The results of this CFD analysis are used to find an expression of the roll moment contribution due to this asymmetry in pressure distribution, it turned out to have a significant contribution to K_v.

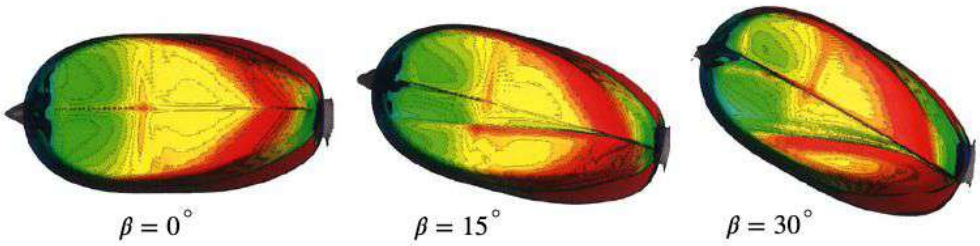

Figure 3.13: Illustration of the asymmetry in pressure distribution for the RSD 2513 sailing under a drift angle [48]

Even though in equation 27 K_{HD} seemed to be independent of the surge velocity, the force contribution due to the dynamic sinkage implies that there is a coupling between surge and the moment around the x-axis. The dynamic sinkage is namely a function of the Froude number, as written in [16].
So it can be concluded that in this research K_v is assumed to be a summation of the moment caused by the vertical force and the force acting in the y-direction, referred as K_Z and K_M respectively.

3.9.2 Dynamic forces

Since the dynamic force contributions K_p and K_r are not included in the method used in TugSim, the derivation and necessity of those terms will be elaborated in this subsection.

K_p represents the roll damping term, often referred as B_{44}. To account for this roll damping a suitable expression should be found. A free-decay test may offer solution. From the results of a free-decay test the total damping at the vessels natural frequency can be derived. However, a free decay test is performed at zero velocity while a non-zero velocity influences the roll damping [49] significantly. In [13] an overview of roll damping prediction methods for ships is provided. One of those methods contributing for the ships forward velocity, is the widely used method developed by Y. Ikeda in 1978. In this method the damping is split in several contributions and can be formulated as in equation 50. Here it is indicated which force contributions are dependent on the vessels forward velocity.

$$B_{44}(\omega, u) = B_{44W}(\omega, u) + B_{44L}(u) + B_{44F}(\omega) + B_{44E}(\omega, u) + B_{44APP}(u) \tag{50}$$

Where:

$$\begin{aligned} B_{44W} &= \text{Wave damping} \\ B_{44L} &= \text{Lift damping} \\ B_{44F} &= \text{Skin friction damping} \\ B_{44E} &= \text{Eddy damping} \\ B_{44APP} &= \text{Appendages contributions} \end{aligned}$$

When using a zero velocity free-decay test to obtain the roll damping, many of the damping terms given in equation 50 are already included implicitly. Those included terms are marked in blue. Some of those damping contributions, are dependent on the forward velocity as well. The absolute in- or decrease of the damping due to forward velocity cannot be approximated using a free-decay roll test, as it is impossible to decompose the damping terms. Nevertheless, the impact of the forward velocity may be quantified for each damping term.
Based on the literature written in [13], it can be concluded that B_{44E} significantly decreases with forward speed. Besides, B_{44L} could even become dominant at high forward speed. The increase of the bilge keel component, mostly included in B_{44APP}, and B_{44F} are relatively large. However, as the contribution to total roll damping of the latter two terms is small, the absolute changes due to forward velocity are often neglected. In figure 3.14 Ikeda's damping decomposition applied to a bare hull for two different roll amplitudes is illustrated [43]. It confirms that the linear damping becomes dominant at higher speeds and it illustrates the ratio's between the different damping contributions.

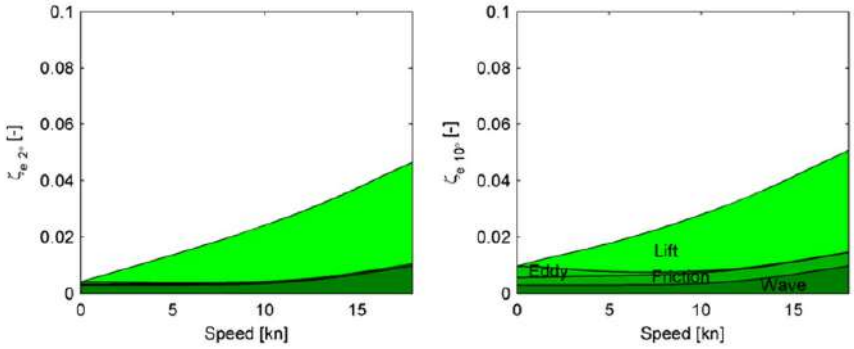

Figure 3.14: Damping decomposition according to method of Ikeda [43]

For this research it is decided to increase the roll damping by addition of $B_{44L}(u)$ and $B_{44APP}(u)$ only. Those additional lift-damping coefficients are calculated using a strip theory based on the method of Ikeda. In table 3.3 the calculated results concern the roll damping with forward velocity are provided.

Table 3.3: Roll damping contributions*

u [kn]	$B_{44PQ}(\omega_e)$ [Nms]	$B_{44L}(u)$ [Nms]	$B_{44APP}(u)$ [Nms]	$B_{44}(\omega_e, u)$ [Nms]
0	-	-	0	-
6	-	-	-	-
10	-	-	-	-

*The roll damping contributions are not public

Besides the dependency on the forward velocity, the roll damping is frequency dependent as well. In subsection 2.4.3 it is explained how damping and added mass terms could be translated from the frequency- to the time domain. However this is a complex and time consuming method, besides it is mentioned that the dominating roll frequency is often the natural frequency. For this reason it is chosen to use the roll damping at natural frequency, $B_{44}(\omega_e, u)$, in the simulation method.

The method described above has a certain level of uncertainty, which is expected to be relatively high. Causes of this uncertainty are:

- B_{44PQ} is obtained from free decay tests on model scale. It does not account for scaling effects. The full scale ship will be surrounded by a turbulent flow in contrast to the model scale model, what will be surrounded by a linear flow. However, those differences are expected to be small as it effects the skin friction, which is only a small contribution to the total damping.
- Ikeda's approximation of $B_{44L}(u)$ is evaluated in [43]. Here experiments show that Ikeda's method overestimates the lift damping. The exact inaccuracy for tugs is unknown, but it shows that the level of uncertainty depends on the ship geometry.
- The tug-tow-system may have a dominating roll frequency which deviates from the natural frequency of the tug itself. This frequency is also depend on the towline stiffness and the mass of the assisted ship. So in free sailing condition it may be valid to take the roll damping equal to the damping at the natural frequency, however during towing operations a correction for the damping may be required.

Whether these uncertainties have an impact on the safety of the tugs or not, will be investigated in the sensitivity analysis provided in chapter 5.

The K_r term is more difficult to obtain, as less literature is written about it. Note that this term is left out in the theory written in [42] as well (equation 25). The effect of the coupling between roll and yaw and its absolute contribution to the total damping is hard to derive, but something could be mentioned about its relative contribution. Just as done for N_r and N_v (figure 3.7) both moment contributions are illustrated in figure 3.15. As the centre of rotation is located at the waterline, the direction of the moment around the x-axis is always opposite to the direction of the y-force. In case of a pure sway motion, the y-forces acting on the bow and stern are acting in the same direction. This results in two contributions to K reinforcing each other. In case of a pure yaw motion, $K_{r,stern}$ and $K_{r,bow}$ act in opposite direction which results in a smaller moment contribution. As the ratio between $Y_{r,bow}$ and $Y_{r,stern}$ is unknown, it cannot be determined whether K_r should be positive or negative. It depends on the geometry of the hull and appendages. However, for specifically the RSD 2513 K_r is expected to be positive. The presence of the skegs cause a large lateral area located at the front of the ship (figure 3.9a). Besides, the location of the point of attachment of the forces acting on these skegs is relatively far beneath the centre of rotation which results in a large moment.

Whether the contribution of K_r is significant, is investigated in the sensitivity analysis reported in chapter 5.

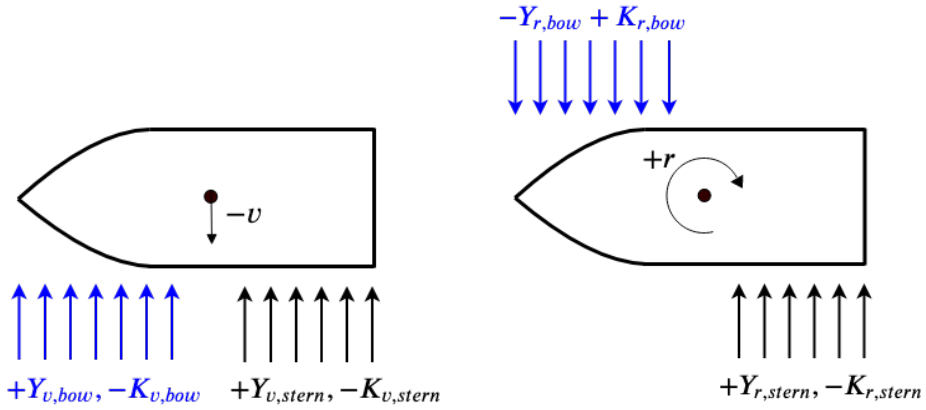

(a) K_v and Y_v

(b) K_r and Y_r

Figure 3.15: Illustration of roll damping contributions

4

Model Validation

If the simulation tool will in the end be used to determine the limits of safety on board of a tug, it should be validated first. This will be done in this chapter following different methods. The desire is to use the simulation tool for evaluating the behaviour of a sailing tug in escort operations. For this the free sailing behaviour as well as the towing behaviour should be validated. To do so, first some straight line captive model tests are simulated to be able to validate the steady state hydrodynamic forces acting on the tug. This will be elaborated in section 4.2. Thereafter a turning cycle and zigzag manoeuvre will be performed in section 4.3 to validate the free sailing behaviour of the tug. Finally, the towing behaviour will be compared with results derived from full scale experiments in section 4.4.

The validation of the simulation tool is done using the data and calculations for a specific DAMEN Tug, of which the characteristics are provided in section 4.1.

4.1 Validation case - DAMEN RSD 2513

From the Reverse Stern Drive Tug 2513, from now on RSD 2513, several model test data is gathered in the past years. This makes it possible to use it for validating the simulation tool. In table 4.1 the main characteristics of the tug are provided.

Table 4.1: Main particulars of RSD 2513*

	Symbol	**Magnitude**	**Unit**
Length between perpendiculars	L_{pp}	22.52	m
Waterline length	L_{wl}	22.77	m
Waterline breath	B_{wl}	12.13	m
Draught at FP	T_f	3.37	m
Draught at AF	T_a	3.26	m
Longitudinal centre of buoyancy	LCB	3.4	% ofL_{pp}
Metacentric height	GM	-	m
Vertical distance from keel to centre of gravity	KG	-	m
Block coefficient	C_B	0.538	-
Displacement	∇	-	m^3
Lateral area of the hull	$A_{lat,hull}$	-	m^2
Lateral area of the skeg	$A_{lat,skeg}$	-	m^2

*Some of the particulars could not made public in this public version of the master's thesis.

With this tug three series of tests are performed, namely: Straight line captive model tests, free sailing model scale tests and full scale towing experiments. The first two series of tests are performed in a tank at MARIN of which the depth is such that deep water can be assumed.

4.2 Validation of hydrodynamic forces

The hydrodynamic forces will be validated using a simulation of a captive model tests as performed at MARIN. Here the tug is fixed in its position under a series of drift angles, so it is unable to move in any direction. With a velocity equal to 8 knots, the tug is towed through the water and the forces are measured. In the simulation tool

these tests are simulated under the same conditions.

In figure 4.1 the non-dimensional forces and moments, with and without skegs, are given as a function of the drift angle. The forces are made non-dimensional as follows:

$$C_x = \frac{X_{total}}{0.5 \cdot \rho \cdot v_s^2 \cdot L_{pp} \cdot T}, \quad C_y = \frac{Y_{total}}{0.5 \cdot \rho \cdot v_s^2 \cdot L_{pp} \cdot T}$$
$$C_k = \frac{K_{total}}{0.5 \cdot \rho \cdot v_s^2 \cdot L_{pp} \cdot T^2}, \quad C_n = \frac{N_{total}}{0.5 \cdot \rho \cdot v_s^2 \cdot L_{pp}^2 \cdot T}$$

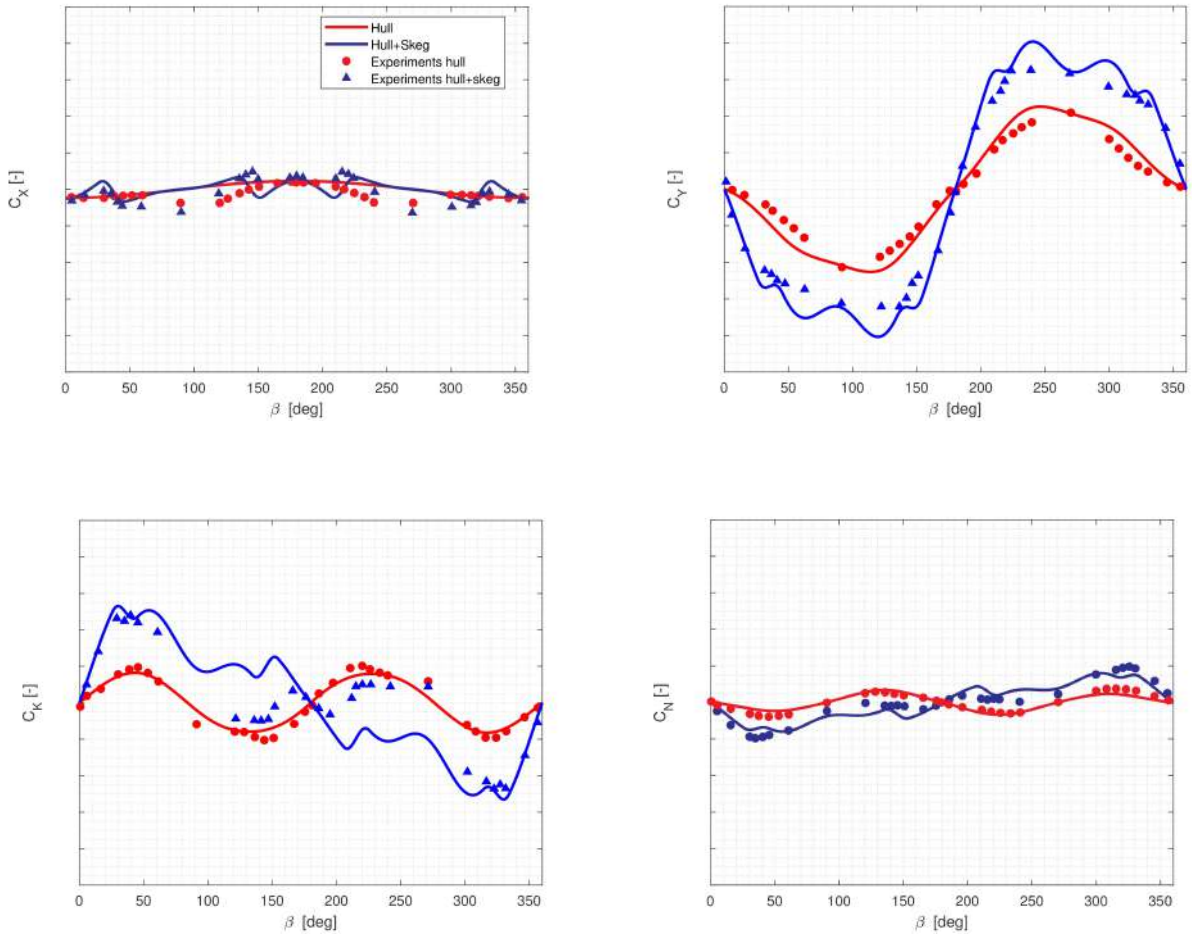

Figure 4.1: Non-dimensional forces and moments obtained in captive model tests

Those captive model tests are initially performed to determine which skeg design results in the best escort performance, for this reason the experiments are performed with and without skegs. Note that the forces acting on the nozzle are not taken into account. It can be seen that the calculated forces in the y-direction and the moment around the z-axis are in good agreement with the experimental results. However, the moment around the x-axis and the forces in x-direction do not collapse with the data retrieved from experiments.

The mismatch between the calculations and experimental data from the force in the x-direction is mainly due to the forces acting on the bare hull, as can be seen in figure 4.1. Here the largest deviation can be found around a drift angle of $90°$, as in the calculations it is assumed that the force in x-direction is zero when sailing under a $90°$ drift angle. This assumption may be valid for low aspect ratio wings being symmetric in two planes. However, the submerged part of the hull is asymmetric in the yz-plane, which causes the pressure to be unequally distributed. This is illustrated in figure 4.2 which is a result of the CFD analysis of the RSD 2315 described in [48].

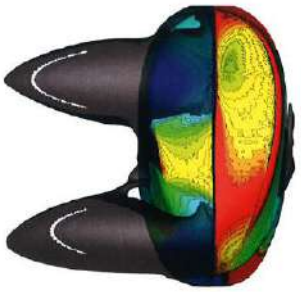

Figure 4.2: Pressure distribution for $\beta = 90°$

For the moment around the x-axis, the differences between the calculation- and the experimental results can mainly be found for drift angles between plus or minus 120 and 160 degree. The deviation is due to the moment generated by the skegs, as the calculation results for a bare hull are in a good agreement with the experimental results.
The moment generated by the skegs is defined as follows: $M_x = z_a \cdot F_y$, in which z_a is the distance to the point of attachment of F_y. In figure 4.1 it can be seen that the calculated C_y is in good agreement with the experimental results and so is F_y, for this reason it can be concluded that the estimation of z_a causes the inaccuracy of the calculation. This distance is assumed to be constant, but due to flow separation under larger drift angles and the interaction between the hull and skegs this distance may be variable.

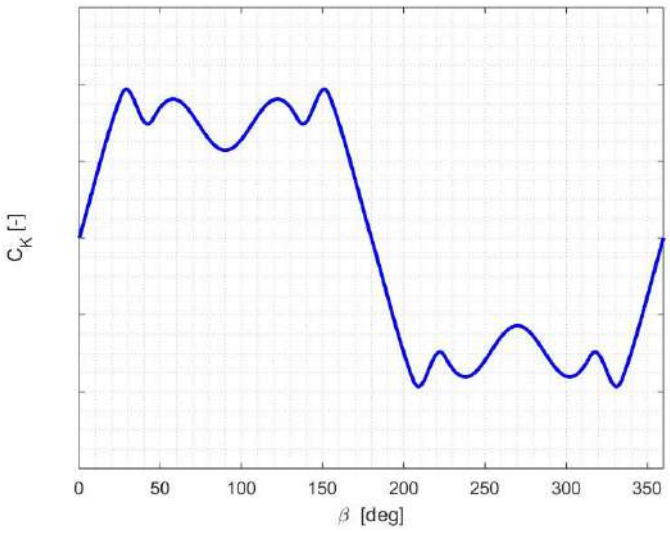

Figure 4.3: C_k generated by both skegs

Experimental results show that, for absolute drift angles between 120 and 160 degree, the calculation of the skeg moment is significantly overestimated. In figure 4.3 the calculated C_k, generated by both skegs, is illustrated. Here it can be seen that the moments calculated for β and $\pi - \beta$ are equal, which indicates that it is assumed that the hydrodynamic forces for a flow approaching from ahead are exactly equal but opposite to the forces resulting from a flow approaching from astern. The mismatch between the calculated and experimental results prove that this assumption is not valid and so influence of the interaction effects between the hull and skeg on the distance z_a should be considered as well.

4.3 Free sailing behaviour

As mentioned in the introduction of this chapter, the turning cycle tests may be used to validate the free sailing behaviour of the vessel. In figure 4.4 the turning cycle characteristics are illustrated, of which some will be used to validate the simulation tool. The data set used to validate the turning cycle characteristics is retrieved

from free sailing model scale tests with the RSD 2513. Before the validation can be completed, first the lacking hydrodynamic for contributions $N_r, Y_r, N_{rr}, Y_{rr}, N_{rv}$ and Y_{rv} should be tuned, this is done in subsection 4.3.1.

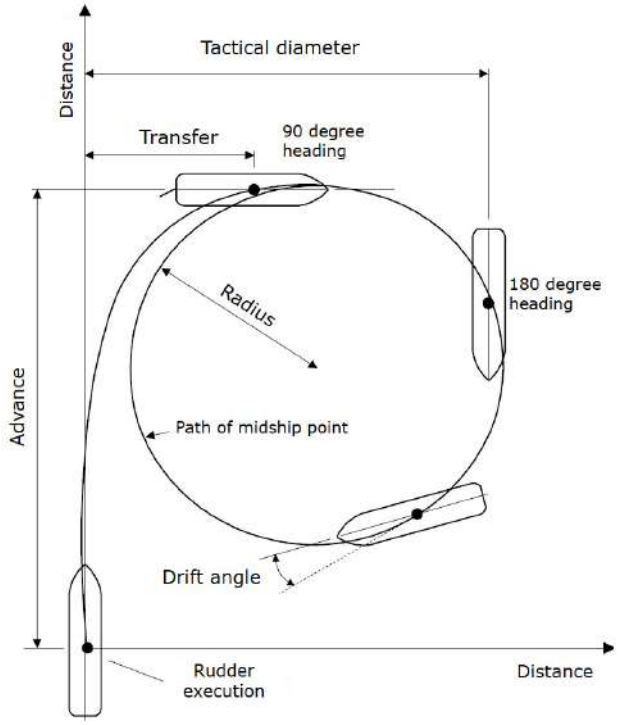

Figure 4.4: Turning cycle characteristics

4.3.1 Tuning hydrodynamic force contributions

In section 3.5 it is described how some of the linear and non-linear damping terms could be obtained, namely by use of the semi-empirical method described in [4]. However, as described in subsection 3.5.4, those terms are expected to be different for tugs. In this subsection it will be determined what should be the correction of the dynamic force terms, such that they are valid for tugs as well. This will be done by comparing the calculation results with results obtained in model tests. It concerns the following terms: $N_r, Y_r, N_{rr}, Y_{rr}, N_{vr}$ and Y_{vr}. Note that in the end the correction of those terms will be valid for only one specific case, namely for the RSD 2513.
Tuning the hydrodynamic force terms is an iterative process as those forces may not be seen as independent. The tuning will be done by multiplying the force terms by a specific factor of which its value will be determined in this section.

From free sailing model tests three steady state turning cycle characteristics are obtained, namely: the yaw rate, drift angle and heeling angle. Because the used semi-empirical method does not consider the roll motion, the focus will be on the yaw rate and drift angle only. Which will mainly be determined by N_r, N_{rr}, N_{vr} and Y_r, Y_{rr}, Y_{vr} respectively. The followed iteration sequence is sketched in figure 4.5. So the N- and Y-terms are tuned on the basis of the available data concerning the steady state yaw rate and steady state drift angle respectively.

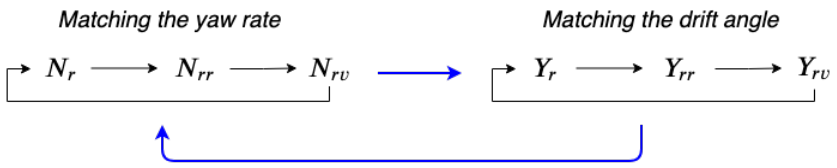

Figure 4.5: Sketch of followed iteration sequence for tuning hydrodynamic force components

A short physical explanation is provided in subsection 3.5.4, here it is explained that the yaw damping as a result of a yaw velocity (N_r) will have a large influence on the manoeuvring behaviour. Besides, it is explained why this moment contribution is expected to be higher for the RSD 2513. In figure 4.6 the steady state yaw rate during turning cycles is given for different steering angles. The black dashed line illustrates the trend obtained form model tests. Here the multiplication factor for N_r has been varied over a certain range, while the other terms are kept at their initial values.

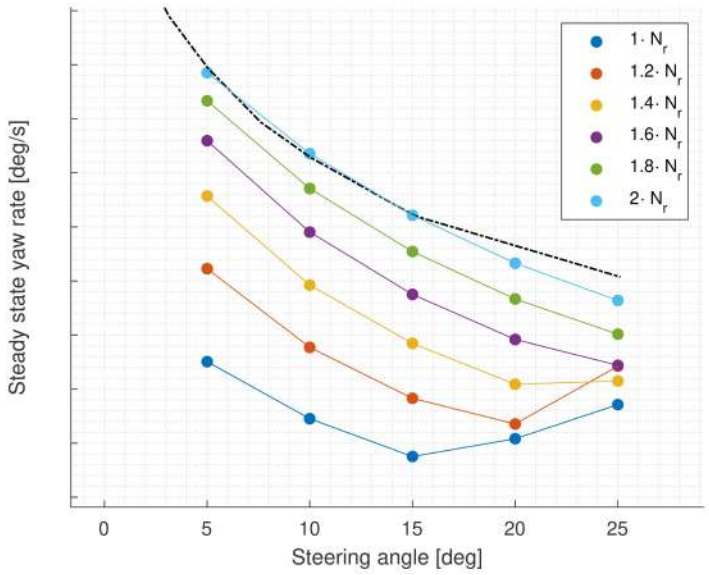

Figure 4.6: Variation of N_r

It can be seen that for multiplication factors between 1.4 and 1.8, the calculation results follow the trend obtained from experiments. Even though this figure shows that the multiplication factor should exceed 1.8, conclusions can only be drawn whenever the iteration process has been completed. To see whether the increase of N_{rr} and N_{rv} influences the required correction factor of N_r, some variations has been conducted. In figures 4.7a and b the multiplication factors of N_{rr} and N_{rv} are varied while the multiplication factor of N_r is kept to 1.8.

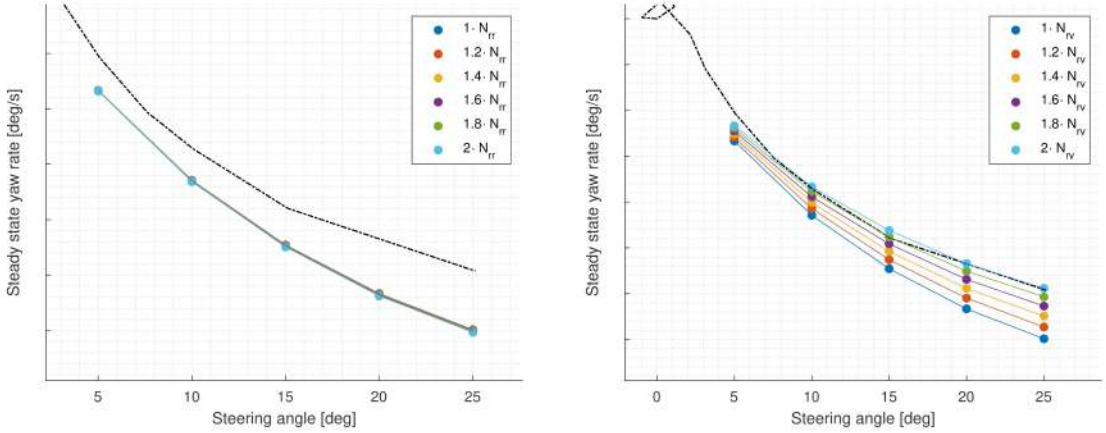

(a) Variation of N_{rr} with constant N_r

(b) Variation of N_{rv} with constant N_r

Figure 4.7: Steady state yaw rate for varying hydrodynamic derivatives

From figures 4.7a and b it can be seen that increasing N_{rr} has a very little influence on the manoeuvring behaviour during turning cycles. The influence of increasing N_{rv} is significantly larger. Knowing this it can be concluded that a good balance should be found between N_r and N_{rv}. After a few iteration steps, the following results are obtained:

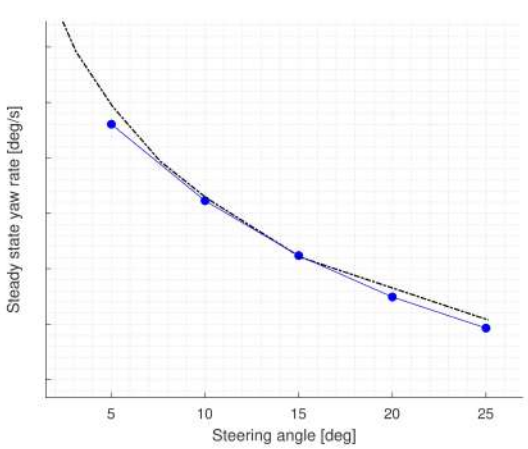

(a) Yaw rate

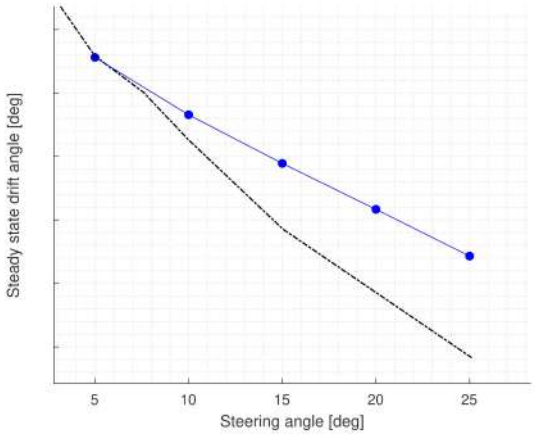

(b) Steady state yaw rate and drift angle after tuning of yaw damping

Figure 4.8: Drift angle

Tuning the N-terms has resulted in a yaw rate being in good agreement with the experimental results, as can be seen in figure 4.8a. The drift angle, which is mainly influenced by the Y-terms, deviates especially at higher yaw rates. Here the non-linear effects are expected to be significant, so tuning Y_{rr} and Y_{rv} is expected to reduce the deviation. In figures 4.9a and b respectively Y_{rr} and Y_{rv} are varied. Note that here the range of multiplication factors is from -0.2 to 1, as those terms are expected to decrease with respect to the original terms obtained from [4] (subsection 3.5.4).

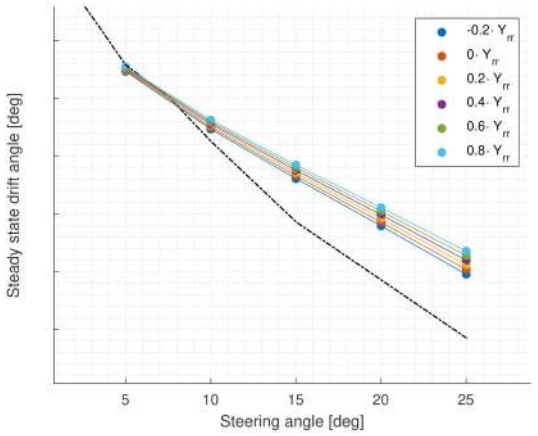

(a) Variation of Y_{rr}

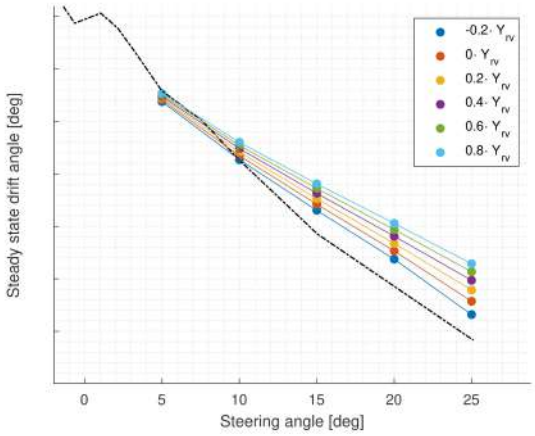

(b) Variation of Y_{rv}

Figure 4.9: Steady state drift for varying hydrodynamic derivatives

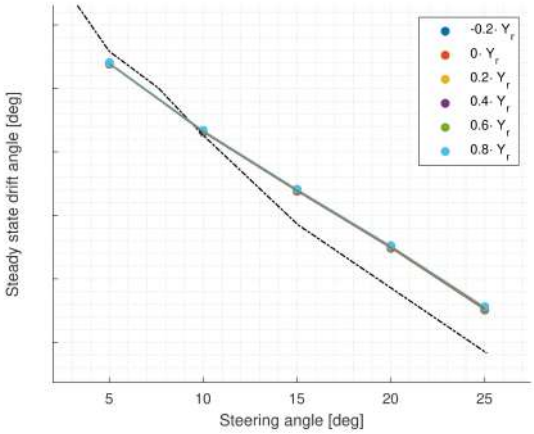

Figure 4.10: Variation of Y_r

Variation of Y_{rr}, Y_{rv} influences the steady state drift angle for this specific case significantly, in contrast to the linear term Y_r. The impact of varying Y_r is shown in figure 4.10, which shows that varying Y_r barely influences the steady state drift angle.
In table 4.2 the derived initial values of the multiplication factors are provided. The multiplication factors for terms which barely influence the yaw rate nor the drift angle, are set equal to those corresponding to the similar terms.

Table 4.2: Initial multiplication factors for hydrodynamic derivatives

Hydrodynamic derivative	Multiplication factor
N_r	1.8
N_{rr}	1.8
N_{rv}	1.8
Y_r	0.1
Y_{rr}	0.1
Y_{rv}	0.1

From the obtained multiplication factors, it can be concluded that the expectations provided in subsection 3.5.4 are met. The yaw damping moments will increase for tugs due to the differences in geometry, like the presence of large skegs located close to the bow. Besides, for the same reason, the total Y-force components coherent with the yaw motion will be smaller for tugs compared to common merchant ships.

Now the yaw rate and drift angle are discussed, an additional turning cycle characteristic will be considered. From the free sailing model tests the speed loss in a turning cycle can be obtained. When performing a turning cycle, the vessel's forward speed will decrease with respect to the initial forward speed at the beginning of the turning cycle. The speeds are respectively referred as u_{ss} and u_0, which means that the following statement is valid: $u_{ss} < u_0$. In figure 4.11 the speed loss ratio, being u_{ss}/u_0, is given as a function of the steering angle. Here the blue dots represent the speed loss ratio resulting from the calculations performed with the developed simulation model.

Using the results presented in figure 4.11, it can be determined whether the lift induced drag terms (X_{vr}, X_{vv} and X_{rr}) should be included. Inclusion of those hydrodynamic force contributions would increase the drag and with that decrease the speed loss ratio. It is expected to improve the match between the calculated and measured results in figure 4.11. However as those terms are dependent on Y_r, of which the magnitude is disputable, inclusion would result in another uncertainty. Besides, the calculated speed loss ratio is already in good agreement with the measured data. To limit the number of uncertainties in the simulation model, it is chosen to neglect the little effect of the lift induced drag terms.

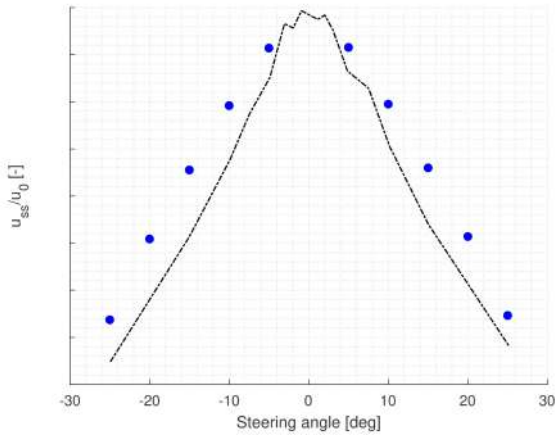

Figure 4.11: Speed loss ratio as function of the steering angle

4.3.2 Turning cycle characteristics

In section 4.3.1 suitable correction factors for $N_r, N_{rr}, N_{rv}, Y_r, Y_{rr}$ and Y_{rv} are found, in this section those values will be used to validate multiple turning cycle characteristics. The first turning cycle characteristic, which will be compared to experimental data, is the radius of the cycle. In the past years several full scale turning cycles are performed with different ASD tugs, of which the underwater part of the vessel is comparable with this of the RSD 2513. Despite the differences in design between the ASD and RSD tugs, the data can be used to check whether the calculated turning cycle radius is of the same order of magnitude as those of the ASD tugs. The speed before rudder execution varies for the performed full scale experiments. Differences in approaching velocity result in differences in turning cycle radius. Nevertheless, as the approaching speed used in the calculations is taken as the average of the full scale experiments, the calculation can still be used to check the order of magnitude. In figure 4.3.2 the results can be seen and in table 4.3 the approach velocity for each tug design is provided.

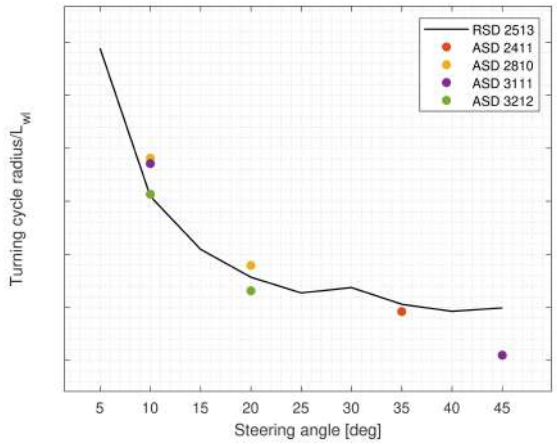

Figure 4.12: Turning cycle radius compared with full scale experiments performed with comparable tug designs

Table 4.3: Approach velocity in full scale tests

Tug	Approach velocity [kn]
ASD 2411	13.2
ASD 2810	13.2
ASD 3111	12.6
ASD 3213	14
RSD 2315	13

Despite the deviations due to differences in design and approach velocity, it can be concluded that the order of magnitude of the turning cycle radius is realistic and it follows the trend found in the results of the full scale turning cycle tests performed with the ASD tugs.

As in subsection 4.3.1 experimental data retrieved in model scale tests are used to tune the hydrodynamic derivatives, the final results will be validated using this data as well. In figures 4.13 to 4.15 the yaw rate, drift angle and heeling angle are compared with the retrieved experimental data.

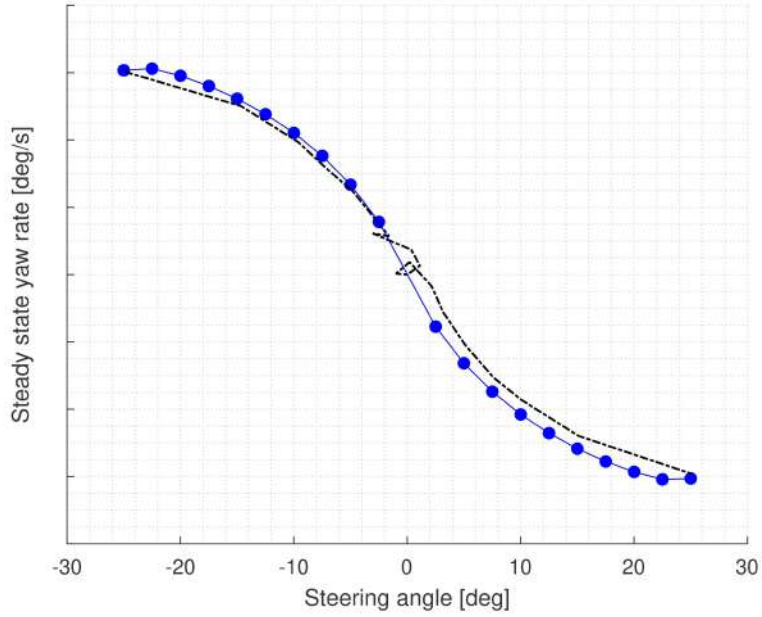

Figure 4.13: Steady state yaw rate as a function of the steering angle

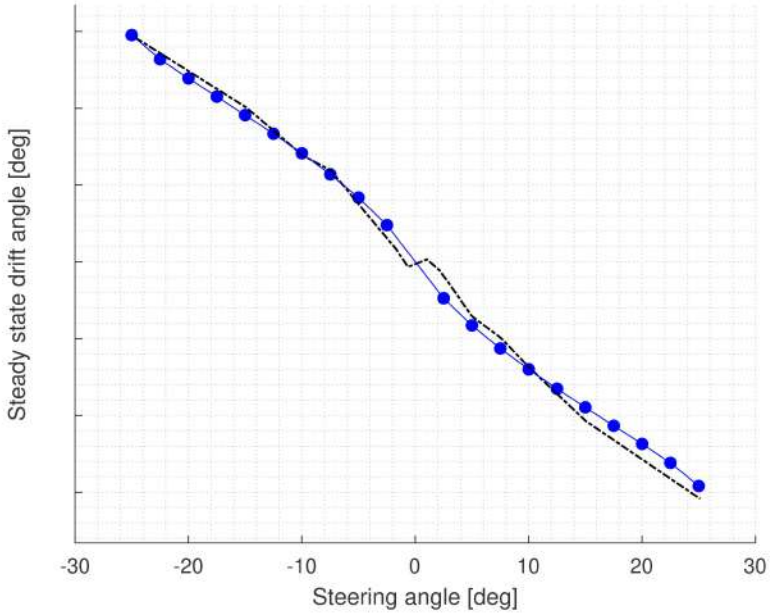

Figure 4.14: Steady state drift angle as a function of the steering angle

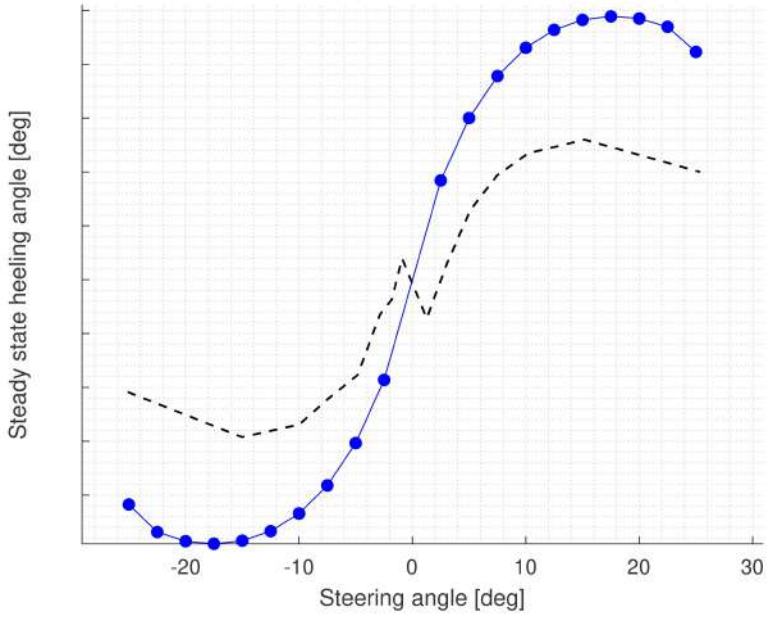

Figure 4.15: Steady state heeling angle as a function of the steering angle

Figures 4.13 to 4.15 show that the calculated yaw rates and drift angles are in good agreement with those obtained with free sailing experiments. The largest deviations may be found between the calculations and experimental results of the heeling angle. The roll moment can be divided into three components, as described in section 3.9, namely:

1. The static roll moment
2. Roll moment as a result of the force acting on the side of the vessel
3. Additional roll moment due to dynamic sinkage

In the simulation tool the force acting on the second contribution only considers the Y-force as a result of a sway velocity. However Y_r and Y_{rr} could possibly influence the roll motion as well. To evaluate whether those y-force contributions would have a significant influence, the steady state Y_v and Y_r contributions are separated and given for a range of steering angles. Those results are presented in figure 4.16a. It can be seen that the absolute contributions of the Y_r, Y_{rr} and Y_{rv} to the total Y-forces are small. So based on this figure, we could already conclude that those will barely affect the side force resulting in a roll moment.

Another cause of the deviations found in figure 4.15 could be the effect of the yaw velocity on the hydrostatic restoring moment. In [19] a CFD study is performed to investigate the effect of a yaw velocity on the static GZ-curve. This research pointed out that the effect of a yaw rate on the GZ-curve is only significant at higher heeling angles. However, as illustrated in figure 4.16b, the static roll moment dominates the total roll moment and small inaccuracies in the approximation of this static roll moment, could result in perceptible inaccuracies in the heeling angle calculations.

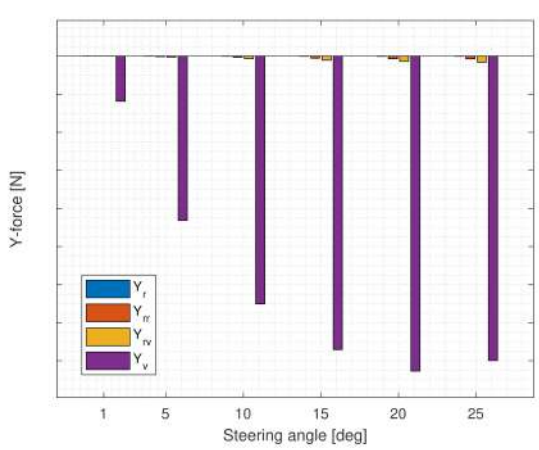

(a) Separation of Y_v and Y_r components

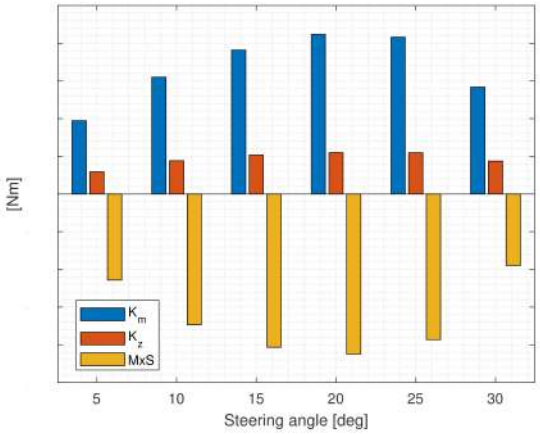

(b) Separation of the different contributions to the roll moment

Figure 4.16: Steady state force decomposition

4.3.3 Zigzag manoeuvre

In [24] it is listed what manoeuvres should be simulated to prove validity of a developed simulation tool. One of those manoeuvres is the zigzag manoeuvre, which has been performed with the RSD 2513 on model scale as well. The measurement results of this experiment are used to validate the developed simulation tool. In figure 4.17a the steering angle over time, as applied in the model scale experiments, is provided. This is used as an input for the simulation model, resulting in the heeling angle, heading angle and yaw rate as illustrated in figures 4.17b, 4.18a and 4.18b respectively. Here the blue lines represent the calculation results and the black dashed lines represent the results obtained from the experiment.

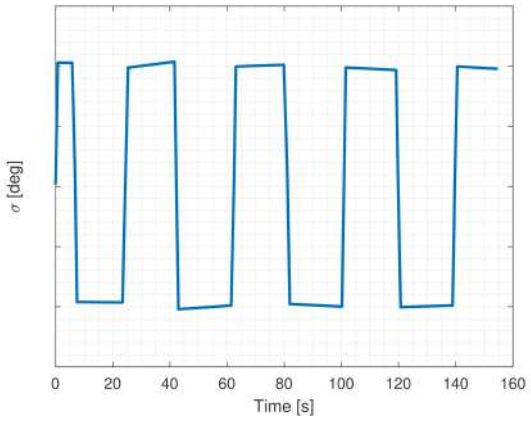

(a) Steering angle as a function of time

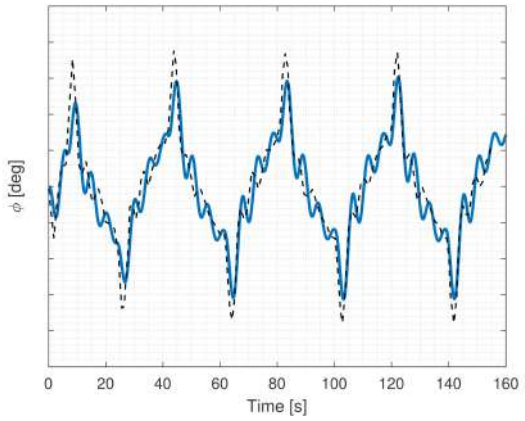

(b) Heeling angle as a function of time

Figure 4.17: Zig-zag manoeuvre characteristics (part I)

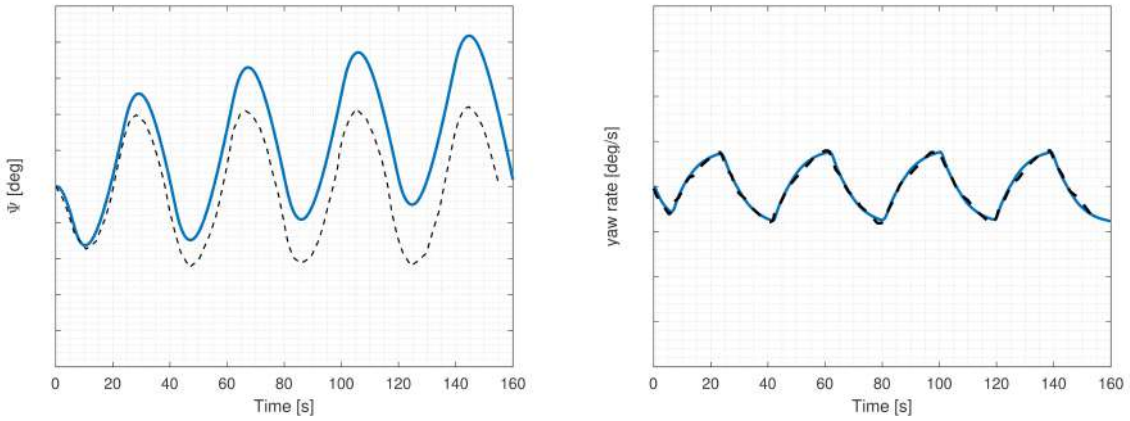

(a) Heading angle as a function of time

(b) Yaw rate as a function of time

Figure 4.18: Zig-zag manoeuvre characteristics (part II)

Those figures show that the calculated heeling angle is in good agreement with the obtained experimental results. Apart from a small underestimation of the heeling angle found at the peaks and a little shift in phase.
The error between the calculated and the measured heading angles become larger when time increases. Those deviations are a result of an accumulation of errors over time, which are caused by small differences in the input parameters. The time over which the steering is kept constant (figure 4.17a) has a major impact on the heading angle. Nevertheless, the calculated yaw rate as illustrated in figure 4.18b is in good agreement with the yaw rate measured in the experiments.

4.4 Towing behaviour

Besides the free sailing behaviour, the behaviour of the tug while escorting mode should be validated. Previously some full scale tests are performed with the RSD 2513, where the velocity of the assisted vessel is claimed to be 8 knots. During these tests the steering angle and engine load percentage are measured, which are used as input signals of the simulation tool. The output of the simulation, consisting of the towline force, heeling and heading angle, is compared with the results retrieved from the full scale tests.

Figures 4.19, 4.20 and 4.21 show respectively the calculated and measured heeling angle, heading angle and towline force. It shows that, unless that the simulation results seems to follow the trend obtained in experiments whenever heeling angles become high, significant deviations arise between the measured and calculation heeling angle, towline force and heading angle. There are several factors which could possibly cause these deviations, those are listed here:

- Measurement uncertainties: *Especially in the measurement results of the towline force a high level of measurement uncertainty is present. This can be seen in figure 4.21 where the towline force stays constant over whilst the heading and heeling angle show a lot of dynamic behaviour*

- Lack of information: *The amount of available information is limited. For example the loading condition of the tug is unknown and the exact speed of the assisted vessel is not measured. Chapter 5 would point out whether the lacking information will have a significant influence on the calculation results. To give an indication, in appendix C the calculation results for different velocities and static trims are shown, as they are expected to have a significant influence on the tug's manoeuvring behaviour.*

- Limits of simulation model: *Several assumptions are made during the implementation of the simulation model, this results in some limits of the model itself. One of the limits is that the thruster interaction is not incorporated in the model. For higher steering angles or whenever both thrusters are steered individually, these interaction effects could have a significant impact on the manoeuvring behaviour. As the steering angle in the full scale experiments will mainly be around 40°, implementation of these interaction effects is expected to improve the results.*

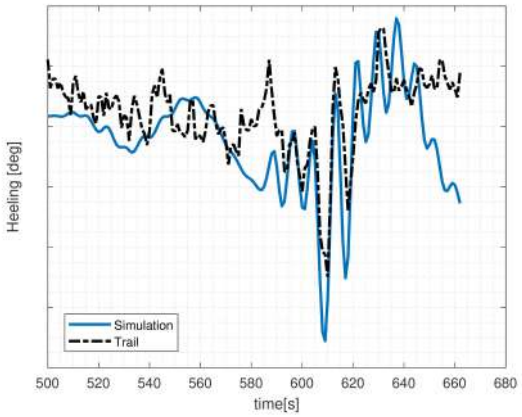

Figure 4.19: Comparison of heeling angle for validation purpose

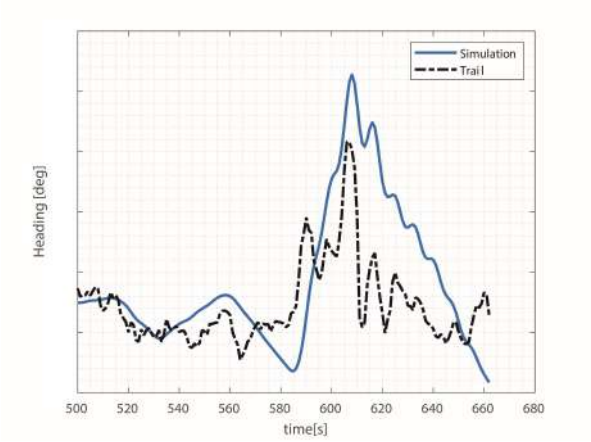

Figure 4.20: Comparison of heading angle for validation purpose

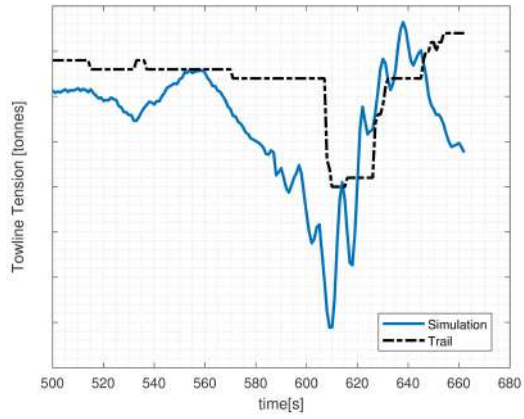

Figure 4.21: Comparison of towline force for validation purpose

4.5 Discussion

Multiple model scale experiments are used to validate the manoeuvring behaviour of tugs. So are the steady state forces validated using captive model tests. The calculation results of the forces are however on full scale. To be able to compare both results, the experimental results should be scaled from model scale to full scale. This has been achieved by multiplying the measured forces and moments by the following appropriate scaling factors:

Forces: $\lambda^3 \cdot \lambda_p$

Moments: $\lambda^4 \cdot \lambda_p$

Where λ is the linear scaling ratio and $\lambda_p = \frac{\rho_{sea}}{\rho_{basin}}$.

This method is somewhat simplified as it scales all force components with the same factor and no corrections for i.a. roughness are applied. Besides, in the recommended procedures and guidelines concern captive model tests [23] it is recommended to use a Froude scaling.
So when using the obtained captive model test results to validate the simulation model, a certain confidence interval should be incorporated. In other words, even though the calculation results would perfectly match the captive model test results, it does not mean that the calculated forces and moments will perfectly match the full scale involved hydrodynamic forces and moments as well. As stated in [23] the scale effects in manoeuvring are not yet fully understood. Besides, it is generally accepted that scale effects are supposed to increase with increasing drift angle. This could be a result of the increasing impact of viscosity which may be one of the causes of the deviations found in figure 4.1.

The straight line captive model tests are used to validated the steady state forces. This method is generally accepted as stated in [23]. However, the dynamic forces could not be validated using the straight line captive model tests. To be able to validate those hydrodynamic force contributions harmonic and steady circular motion tests should be performed (section 2.3.2). These tests may be used to calculate the involved forces during pure yaw as well as coupled yaw-sway motions.
To further improve the validation of the simulation model a method to predict the added mass and damping is desired. A series of forced oscillation tests would offer solution. In [26] a method is provided which can be used to obtain the damping and added mass terms in each degree of freedom. The damping and added mass seem to be dependent on the amplitude of the oscillation and the phase found between the involved hydrodynamic force and the displacement over time.

The last discussion point regards the applicability of the model to different tugs designs. The hydrodynamic forces, the turning cycle characteristics and the dynamic behaviour during zigzag manoeuvres have been validated for the Damen RSD 2513. However, the question remains whether the developed method is suitable for other tug designs as well.
First of all, TugSim has been developed for multiple tug designs and it is able to predict the steady state forces for several combinations of hulls, skegs and nozzles. Most of the hydrodynamic force contributions which could not be calculated using TugSim, are calculated using the method described in [4]. To make this semi-empirical method applicable to tugs, the hydrodynamic derivatives are tuned in section 4.3.1 using data retrieved from turning cycle tests. The fact that the calculated turning cycle characteristics are in good agreement with the measured characteristics (figures 4.13 to 4.15), is therefore not coincidental. However, it is expected that the obtained correction factors provided in table 4.2 are not directly applicable for every tug design. Nevertheless, the physical background behind the tuning, as described in section 3.5.4, is suitable for tugs in general. Besides, figure 3.8 shows that the correction factor is expected to be mainly dependent on the applied skeg design instead of the bare design itself. As the method written by Ankudinov [4] gives a well approximation of the side forces acting on a bare hull of tug, especially at smaller drift angles. To confirm this assumption, it is recommended to perform harmonic and steady circular tests once with only a bare hull and once with skegs attached to it. Using this results it can be investigated whether the measured hydrodynamic force contributions of a bare hull are in good agreement with the ones calculated using the method described in [4]. And if they are in good agreement, a correction for the attached skegs should be found.

5

Sensitivity Analyses

An inaccurate approximation of one of the input parameters could possibly result in inaccurate calculation results. A sensitivity analysis is a method to find out which of the systems input parameters have a significant influence on the final results and to what extent. By varying the chosen properties over a certain range and performing a specific calculation for each value in this range, it can be investigated whether changes in those properties result in significant changes of the final results or not. In this chapter sensitivity analysis will be performed for several input properties, which are divided in two groups. The first group contains all 'simulation related parameters'. For some input parameters an initial estimation had to be made, because the exact value is unknown. A sensitivity analysis for these parameters will point out whether an inaccurate estimation of these input parameters will influence the simulated manoeuvring behaviour and to what extend.
The second group contains the 'design and operation related parameters'. Even though those parameters are often well known, it is interesting to see what is the effect of their variation on the manoeuvring behaviour of tugs. It enables to evaluate whether the limits of safe operation should be dependent on one of those parameters or not.

When keeping an eye on the research goal, which is defining the limits of safe operation considering the hydrodynamic forces, the amplitude of the heeling angle is of great importance. The heeling angle defines whether, after impact loads, the tug stays in safe position or will collapse. In this sensitivity analyses three situations has been simulated in which the heeling angle may become significantly large, those are provided in section 5.1. The sensitivity analysis will focus on what input parameters have a significant influence on the heeling angle in the different dynamic scenarios.
In section 5.2 the sensitivity analysis is performed concerning the simulation related parameters. Thereafter, in section 5.3, the sensitivity analysis concerning the design and operation related parameters is conducted.

5.1 Dynamic scenarios

To be able to analyse the sensitivity of the system, three dynamic scenario's has been simulated with the RSD 2513. The first dynamic scenario is one often present in standard escort towing operations, namely the transition from sailing behind the assisted vessel to sailing aside being in a combined towing mode. Even though this scenario is common, high heeling angle overshoots could occur as a result of an unnecessary large amount of thrust.
The latter two scenarios include less common events. To be able to define the tug's limits of safety dynamic situations, where impact loads play a major role, should be simulated. The dynamic behaviour during these unforeseen situations are nowadays barely analysed, nevertheless they could be crucial for defining the tugs limits of safety. One of those dynamic scenarios, which is claimed to be critical in i.a. [3] and [2], is the instantaneous loss of towline tension. Loss of towline tension is expected to result in an instantaneous change of the moment around the x-axis and so an increase of the acceleration, velocity and heeling angle. Another scenario, dealing with high impact loads and possibly high heeling angles, concerns the loss of full thrust.

To summarise, the dynamic scenario's are referred as follows:

1. Transition from behind the assisted ship to aside in a combined towing mode
2. Instantaneous loss of towline tension
3. Instantaneous loss of full thrust

Figures 5.1a and b illustrate respectively the steering angle and engine load percentage as a function of time during the simulation of all three scenarios. However, for scenario 3 the engine load percentage is set to zero after running a while.

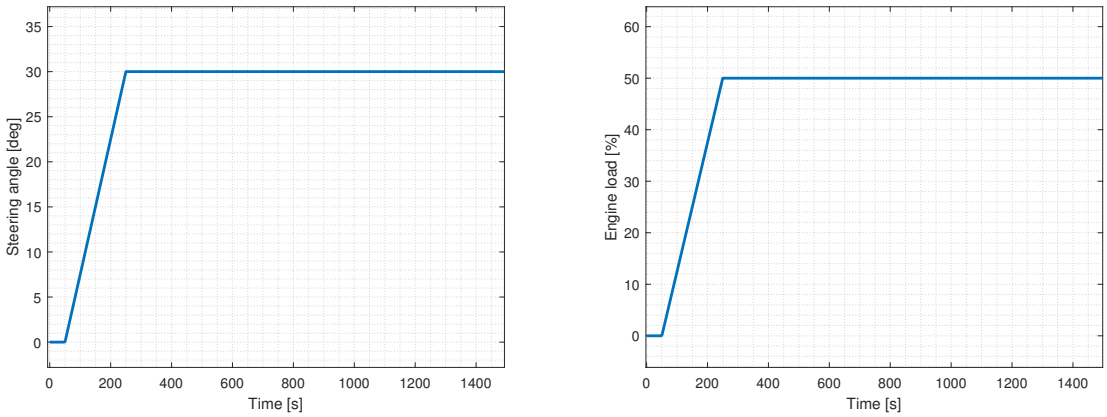

Figure 5.1: Steering angle and engine load during simulation of dynamic scenarios 1

In figures 5.2 and 5.3 examples are provided of time simulations of all three scenarios, those are used to illustrate the definition of the reference values. An in- or decrease of these reference values as a result of varying one of the input parameters, will not directly in- or decrease the danger involved in the considered dynamic scenarios. Nevertheless, they are related to safety, as *they indicate the ease with which the tug starts to roll after impact loads*.

In figure 5.2a it can be seen that an overshoot in heeling angle occurs before steady state is reached. The height of the overshoot depends on the input parameters of which the sensitivity will be analysed in this chapter. In figure 5.2b the reference value of scenario two is illustrated, which is defined as the difference between the steady state heeling angle and the first minimum after the towline has been released. In figure 5.3 the reference value for scenario 3 is indicated, which is again the difference between the steady heeling angle and the first minimum after loss of thrust.

Investigating the sensitivity to the parameters based on the defined reference values, gives an indication about the dynamics of the system, whether or not dealing with impact loads. It illustrates how the system recovers its static equilibrium or changes to a new one.

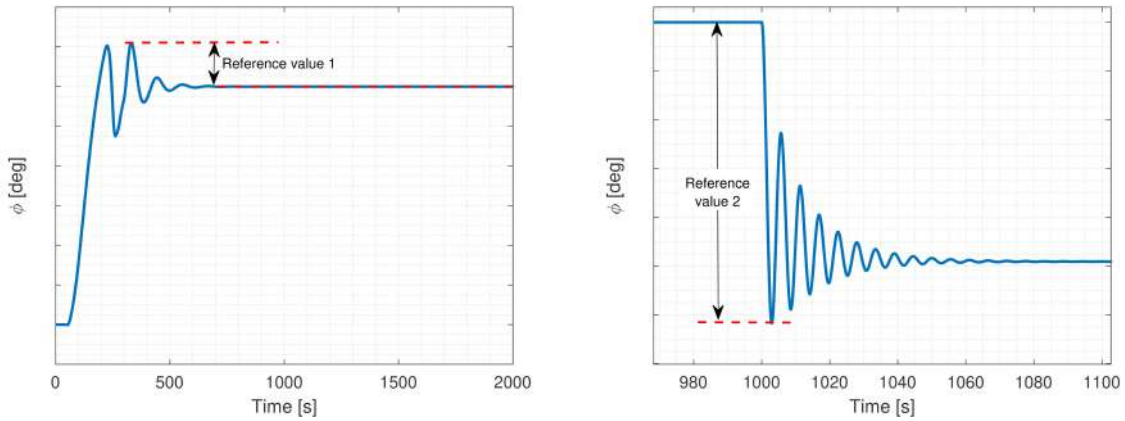

(a) scenario 1 (b) scenario 2

Figure 5.2: Definition of reference value

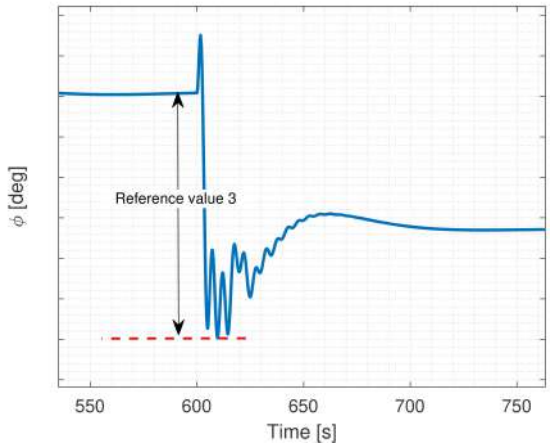

Figure 5.3: Definition of reference value in scenario 3

5.2 Sensitivity to simulation related parameters

Inaccurate estimation of input parameters could lead to significant errors in calculation results. The numerical method is already provided in chapter 3, here initial values are derived for multiple input parameters. Many of those parameters could not be calculated exactly due to lack of knowledge or data. In this section the systems sensitivity to those parameters has been analysed and expressed in terms of the reference values defined for each different dynamic scenarios. In every subsection the sensitivity to a change in one specific parameter or a group of coherent parameters will be analysed. To start with the inertia moments, followed by the added mass terms and the different damping terms.

5.2.1 Inertia moments

The derivation of the initial values of the moments of inertia has been described in subsection 3.8.1. The method described in [26], which is often used, calculates the moments based on radii of inertia. Each radii varies over a certain range, this range is also the range over which the inertia moments will be varied in this sensitivity analysis. In table 5.1 the lowest and highest values in the range are provided. The lowest values are chosen to be the initial values. Note that I_{xz} is initially set to zero, as it is assumed to be very small compared to I_{zz} and I_{xx}. In this analysis it is investigated whether addition of a small I_{xz}, being 10% of I_{zz}, will influence the manoeuvring behaviour. The results of the sensitivity analysis, concerning the inertia terms, are provided in figure 5.4. Here the percentage change with respect to the initial conditions is given on the y-axis and the compared property, with a subscript indicating the scenario, on the x-axis.

Table 5.1: Initial inertia moments

Property	I_{xx}	I_{zz}	I_{xz}
Lowest value in range	6.554e6	12.419e6	0
Highest value in range	11.621e6	20.118e6	1.162e6

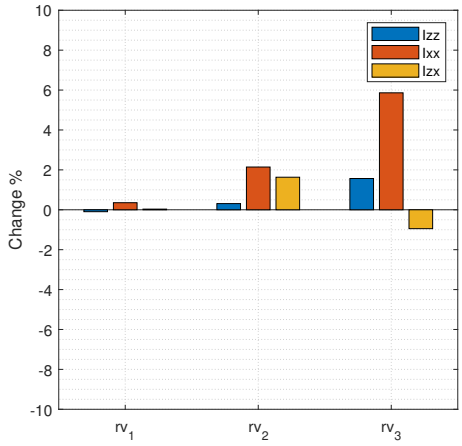

Figure 5.4: Sensitivity analysis inertia moments

5.2.2 Added mass

In section 3.8.2 it is described how the initial values of the added mass terms are obtained. Those educated guesses are based on literature combined with potential flow theory, however with an unknown accuracy. In order to determine the influence of estimation errors in the added mass terms, a sensitivity analyses has been conducted. Table 5.2 shows the initial values of the added mass terms. The order of uncertainties determines what should be the range of variation, however this order is unknown. In [47] a similar sensitivity analysis has been performed for free sailing common merchant ships, here the added mass terms are varied by 10%. As stated in [49] a potential flow method, used to calculate the bare hull added mass terms, gives a good approximation of the actual added mass. Addition of appendages requires additional added mass terms, of which the approximation method has a higher uncertainty. This higher uncertainty has resulted in a variation range of 20%. In figure 5.5 the results of the sensitivity analysis are shown.

Table 5.2: Added mass initial values*

Property	a_{11}	a_{22}	a_{44}	a_{66}	a_{26}	a_{24}	a_{46}
Initial value	-	-	-	-	-	-	-

*Added masses could not made public

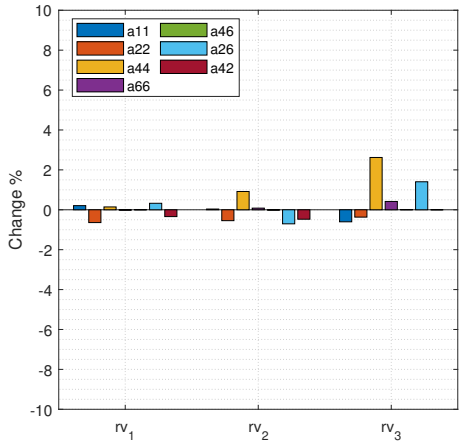

Figure 5.5: Sensitivity analysis added mass terms, with 20% increase

5.2.3 Damping terms

As described in section 3.5 some of the damping terms are not included in the method used in TugSim and should for this reason be estimated using semi-empirical methods. Those semi-empirical methods are mainly suitable for relatively large merchant ships. To make them suitable for tugs as well, the damping terms should be multiplied by a specific factor. The initial values of these factors are determined in section 4.3.1 and based on data obtained from model scale turning cycle tests. The iteration process followed in subsection 4.3.1 shows already the impact of changing the damping contributions, however the question remains whether these impacts are the same in the provided dynamic scenarios. This will be investigated in this subsection.

The initial values of the hydrodynamic derivatives could be very inaccurate, as it is based on turning cycle data only. The order of uncertainties determines the range over which the terms should be varied. Because of the large uncertainties, this range should be relatively large. It is chosen to analyse two cases, namely: an increase of 20% and a decrease of 50%. The percentage increase is chosen to be smaller, because a large increase should result in damping terms deviating significantly from the original damping terms derived with the semi-empirical method. This large deviation would be physically inexplicable. The percentage decrease of 50% is based on original values of the damping terms as well. The initial damping terms N_r and N_{rv} are almost twice the original damping terms from [4], so a variation of 50% indicates that the damping terms could variate between the original and the found initial value. The results of the sensitivity analysis are provided in figure 5.6.

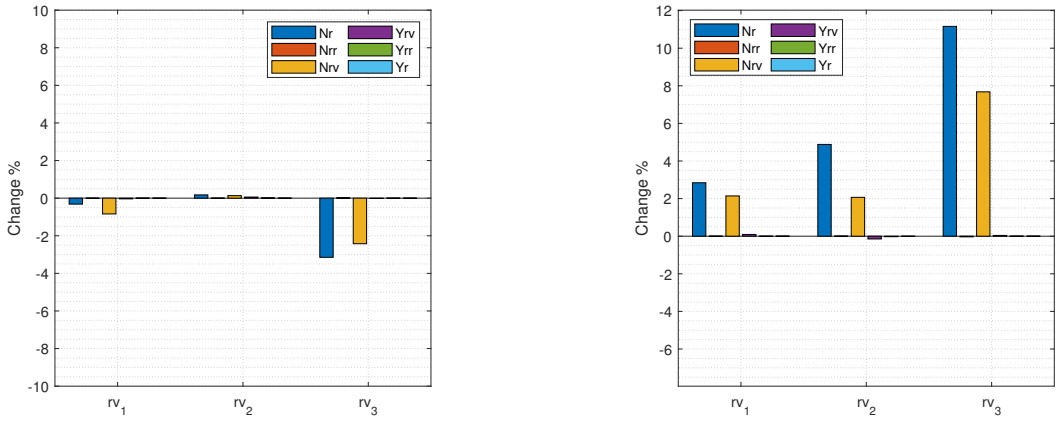

(a) 20% increase of damping terms

(b) 50% decrease of damping terms

Figure 5.6: Sensitivity analysis damping terms

Besides the above investigated hydrodynamic damping contributions, some additional damping terms are used in the calculation, namely: K_p and K_r. In subsection 3.9.2 it is explained how the roll damping in this simulation method is obtained. With that, it is elaborated what assumptions are made. For example, the effect of forward velocity on eddy and frictional damping coefficients is neglected. Besides the effects mentioned in subsection 3.9.2, in [13] it is concluded that the roll damping at full scale exceeds the roll damping obtained with free decay tests at model scale. Due to the presence of a turbulent flow, instead of a laminar flow at model scale, especially the frictional and bilge keel damping coefficients are higher at full scale.

Because of the large uncertainty, the roll damping is varied over a large range. This range covers the both the damping at zero velocity obtained from free decay roll tests and the damping including the approximated lift damping coefficients. In terms of percentages the variation will be between 35% and 120% of the initial approximated value in subsection 3.9.2. The results of the sensitivity analysis are illustrated in figure 5.7a.
Concern the coupled roll-yaw damping term K_r. The contribution of this term is unknown, however to be able to analyse the systems sensitivity a rough estimation is made. In figure 3.15 it can be seen that K_r is a result of vertical forces $Y_{r,bow}$ and $Y_{r,stern}$. Those forces could be calculated using the method developed by Ankudinov [4], such as in section 3.5. Y_r, Y_{rr} and Y_{rv} are tuned for the RSD 2513 in section 4.3.1, the obtained initial values of those forces are used to predict K_r. This results in the following expression of K_r:

$$K_r = z_a(\varphi) \cdot (Y_r r + Y_{rr} r|r| + Y_{vr} r|v|)$$

Here $z_a(\varphi)$ is the vertical distance from the point of attachment of the total y-force to the centre of rotation. As this distance is unknown, it is chosen to take largest possible distance. Being the distance between the point of attachment of the y-force acting on the skeg and the centre of rotation.
To account for the large uncertainty in the estimation of K_r, the sensitivity range will be from -200% to +200%. The results are illustrated in figure 5.7b.

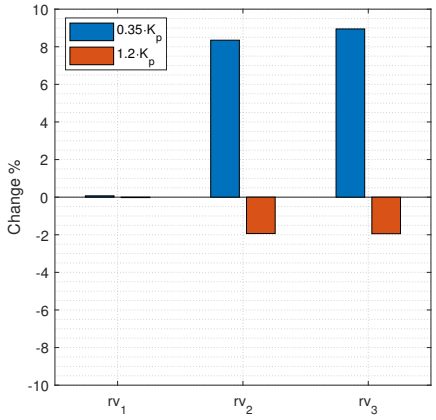

(a) K_p being 35% and 120% of its initial value

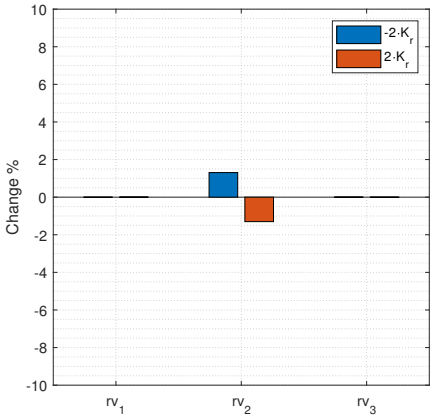

(b) Addition of K_r being $\pm$200% of its initial value

Figure 5.7: Sensitivity analysis K_p and K_r

5.2.4 Discussion of results

In subsections 5.2.1 to 5.2.3 the sensitivity to added mass-, inertia- and damping terms has been investigated. In this subsection the results of these analysis will be discussed. To start with the sensitivity to the inertia terms.

The uncoupled inertia terms I_{zz} and I_{xx} are expected to decrease the accelerations $\dot{r}$ and $\dot{p}$ respectively. A large increase of I_{zz} will therefor significantly slow down the yaw motion. In [9] the following hypothesis is provided:

"*It is obvious that an extremely long tug will roll over before its starts to yaw, while a short tug easily yaws*".

According to this hypothesis, an increase of I_{zz} is expected to result in a larger heeling angle as it will start to roll over before it starts to yaw. The results of the sensitivity analysis provided in figure 5.4 matches this expectation. It shows that an increase of I_{zz} results in larger changes of the heeling angle. The cause-and-effect relationship can be defined as follows:

$$+I_{zz} \longrightarrow -r \longrightarrow +p \longrightarrow +\Delta\varphi$$

The same reasoning could be used for the impact of increasing I_{xx}. The following cause-and-effect relationship is expected:

$$+I_{xx} \longrightarrow -p \longrightarrow +r \longrightarrow -\Delta\varphi$$

So now the tug is expected to start yawing before it starts to roll over, which should result in smaller changes of the heeling angle. However, figure 5.4 proves the contrary. Increasing I_{xx} results in larger changes of φ. This phenomena is a result of the changing drift angle, which goes together with an increasing moment around the x-axis (K). The expected cause-and-effect relationship should be corrected, resulting in:

$$+I_{xx} \longrightarrow -p \longrightarrow +r \longrightarrow +\beta \longrightarrow +\Delta\varphi$$

Concern the coupled inertia term I_{zx}, it is remarkable that addition of this term has a perceptible influence on the heeling angle, as it is mostly neglected in manoeuvring and seekeeping theory. However, the changes are relatively small and conclusions are hard to draw as the absolute value of I_{zx} is unknown.

When looking at the results of the sensitivity analysis concerning the added mass terms, shown in figure 5.5, it can be concluded that in general a 20% increase of the added mass terms has a relatively small effect on the change of the heeling angle after impact loads. The same trend can be observed like for the inertia terms, namely: An increasing a_{44} results in a rapidly change of the drift angle which goes together with a change of the heeling angle. Besides a_{44}, the coupled sway-yaw added mass (a_{26}) has a relatively large impact on φ, especially in scenario 3. In this scenario the loss of thrust causes large sway and yaw velocities which are both influenced by a_{26}. It indicates

that there is a strong coupling between sway, roll and yaw.

The largest percentage changes can be found while varying the damping terms. Figures 5.6a and b show that especially an in- or decrease of the N_r or N_{vr} term has a significant influence on the heeling angle. This indicates again the strong coupling between yaw and roll. $N_r r$ and $N_{rv} r|v|$ are both moments counteracting the yaw motion. So a decrease of N_r or N_{vr} eases the yaw motion, which results in larger drift angles and with that larger heeling angles.

$$+N_r \longrightarrow +r \longrightarrow +\beta \longrightarrow +\Delta\varphi$$

Note that variation of all Y-terms does barely influence the heeling angle, this is in contrast with the findings described in [47]. Here Y_{rr} seems to have a significant influence on especially the tactical diameter of a turning cycle, a characteristic which is not investigated in this research. This research points out that towline release or engine failure does not instantaneously cause large sway accelerations, as it starts to roll and yaw before it starts to sway.

The last two analysed simulation related input parameters are K_p and K_r, of which the results are illustrated in figure 5.7. It can be seen that even though the variation range for K_r is large, the impact of adding this term on the dynamic behaviour of the tug is minimal. In contrast to the impact of changing K_p, which is significant. As expected the reference value in all scenarios increases when K_p decrease and vice versa, as the roll damping prevents the tug from rolling.

It is important to note that, even though large percentage changes are found after varying some input parameters, nothing can be said about the tugs safety yet. It only helps to find out which input parameters should be estimated more accurately since they possibly have a large influence on the heeling angle in the three different scenarios. In appendix A all data required for this sensitivity analysis for the given dynamic scenarios is provided.

5.3 Design and operation related parameters

In section 5.2 a sensitivity analysis concerning inertia, added mass and damping terms is provided. Those terms together are named 'the simulation related parameters'. In this section the focus will be on the sensitivity to more operation and design related parameters. To define what are the limits of safe operation, it should be defined to which design and operation related parameters the tug-tow-system is sensitive. One of the parameters which differs for every towing operation, is the velocity of the assisted vessel. The sensitivity to the velocity of the assisted vessel, known as U_0, is analysed in subsection 5.3.1. Besides the sensitivity to U_0, the influence of the loading condition has been investigated, this is elaborated in subsections 5.3.2 to 5.3.4. Here multiple loading condition related parameters have been investigated separately.
For this group of input parameters an additional result will be compared. Besides the reference values elaborated in section 5.1, the steady state heeling angle will be compared. The concerned input parameters in this section possibly influence the steady state heeling angle as well, in contrast to the parameters analysed above.

5.3.1 Velocity of assisted vessel

Changing the velocity of the assisted vessel is similar to a change of current velocity. So analysing the sensitivity to U_0 will also help to investigate the effect of a non-zero current velocity during a towing operation. Besides the hydrodynamic forces acting on the vessel, the thrust force is dependent on the inflow velocity as well. This could result in significantly different results for various inflow velocities.

In the previous calculations U_0 is set to 8 knots, as the hydrodynamic forces are well validated for this velocity (section 4.2). 8 knots is taken as the initial value of U_0. To make sure the simulation is realistic, a variation range up to 20% has been chosen. For this range of inflow velocities, together with the given thrust defined in the dynamic scenarios, the maximum heeling angle does not exceed the angle where deck immersion takes place. Figure 5.8 shows the results of the sensitivity analysis concerning the velocity of the assisted vessel, i.e. the current velocity.

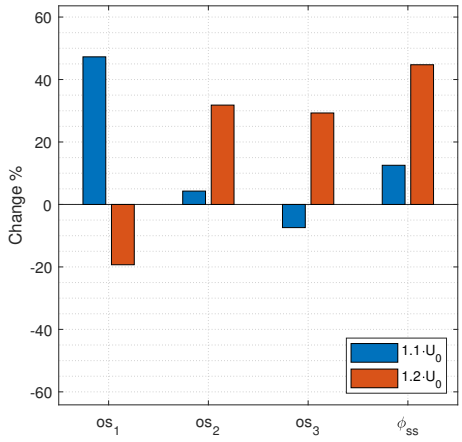

Figure 5.8: Sensitivity analysis U_0

5.3.2 Geometric metacentre height

Figure 4.16b shows that the hydrostatic roll moment, defined as $\rho g \nabla \cdot GZ$, has a significant contribution to the total roll moment. Here GZ represents the righting lever. In the existing manoeuvring models [42] this GZ-curve is assumed to be speed independent. However when sailing at high speed, this GZ-curve possibly changes.
Figure 5.9a shows the definition of the righting lever GZ and the meta center height GM.

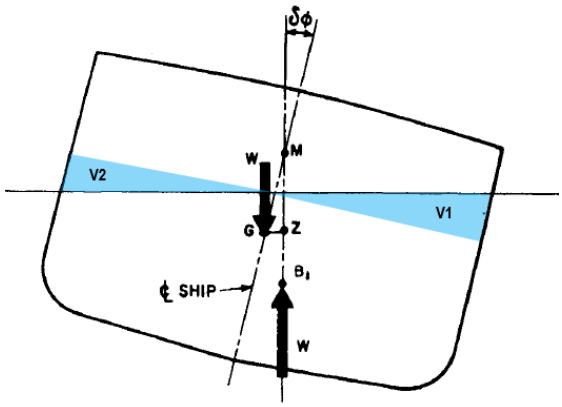

(a) Metacenter and righting lever [31]

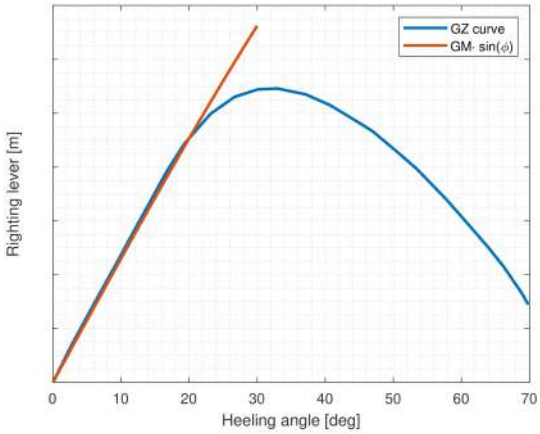

(b) GZ-curve for RSD 2513

Figure 5.9: Explanation righting lever

The hydrostatic moment is a restoring moment caused by the displaced water. For the derivation of the righting lever, it is assumed that the volume of the additional displaced water as a result of a heeling angle (V1 in figure 5.9a) equals the loss of displacement (V2). However, whenever the Froude number or yaw rate becomes large, the free surface effects should be considered. The change of the wave pattern around the ship could result in different volumes V1 and V2 and so a in- or decrease of GZ.

In [19] the lessons learned from the accident with the JMS Delta, as described in chapter 1, are listed. In response to this accident, the influence of a changing wave pattern on the righting heeling curve is investigated. In this document the change of GZ during the yaw motions is claimed to be the cause of the accident.

To find out what is the impact of a speed dependent GZ, a sensitivity analysis has been performed. Whether GZ will in- or decrease and to what extend is unknown, for this sensitivity analysis it is chosen to vary GM with $\pm 10\%$. As for small heeling angles GZ could be replaced by $GMsin(\phi)$, this is illustrated in figure 5.9b. The results of the sensitivity analysis are provided in figure 5.10.

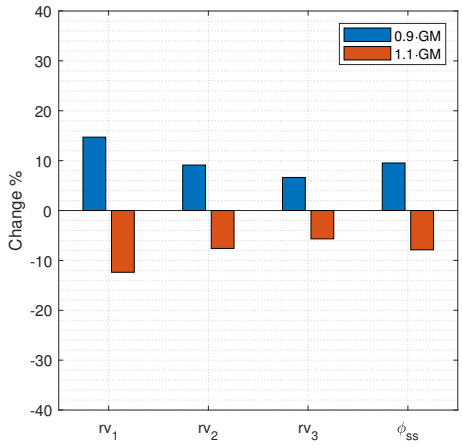

Figure 5.10: Sensitivity analysis GM

5.3.3 Static trim

In [20] it has been proven that the static trim strongly effects the ship manoeuvring. Besides a trim correction, being a function of $\frac{\tau}{T_{mean}}$, is derived. Even though this correction is derived for relatively large slender ships, it is applied to the linear terms N_v and Y_v in this simulation model. To determine the impact of the trim, a sensitivity analysis will be performed in this section. In this analysis the ratio $\frac{\tau}{T_{mean}}$ will be increased and decreased by 200%, assuming that T_{mean} is constant. This range of variation seems to cause a major deviation, however the absolute changes of draught and trim are realistic. They can be found in table 5.3. As indication: For the RSD 2513 there is 2864 kNm required to increase the trim by one centimetre.
The results of the sensitivity analysis are shown in figure 5.11.

Table 5.3: Absolute changes of draught and trim

	τ/T_{mean}	T_a[m]	T_f[m]	τ[m]
Increase	+200%	+0.168	-0.168	+0.112
Decrease	-200%	-0.168	+0.168	-0.112

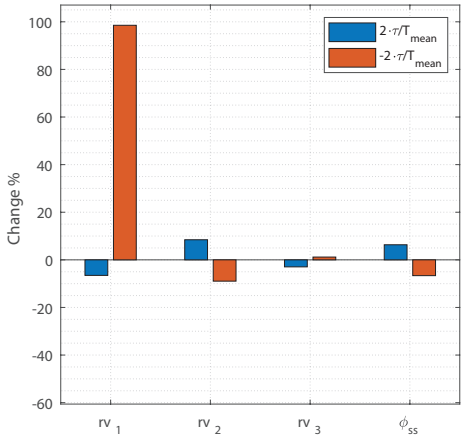

Figure 5.11: Sensitivity analysis trim

5.3.4 Loading condition

In subsections 5.3.2 and 5.3.3 the sensitivity to a change of GZ and the trim is given. Those parameters are dependent on the vessels loading condition. The parameters differ significantly for each loading condition. In this subsection the impact of changing the loading condition will be analysed. From trim and stability calculations the concerned parameters are obtained for every loading condition, the percentage change with respect to the initial conditions is provided in table 5.4.

The dynamic scenarios are performed for various loading conditions. In this research the initial loading condition is chosen to be 50% of fully loaded. Two variants are investigated to be able to judge the system's sensitivity, namely: 10% and 98% loading condition.

Table 5.4: Percentage change of loading condition dependent input parameters for the RSD 2513

	T_f	T_a	∇	GM	τ	τ/T_{mean}
10%	-10.1%	+1.7%	-5.6%	+1.3%	+262.7%	+381.8%
98%	+6.5%	+3.5%	+6.5%	-2.6%	-61.9%	-63.0%

In figure 5.12 the results of the sensitivity analysis concerning the loading condition dependent parameters are shown.

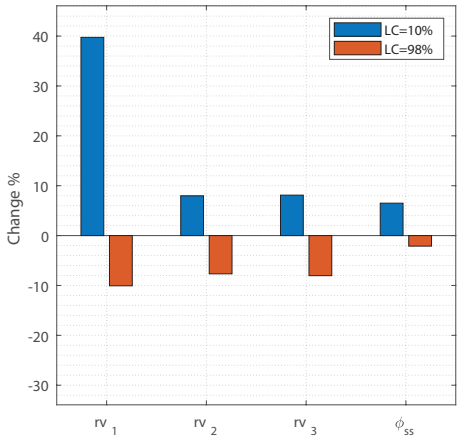

Figure 5.12: Sensitivity analysis loading condition

5.3.5 Discussion of results

In subsections 5.3.1 to 5.3.4 the systems sensitivity to a change of the velocity of the assisted vessel, the geometric metacentre height, trim and loading condition is provided. In this subsection, the results will discussed.

To start with a change of the the velocity of the assisted vessel, of which the sensitivity analysis give no consistent results. Whether the system is more or less sensitive to impact loads depends on the percentage change of the velocity U_0. Differences can especially be found in the results of scenario 1. Here a 10% increase results in a significant increase of the reference value, while an increase of 20% causes a decrease. Just as concluded in subsection 5.2.4 this is a result of the interaction between accelerations $\dot{r}$ and $\dot{p}$.

Apparently, with a velocity increase of 10% the ratio between the roll velocity and the yaw velocity ($\dot{p}/\dot{r}$) is larger compared to the case where the velocity has increased by 20%. Which means that the tug seems to start rolling before it starts to yaw.

The 10% variation of the metacentre height resulted in changes of reference values up to about 15%. A decrease of GM results in increasing reference values, while an increase of GM results in decreasing reference values. The reference values in all scenarios seems to increase linearly with a decreasing GM. This is well explainable, as the restoring moment is linearly dependent on GM. However, for larger heeling angles the impact of the wave pattern on the hydrostatic GZ-curve could easily exceeds 10%, according to the investigation described in [19]. In figure 5.13 the with CFD obtained GZ-curve at high yaw rate is illustrated in yellow.
According to those findings, it can be concluded that GZ up to 10° does not change with forward or yaw speed. However, the GZ curve starts to decrease earlier which means that less resultant up-righting energy will be left when sailing at relatively high forward or yaw speed under a heeling angle larger than $\pm 10°$ (section 6.1).

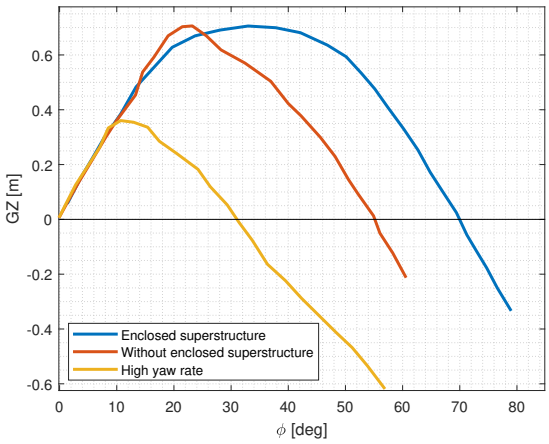

Figure 5.13: Yaw speed dependent GZ-curve

The variation of the trim show significant changes of the reference value (figure 5.11). Those changes arise especially when the trim becomes negative ($T_f > T_f$). The trim correction applied in the used method, has a great influence on the longitudinal location of the point of attachment of the y-force. To calculate N_v the following relation is used:

$$N_v = x_a \cdot Y_v$$

N_v is assumed to be linearly dependent on x_a, being the longitudinal location of the point of attachment of the y-force. It already turned out that the yaw and roll motions are coupled, such that heeling angle generally increases with the drift angle.

At last, the results shown in figure 5.12 combine the variation of multiple input parameters. Here their absolute values are based on different loading conditions. A clear trend can be seen, namely: The more consumables on board, the lower the changes are expected to be after impact loads.

6

Case Studies

Now a numerical simulation tool has been developed and its sensitivity to multiple input parameters has been analysed, crucial situations could be simulated. Nowadays regulations evaluate the tug's safety based on their steady state heeling angles, however the dynamic behaviour before those steady state positions are reached is not necessarily analysed. Overshoots of the heeling angle are expected right before (a new) steady state is reached and in this chapter it is investigated whether this expectation is correct.

The simulated dynamic scenarios considered in this research include the following events:

- Towline failure
- Engine failure
- Performing a turning cycle
- Performing a zigzag manoeuvre
- Transition from indirect steering to port side to indirect steering to starboard side

The purpose is not to identify the worst case scenario, but to judge to what extent the dynamic scenarios pose real risks to escort tugs. Besides, the absolute impact as a result of variation of influential input parameters will be analysed. Here variation of the so called "simulation related parameters" will emphasise the importance of accurate estimation of those input parameters. The variation of the "design and operation related parameters" enables to evaluate the current method used to indicate the risk on board. Nowadays a traffic light based colour coding is used to define whether the instantaneous heeling angle is either safe, risky or dangerous. Here the limits of each zone are independent of i.a. loading condition and velocity. Analysing the absolute changes after variation of this group of parameters will prove whether the limits of safe operation should be dependent on those those parameters.

The outline of this chapter will be as follows: In section 6.1 the current regulation will be elaborated, which will later be used to drawn conclusions. In sections 6.2 to 6.6 dynamic scenarios are provided, in the same order as listed above. And to finalise, an overview and short discussion is given in 6.7.

6.1 Quasi-static safety determination

A tugboat sailing under Class needs to comply with the stability criteria of that particular classification society or the requirements of the Flag authority, however each classification may have its own method to determine tug stability. Most classification societies apply the so called classical approach, using a stability diagram. An example of such a stability diagram is given in figure 6.1a, it shows the righting lever (GZ) and the heeling lever. At the position where the heeling lever and righting lever intersect, the equilibrium heeling angle is found. The dynamics are covered by an energy approach. Here the tug is required to have enough up-righting energy to overcome the heeling moment and return to upright position, this up-righting energy is referred as the residual area in figure 6.1a.
A vessel may be considered having sufficient up-righting energy if the area marked in blue is greater than or equal to the area marked in green. Differences between the definition of the blue area, corresponding with the amount of up-righting energy, arise between the classifications. The differences are indicated in figure 6.1a with different shades of blue. The largest safety margin is considered when the amount of up-righting energy is defined being the area between θ_{C1} and θ_M. When the residual area is limited by θ_{C1} and θ_{C2} there is no safety margin considered.

Damen TugSim uses a variant of the classic approach to find as many as possible static equilibrium positions, in which the escort tug will have sufficient up-righting energy to overcome the heeling moment resulting from

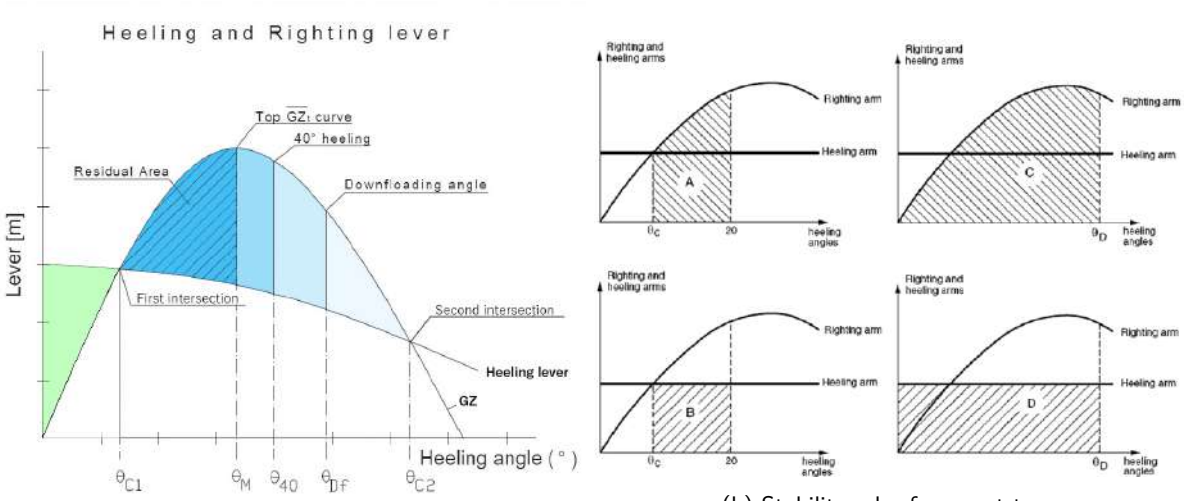

(a) General stability diagram

(b) Stability rules for escort tugs

Figure 6.1: Stability regulation

the towline and hydrodynamic forces. An example of the TugSim output has been provided in figure 1.2. In the applied method the maximum allowed heeling angle is obtained using the stability criteria developed especially for escort tugs operating in calm water [8] which are illustrated in figure 6.1b. Additional requirements are developed for escort tugs, cause they are considered to operate with large drift angles and relatively high speeds. Those escort tug regulations are more stringent than the criteria for self-tripping and tow-tripping [8]. However, they are based on the same classical approach as described above. The tug in escort operation is assumed to have enough up-righting energy when it complies the following:

$A \leq 1.25B$
$C \leq 1.40D$

So whenever the tug's heeling angle does not exceed the obtained maximum heeling angle, the equilibrium is assumed to be safe and there is enough up-righting energy left. This maximum heeling angle seems to be dependent on the loading condition, as the GZ-curve is loading condition dependent as well.

Residual up-righting energy is required to resist heeling angle peaks as a result of impact loads or during manoeuvres. The definition of the residual area (figure 6.1a) is related to the definition of safety, i.e. the upper limit of the residual area may be seen as the limit of safety. In this research the angle of deck immersion has been chosen as the limit of safety, due to the limitations of the simulation model. The simulation tool is not able to quantify the impact of water on deck on the stability of the tug. It is assumed that the restoring moment will decrease as a result of water on deck. ***So in this research, the tug is considered to be safe whenever the angle of deck immersion is not exceeded.*** To check whenever this angle of deck immersion will be exceeded, time domain simulations of different scenarios are provided in the following sections.

6.2 Simulation of towline failure

One of the dynamic scenarios claimed to be dangerous [2] is the release of the towline. To check whether this situation is indeed risky, a time domain simulation will be performed. From the sensitivity analysis in chapter 5 it can be concluded that whenever the loading condition is 10% of fully loaded, the changes of the heeling angle as a result of impact loads will be the most significant. To visualise the effect of parameter variation the best, it is chosen to perform the simulation with a 10% loading condition. Remaining input parameters are provided in table 6.1.

Table 6.1: Input parameters simulation

Loading condition [%]	$U_0[kn]$	Engine load [%]	$\sigma[^\circ]$
10	8	50	30

In this simulation of towline failure, the towline will be released when sailing in steady state position. In steady state, the force equilibrium will be as illustrated in figure 6.2. This results in the following sum of moments:

$$\sum K = K_{tow} + K_{HD} - K_{HS} - K_{prop} \tag{51}$$

The towline failure from a steady equilibrium, with all input parameters kept at their initial values, is illustrated in figure E.1. Before towline release the heeling and heading angles are equal to respectively 11° and -50°, which means that according to the regulations the tug sails in safe position. The release of the towline does not seem to increase the danger, as the absolute heeling angle will not exceed the maximum allowable heeling angle as illustrated in figure E.1. As expected, the hydrodynamic damping prevents the tug from rolling over to the other side, even if the propulsion force still causes a rotational moment around the x-axis. Besides, the tug turns away from the escorted vessel. Apart from the unknown consequences of the assisted vessel sailing without assistance after towline release, no hazardous situations will arise.

The sensitivity analysis (subsection 5.2.3) pointed out that the dynamic behaviour after towline release changes significantly with damping terms N_r and N_{rv}. To check what is the absolute impact of this reduction of those yaw damping terms, the towline failure has been simulated with N_r and N_{rv} being half of its initial values. This

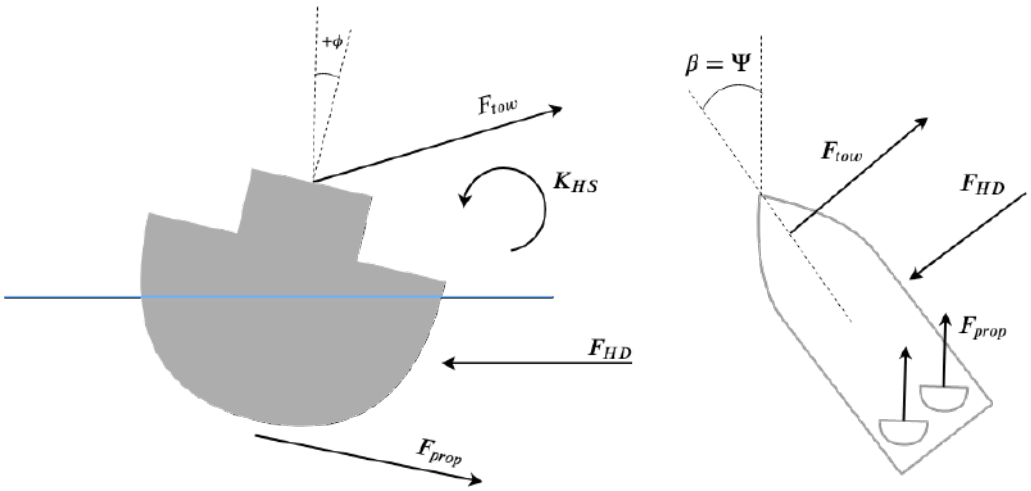

Figure 6.2: Static force equilibrium

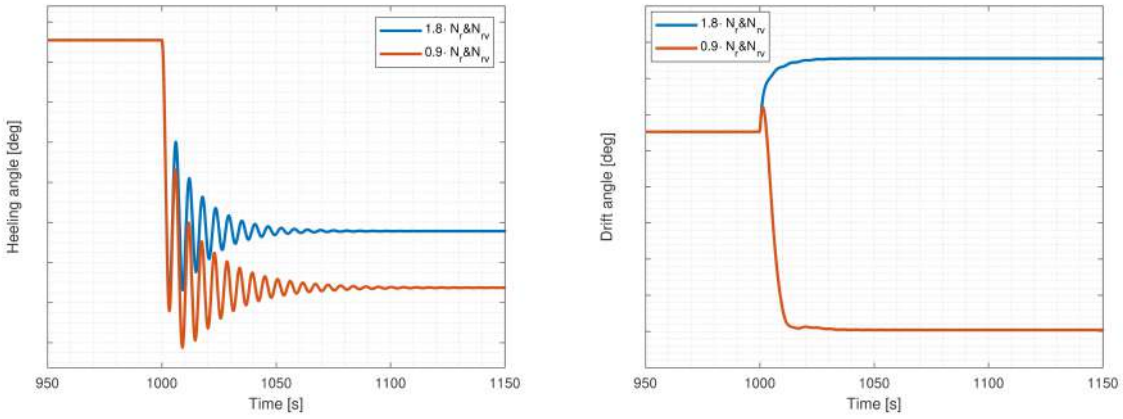

Figure 6.3: Heeling angle after towline failure for different values of N_r and N_{rv}

is illustrated in figure 6.3a.

It can be noticed that the heeling angle overshoot to the other side becomes larger, but the maximum angle after towline release does still not exceed the steady state heeling angle. Even with little yaw damping, no dangerous situations arise. Apart from that, it is remarkable that for N_r and N_{rv} being half of its initial values, the second minimum after towline release exceeds the first one. This seems to be a result of an overshoot in the drift angle, as indicated in figure 6.3b.

Other input parameters having a significant impact on the dynamic behaviour of the tug after towline release, are K_p and U_0. Variation of those parameters results in a higher heeling angle overshoot, but will not cause the tug to exceed the maximum allowable heeling angle. The absolute changes due to variation of the influential parameters can be found in appendix F.

Besides the heeling angle, heading angle, roll rate and yaw rate, the ratios between the different force and moment components has been illustrated in figure E.1. It shows the ratios between the moment contributions generated by the towline, the propulsion and the hydrodynamic forces. Note that K_{tow} and N_{tow} are both results of the moments generated by the hydrodynamic and propulsion forces.

It clearly shows that for both the moments (N and K), the hydrodynamic force contribution is dominant before the towline has been released. To show which contributions to the hydrodynamic force are significant, the hydrodynamic forces are decomposed as well. From the decomposition of the hydrodynamic forces provided in figure E.1 the following can be concluded for N_{HD}, K_{HD} and Y_{HD}:

N_{HD}: Before the towline has been released, the yaw rate is zero and with that N_r, N_{rr} and N_{rv} are zero as well. The only significant moment contribution seems to be N_v. After towline failure the tug will start to perform turning cycles, here N_{rv} and N_r become important as well.

K_{HD}: The K-moment is decomposed in three contributions, namely: K_z,K_m and K_p. K_z and K_m together form the commonly used K_v (subsection 3.9.1). In steady state the moment caused by the side force seems to be dominant, however K_z seems to have significant contribution as well. After towline failure, K_p, being linearly dependent on the roll rate, causes the roll velocity to damp out.

Y_{HD}: From the sensitivity analysis in chapter 5 it was already concluded that variation of the Y-force contributions does barely influence the dynamic behaviour of tugs in escort operations. Figure E.1 emphasises this finding. The only significant force contribution seems to be Y_v.

6.3 Simulation of engine failure

The failure of engines, i.e. loss of thrust, is claimed to cause dangerous situations as well [2]. The time domain simulation of this situation is illustrated in figure E.2. Here the same input parameters are used as for the simulation of towline failure (table 6.1). When looking at the simulation of the heeling angle, it can be seen that directly after loss of thrust there is an overshoot of the heeling angle. From figure 6.2 it can be concluded that in steady state the propulsion force prevents the tug from rolling over. Whenever this force becomes instantaneously zero, the total moment around the x-axis becomes positive and the heeling angles starts to increase. However, at the same time the tug start to yaw as well, which causes together with the hydrostatic restoring force the heeling angle to decrease again. In figure 6.4a the trace of the tug after loss of thrust is illustrated. Here the tug starts at steady state position, marked in yellow, and ends in a new equilibrium position, marked in blue. The illustrated tugs are included to give an indication of the heading angle at the moment in time, the arrows in 6.4b point to those moments in time. Note that the illustrated tugs are not on scale.

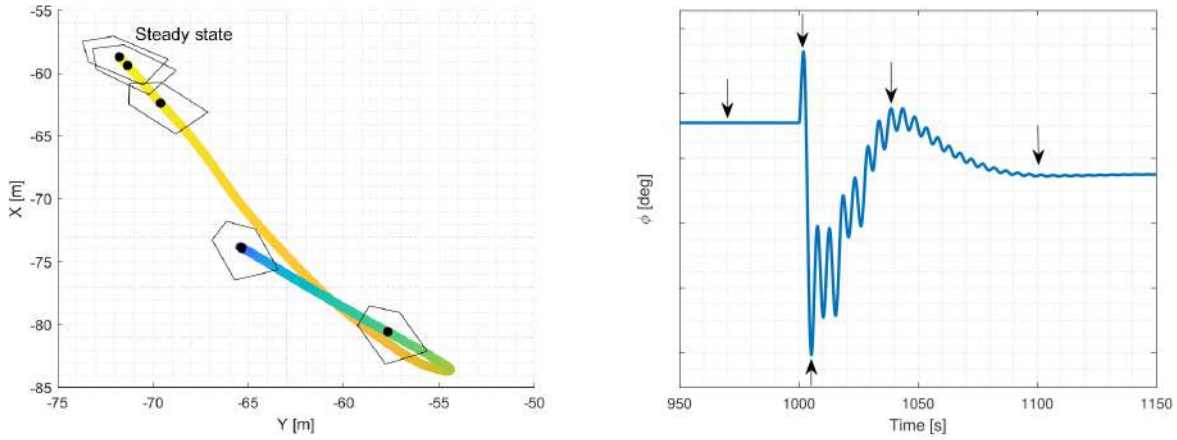

Figure 6.4: Trace after loss of thrust

Besides the overshoot of the heeling angle immediately after loss of thrust, another peak can be found in figure 6.4b. This peak occurs right before reaching its new equilibrium, due to the overshoot in heading angle. This peak is strongly dependent on the initial steering angle. In figure 6.5 the maximum arising heeling angle as well as the steady state heeling angle are given as a function of the initial steering angle. Here the first and second peaks, as indicated in figure 6.4, are provided in respectively figures 6.5a and b. These figures show that, even though the steady state heeling angle is lower for higher steering angles, the heeling angle peak is not necessarily lower as well. From figure 6.5b it can be concluded that for steering angles larger than 34°, the second peak exceeds the steady state heeling angle. In figure F.3 the impact of varying the initial steering angle is simulated over time.

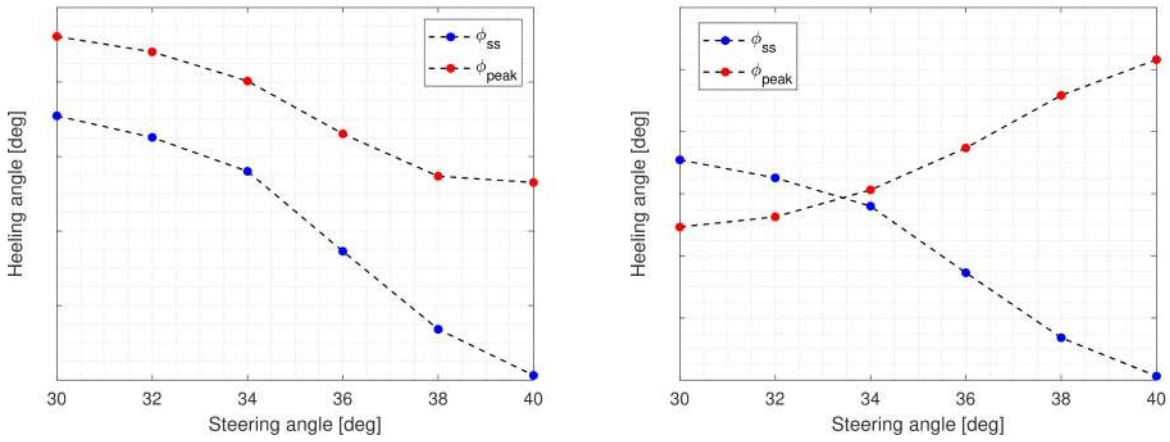

(a) First peak

(b) Second peak

Figure 6.5: Heeling angle peaks after engine failure

Besides the steering angle, the sensitivity analysis in chapter 5 pointed out that N_r, N_{rv}, I_{xx}, K_p and U_0 have a significant influence on the dynamic behaviour of the tug after loss of thrust. In appendix F the absolute changes due to variation of those parameters are illustrated. It can be seen that the variation of N_r and N_{rv} causes significant changes in the second heeling angle peak. Besides, a decrease of the velocity of the assisted vessel causes the difference between φ_{ss} and the second heeling angle peak to increase significantly, however the angle of deck immersion will not be exceeded in any of the considered cases.

Concern the different contributions to the hydrodynamic forces and moments, similar conclusions could be drawn as for the towline failure described in section 6.2. Although the forces due to the sway velocity, indicated with subscript 'v', are even more important for the simulation of the engine failure. This is due to the fact that the tug will, after engine failure, be towed by the assisted ship. So the tug is still facing the inflow velocity (v_a) due to the velocity of the assisted ship.
In the end we can conclude that, regardless of the input parameters, two significant heeling angle peaks arise after the loss of full thrust. The second peak is a result of an overshoot of the heading angle. Even though two heeling angle peaks arise, in not any case the angle of deck immersion will be exceeded. It can be concluded that no dangerous situations will arise after the engines have failed.
Besides, this second heeling angle peaks could be prevented by reducing the steering angle after loss of thrust. From the simulations provided in figure F.3, it can be concluded that whenever the steering angle has been decreased to zero within approximately 20 seconds after loss of thrust, the second heeling angle peak would be prevented. To confirm this assumption, a time domain simulation is provided in figure F.7 where the steering angle is decreased to zero after 20 seconds.

6.4 Turning cycle

In the introduction of this report (chapter 1) the fatal accident with the tug named 'JMS Delta' is claimed to be one of the accidents that encouraged the discussion concern the safety of tugs. The casualty happened in free sailing condition, at the start of a turning cycle. In [19] the casualty has been analysed. Here it is claimed that the effect of a changing wave pattern when sailing with a large yaw speed, is the mean reason for the loss of stability during a turning cycle. In figure 5.13 the results of the research performed in [19] are illustrated, it shows the static GZ-curve as a function of the heeling angle for multiple situations. From this figure it can be concluded that, for the JMS Delta in specific, the effect of a yaw rate on the GZ-curve starts to become significant for heeling angles larger than 10°. However, the question remains whether the heeling angle exceeds these 10°. According to the experimental results presented in figure 4.15 the steady state heeling is expected to stay far below. However the heeling angle before this steady state is reached, is expected to be significantly larger. In this section it will be investigated whether is expectation will be met.

The time domain simulations will be performed for the RSD 2513 sailing with full power. The steering angle will increase with $15°/s$, which is according to trail measurement data the highest possible steering velocity. Figure 6.6 shows the maximum heeling angle for a range of steering angles. It shows that the highest heeling angle appears when the steering angle equals 25°. During this manoeuvre the heeling angle seems to increase the maximum allowable heeling angle, however the angle of deck immersion (18.4 °) will not be exceeded.

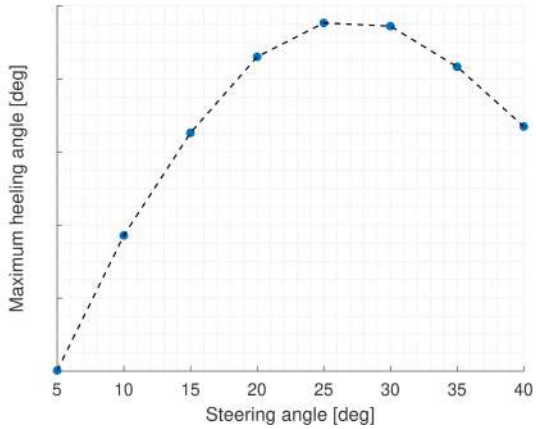

Figure 6.6: Heeling angle peak for a range of steering angles

Figure 4.13 shows that, besides the heeling angle, the yaw rate is the highest for a steering angle of 25°. In [19] it is claimed that the impact of a changing wave pattern on the GZ-curve is the highest when having a large yaw rate. This means that the heeling angle peak for $\sigma = 25°$ is expected to be higher when accounting for the effect of the changing wave pattern. So even though the angle of deck immersion of 18.4° is not reached in the time simulation, conclusions about the safety could not yet be drawn. To be able to draw valid conclusions, the effect of the changing wave pattern on the GZ-curve should be investigated.

Regarding the effect of variation of the influential input parameters; even though the sensitivity to the heeling angle during a turning cycle has not been investigated in chapter 5, the same conclusions could be drawn as in section 6.3. Only the yaw damping terms N_r and N_{rv} are expected to have an impact on the heeling angle peak. Less damping will result in higher yaw rates and with that larger heeling angles (figure 4.13). The full result of the time domain simulation of the turning cycle with $\sigma = 25°$ is provided in figure E.3.

6.5 Zigzag manoeuvre

In section 4.3.3 a zigzag manoeuvre has already been performed and used for validation purposes. Figure 4.17a shows that the maximum heeling angle is far below the angle of deck immersion, however this experiment is performed at only 15% maximum power. In this section it will be investigated whether the angle of deck immersion will be exceeded during zigzag manoeuvres executed with full power, representing the worst case scenario.

Different zigzag manoeuvres has been performed, they can be distinguished based on their ratio between the steering angle and the length of the period in which the steering angle is kept constant. The maximum heeling angles during those different manoeuvres are provided in figure 6.7. It shows that when the steering angle equals $20°$ and is kept constant during 20 seconds, the heeling angle peak is the highest. However, in not one of the simulated cases the angle of deck immersion is exceeded and so it can be concluded that no dangerous situations arise when zigzag manoeuvres will be performed. In figure E.4 the full time domain simulation of the 20/20-zigzag manoeuvre is shown.

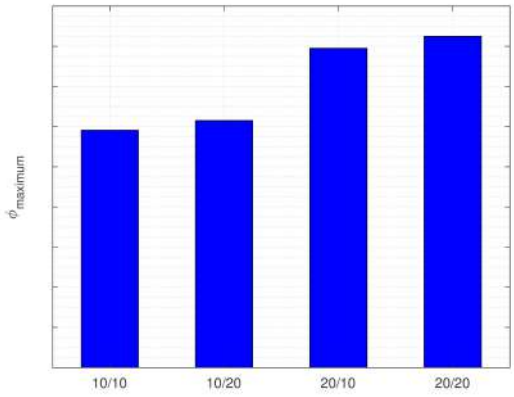

Figure 6.7: Maximum heeling angle for multiple zigzag manoeuvres

6.6 Transition from indirect steering (port) to indirect steering (starboard)

According to the regulations escorting is considered to include active (emergency) steering, breaking and controlling the escorted vessel sailing with a forward speed between 6 and 10 knots. Escort tugs should therefore be able to switch their modes as fast as possible. In figure 6.8 the different indirect towing modes are illustrated. Note that in this research all time domain simulations start from operating in indirect steering mode (figure 6.2), where the objective is to maximise the steering force. The objectives for the indirect braking and the basic indirect mode are respectively: Maximising the breaking force and controlling the escorted vessel by use of primarily its hydrodynamic forces.

The transition from indirect steering to port side to indirect steering to starboard side is an example of active steering which claimed to be dangerous in [2]. In this section this manoeuvre will be simulated, such that the stability of the tug could be assessed.

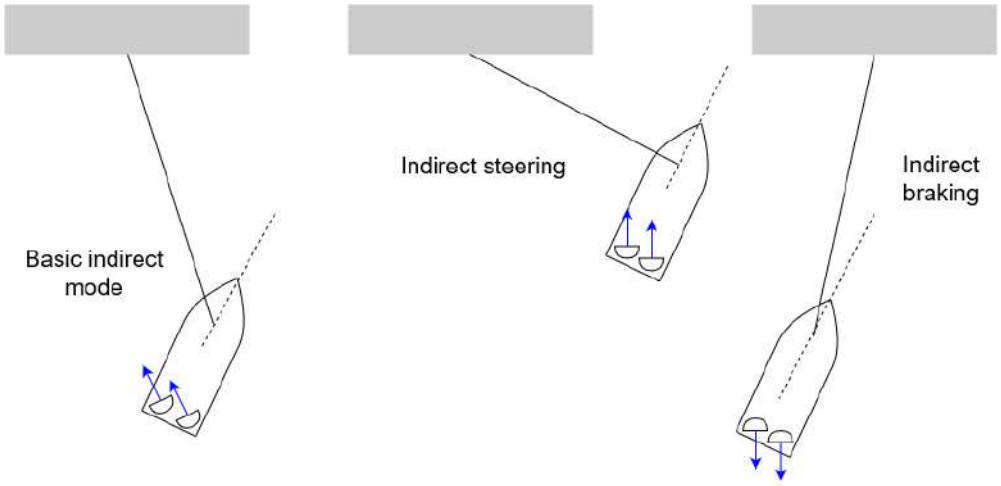

Figure 6.8: Overview of different indirect towing modes [8]

Note that, as mentioned in the introduction of this chapter, the challenge is not to identify the worst case scenario, but to judge the scenarios itself and the impact of variation of input parameters. Even tough, there are many possible combinations of input parameters what would lead to the change of steering direction, for the given purpose only one specific method will be picked. In this research the manoeuvre is simulated in a simplified manner, with the steering angles transitioning from $+30^{\circ}$ to -30° and within the same time the thrust is decreased to 0 and increased to its initial value afterwards. This combination of input parameters is chosen to make sure that the simulations are within the limits of the simulation tool. One of those limits concerns the towline dynamics,

as the implemented towline dynamics are greatly simplified and not validated. For this reason the so called slack forces, which could result in high heeling angles, can not be simulated accurately.

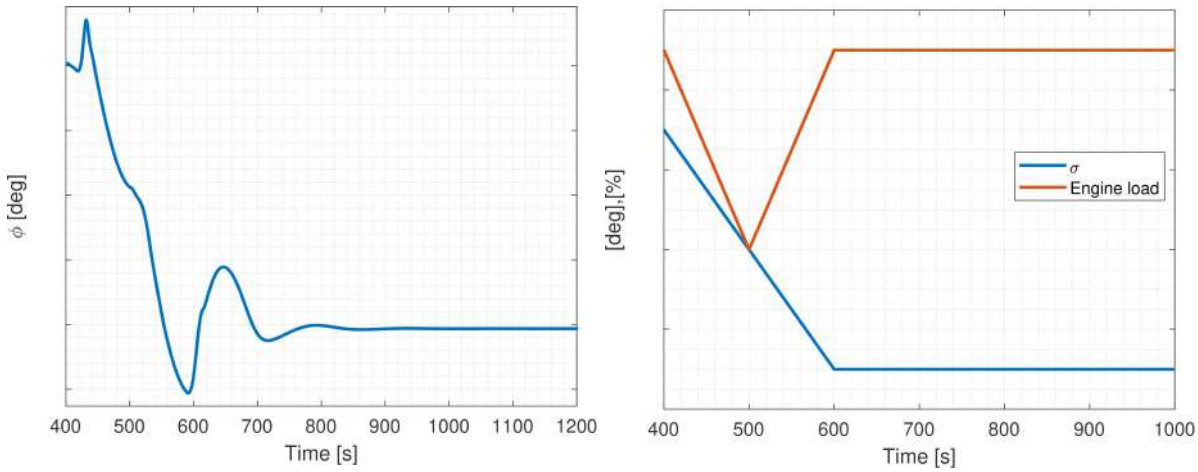

(a) Heeling angle

(b) Engine load and steering angle

Figure 6.9: Transition from steering to port side to steering to starboard side

In figure 6.9a the heeling angle over time is given, resulting from the input provided in figure 6.9b. In figure 6.9a two absolute peaks can be found, one right after the manoeuvre started (t≈450 s) and one just before the new equilibrium is reached (t≈600 s). Both peaks seem to be dependent on the applied steering speed and with that the speed of changing of thrust. In figures 6.10a and b respectively the first and second peak arising during the transition are given as a function of the steering speed. It shows that the first peak decreases with an increasing steering speed, in contrast to the second peak which increases with an increasing steering speed.

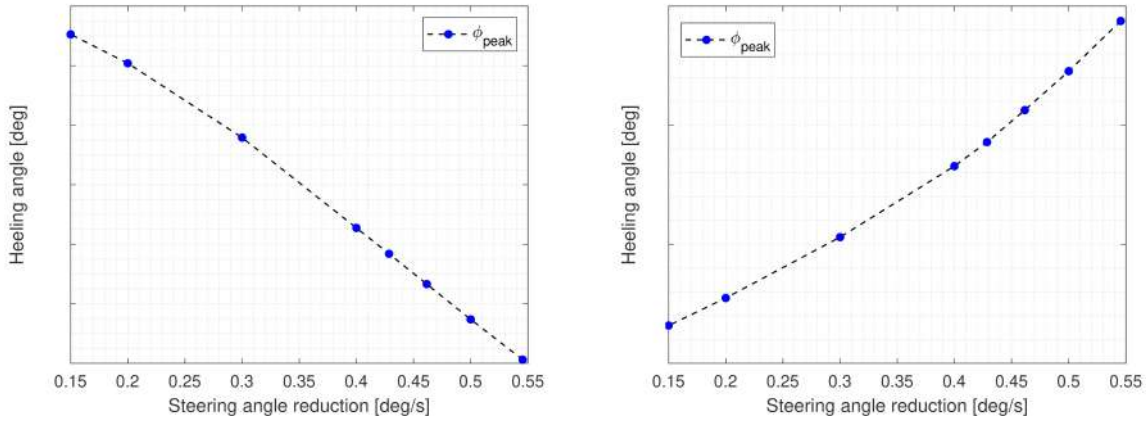

(a) First peak

(b) Second peak

Figure 6.10: Transition from steering to port side to steering to starboard side

Figure 6.10b shows that the absolute heeling angle exceeds the angle of deck immersion for higher steering velocities, which means that dangerous situations could arise during the considered transition. The dependency on the steering speed and speed of changing power is inherently related to the tug's velocity when approaching its new static equilibrium. Further research should point out what is the exact relation between the velocity components and the heeling angle overshoot.

The second heeling angle peak in figure 6.9 seems to be an overshoot due to high velocities as approaching a new equilibrium. This behaviour seems to be similar to the behaviour in the first scenario analysed in the sensitivity

analysis (chapter 5). The sensitivity analyses pointed out that in scenario 1 the velocity of the assisted vessel (U_0), the trim and the loading condition have a great impact on this heeling angle peak. Due to the similarity of both scenarios, those input parameters are expected to have a great influence on the heeling angle arising when changing the direction of the steering force as well.

6.7 Overview and discussion

To finalise this chapter, the results of the simulations are summarised in table 6.2. Here the potential risk is indicated and a short description about the situation is given.
Besides, a discussion is provided about the validity of the results obtained during the simulation of each situation. It is discussed whether additional research is required before the simulation tool could be used to ensure safety on board of a tug.

Table 6.2: Overview of simulated dynamic scenarios

Manoeuvre	**Potential risk**	**Description**
Towline failure	Low	Tug starts to heel to the other side, but its overshoot is small due to the presence of roll damping.
Engine failure	Low	Two heeling angle peaks will arise, of which the second is mostly higher. However, this second peak could be prevented by reducing the steering angle after engine failure. Both peaks will not exceed the angle of deck immersion.
Turning cycle	Moderate	A heeling angle peak arises just after the turning cycle has been started. The highest heeling angle is expected for steering angles resulting in the highest yaw rates.
Zigzag	Moderate	The 20/20 zigzag manoeuvre results in the highest maximum heeling angle. The maximum heeling angle occurs at the moment in time where the yaw rate is the highest as well, just as for the turning cycle performance
Transition indirect steering direction	High	During the transition from steering to port side to steering to starboard side, two heeling angle peaks arise. In most performed simulations of this scenario, the second heeling angle exceeds the angle of deck immersion and so hazardous situations could arise. This peak seems to be dependent on the tug's velocity when approaching its new equilibrium position

6.7.1 Towline failure

Regardless of the input parameters, failure of the towline will not result in dangerous situations. It can be concluded that no further research is required.

6.7.2 Engine failure

Considering a small safety margin would be enough to resist the first peak arising after engine failure. When using the current regulations, a small safety margin has already been taken into account. Regarding the second heeling angle peak, the dependency of this peak on the initial steering angle has been investigated up to a steering angle of 40°. For the RSD 2513 a larger steering angle, together with 50% engine load, would result in an unstable position. As the towline moment is not able to compensate the moment caused by the propulsion and hydrodynamic force

anymore. To guarantee safety after engine failure, it should be investigated whether the second peak will stay below the angle of deck immersion even if higher steering angles are initially applied.

6.7.3 Turning cycle

During turning cycles, high yaw rates are expected. Even though the calculated results show that the maximum heeling angle stays below the angle of deck immersion, safety can not yet be guaranteed. To ensure safety, the impact of the wave pattern around the tug on the static GZ-curve due to high yaw rates should be quantified. This impact is nowadays not well defined, but according to [19] the righting lever (GZ) is expected to decrease as a result of the changing wave pattern. So the question remains whether the hydrostatic restoring moment, implemented as $\rho g \nabla GZ(\varphi)$, is sufficient to balance the involved moments whenever the effect of the changing wave pattern is considered.

6.7.4 Zigzag manoeuvre

Just as during the turning cycles, high yaw rates are expected in zigzag manoeuvres. To guarantee the safety, the effect of the yaw rate on the GZ-curve should be analysed as well.

6.7.5 Transition from indirect steering to port side to indirect steering to starboard side

It is hard to define how the considered transition is performed in a realistic manner. The approach used in this simulations has shown that the second heeling angle peak is dependent on the tug's velocity when approaching its new equilibrium. However, it is unknown what combination of velocity components results in a worst case scenario. To be able to advice the captain sailing on board of the tug, it should be investigated what exactly causes the large heeling angle overshoot. Besides more information should be gathered about how such a transition is commonly carried out.

7

Conclusions and recommendations

In this chapter the conclusions drawn from the findings presented in this thesis will be presented. Besides recommendations for future work will be covered. This will be done is section 7.1 and 7.2 respectively.

7.1 Conclusions

The main objective of this research is formulated as follows:

"Develop a numerical time domain simulation tool, considering four degrees of freedom, being able to analyse and predict the dynamic behaviour of tugs in escort operations"

A combination of classical manoeuvring theory and the calculations used for TugSim has resulted in a simulation tool suitable for tugs, especially in escort operations. This tool is used to analyse the dynamic behaviour of escort tugs just before and right after steady state and to identify the sensitivity of the tug-tow system to the variation of input parameters. The conclusions of this research are divided in three categories, each considered in a different subsection.

7.1.1 Sensitivity to hydrodynamic force contributions arising from manoeuvring theory

The literature review resulted in a list of hydrodynamic force contributions arising from manoeuvring theory. A sensitivity analysis has been performed to investigate whether all of those hydrodynamic force contributions are significant for tugs in escort operations and what is the impact of inaccurate approximation of these terms. Here the focus is on the impact on the heeling angle. From all the hydrodynamic force contributions in three degrees of freedom, the coupled sway-yaw damping and the pure yaw damping seem to be the most influential. This indicates that there is a strong coupling between yaw and roll. A large yaw rate causes to increase the hydrodynamic roll moment as this moment increases with the drift angle. The coupled sway-yaw and the pure yaw damping terms (N_{rv} and N_r) prevent the tug from yawing, which results in smaller heeling angles.
Besides, the sensitivity analysis turned out that the impact of variation of the added mass terms has just a little effect on the dynamic behaviour after impact loads. The same yields for the Y-force contributions coherent with the yaw motion (Y_r, Y_{rr} and Y_{rv}).

Time domain simulations of escorting tugs indicate that pure sway damping terms are dominant, as the facing inflow velocity due to the velocity of the assisted ship is relatively high. The sensitivity of those terms has not been investigated, as their absolute contributions are well known for the validation case.
To the question *"Which hydrodynamic force contributions are essential for simulating escorting tugs?"*
The answer is as follows: N_v, N_{vv}, Y_v and Y_{vv} are dominant. However N_r and N_{rv} prevent the tug from yawing and are therefore essential as well.

7.1.2 Roll moment contributions and its influence on escorting tugs

One of the challenges in this research was to find an accurate formulation of the roll moment, being suitable to use in a time domain simulation tool. From a first order Taylor expansion concern the hydrodynamic moment around the x-axis, several moment contributions appeared (27). Sensitivity analyses and time domain simulations pointed out that the roll moment for escorting tugs is dominated by the roll moment as a result of a sway velocity. This roll moment contribution appeared to be a summation of two components, namely: The moment as a result of the side force and the moment as a result of a resulting vertical force. The performed time domain simulations has shown that both contributions are essential and will increase with the drift angle and facing inflow velocity.

From the sensitivity analysis it can also be concluded that an increase of the roll related added mass and inertia terms will automatically result in lower roll velocities. Therefore the tug starts to yaw before it start to roll and

higher yaw velocities are expected. Because of the velocity of the assisted ship, that may be seen as a facing current velocity, the drift angle will increase whenever the heading angle increases due to the yaw velocity. This results in an increase of the hydrodynamic roll moment and so the heeling angle. It indicates again that there is a strong coupling between yaw and roll.

Besides the roll damping as a result of a sway velocity, the pure roll damping should be incorporated as well. This term prevents the tug from incessantly oscillating around it's local x-axis. However, due to the relatively high facing current velocity this term is small compared to K_v and a variation of it's magnitude will not directly influence the safety of an escorting tug.

7.1.3 Simulation of dynamic behaviour and evaluation of the current regulation

One of the, usually unfulfilled, requirements set by class is that dynamic effects before a steady state is reached should be analysed. In this research it is investigated whether the safety margin set by class is sufficient to resist heeling angle peaks arising after impact loads or during specific manoeuvres. This is done by performing time domain simulations of tug in four degrees of freedom. From this time domain simulations, the following can be concluded:

- 4DOF time domain simulations show that high heeling angles, exceeding the angle of deck immersion, could appear when transitioning from indirect steering to port side to indirect steering to starboard side. Which could result in dangerous situations.
- Heeling angles higher than the maximum allowable heeling angle according to regulation could appear during turning cycles tests, zigzag manoeuvres and after engine failure. However, the safety margin seems sufficient as the deck will not start to immerse.
- Towline failure will not result in dangerous situations

So in most of the simulated dynamic scenarios, the maximum calculated heeling angle stays below the angle of deck immersion and it can be concluded that for those scenarios performed with the RSD 2513, the considered safety margin is sufficient. However, the sensitivity analyses and time domain simulations pointed out that these maximum heeling angles may be dependent on multiple design and operation related parameters. From this it can be concluded that the limits of safe operation, nowadays indicated with a traffic light based colour coding, should at least be dependent on the loading condition (including trim and displacement) and the velocity of the assisted vessel.
The research also indicates that a change in the static GZ-curve, used to calculate the restoring moment, strongly influences the stability of the tug. The effect on GZ of a the wave pattern around the tug when sailing with a high yaw velocity, is expected to have consequences for the safety assessment of tugs.

7.1.4 Overall

The research performed in this thesis contributes to the discussion about safety of tugs in response to multiple accidents happened with tugs. It provides a method suitable for simulating tugs in escort operations and analysing their dynamic behaviour. A combination of semi-empirical manoeuvring methods and an existing performance prediction tool has resulted in a well validated simulation tool. The research emphasises which hydrodynamic force contributions are essential and how those relate to each other. Besides it indicates which design and operation related parameters should be considered when evaluating the tugs safety and what dynamic scenarios should be analysed.

7.2 Recommendations

Following from this research there are some recommendations for further research. These will be described in this section.

- The developed simulation tool assumes that the GZ-curve is constant. However this righting lever is expected to be dependent on the forward as well as the yaw speed, due to the change of the wave pattern around the tug. The performed sensitivity analyses indicates that the dynamic behaviour is strongly influenced by

this GZ-curve. To be able to implement an accurate approximation of the righting lever, investigation to the influence of forward speed and yaw rate on the instantaneous righting lever should be conducted.

- The developed simulation tool is suitable for tugs escorting in calm, deep water. The effect of shallow water and waves on the hydrodynamic forces will be significant. To improve the simulation tool and make it widely applicable, the effects of shallow waters and waves should be implemented in the simulation tool.

- The simulation tool does not account for the effect of water on deck. Which means that the calculated hydrodynamic forces will be valid up to the heeling angle where the deck start to immerse. However, this will probably not directly lead to capsizing when performing an escort operation. To be able to analyse the absolute worst case scenario, the effect of water on deck should be included in the simulation tool.

- Another important lacking effect in the simulation tool, is the thruster interaction. The simulation tool is able to simulate the behaviour of a tug equipped with two azimuth propulsion systems, however the interaction between the two thrusters is not considered. A captain of such a tug will be able to steer each thruster individually, which causes interaction effects to be significant. To simulate the manoeuvring behaviour more accurately and to enable steering each thruster separately, those interaction forces should be included. This will also help to validate the towing behaviour more accurately.

- The sensitivity analyses pointed out that N_{rv} and N_r are both essential damping terms. The derivation of those terms is based on semi-empirical methods using data retrieved from relatively large merchant ships. Even though those damping terms are made suitable for the RSD 2513 by deriving a certain correction term, a more accurate and widely applicable approximation of the damping terms is desired. Preferable, this should be a more on physics based calculation method, such as a strip theory. Besides, harmonic and steady circular motion tests could be used to validate or obtain the yaw damping terms.

- The drawn conclusions are valid for the RSD 2513. However a higher reliability of the obtained results is desired. To increase the reliability, multiple tug designs should be analysed.

- Dangerous situations could arise during the transition from steering to port side to steering to starboard side. The heeling angle peak in this scenario seems to be dependent on the velocity when approaching a new equilibrium position. To find out what is the exact cause of this heeling angle overshoot, further research should be performed to investigate what is the exact relation between the velocity components and the heeling angle overshoot.

References

[1] Robert G Allan. "Escort Tug Performance Prediction Using CFD". In: *Proceedings of the 5th Tugnology Symposium, London* (2013).

[2] Robert G Allan. "Escort Tug Safety: Accounting for dynamic Scenarios in Design and Operations". In: *Proceedings of the 11th Tugnology Symposium, Liverpool* (2019).

[3] Robert G Allan. "The State of Tug Safety Today". In: Proceedings of the 8th Tugnology Symposium, Boston. 2016.

[4] V. Ankudinov. "Ship manoeuvring simulation model including regimes of slow speeds and large drift angles". In: *Report for the First International Maritime Simulation Symposium* (1985).

[5] C. Aydin et al. "Practical computational procedures for predicting steering and braking forces for escort tugs". In: *Ocean Engineering* 166 (2018), pp. 159–171. DOI: https://doi.org/10.1016/j.oceaneng.2018.08.021.

[6] Kor Kian Beng. *22 people confirmed dead in tugboat tragedy in China's Yangtze river*. 2015. URL: https://www.straitstimes.com/asia/east-asia/22-people-confirmed-dead-in-tugboat-tragedy-in-chinas-yangtze-river.

[7] Pablo Carrica et al. "Turn and zigzag maneuvers of a surface combatant using a URANS approach with dynamic overset grids". In: *Journal of Maritime Science and Technology* 18 (2013), pp. 166–181. DOI: 10.1007/s00773-012-0196-8.

[8] Gijsbert de Jong. "Enhancing Tug Safety Through Internationally Harmonised Stability Regulations". In: *Proceedings of the 9th Tugnology Symposium, Rotterdam* (2017).

[9] Jochem de Jong, Jeffrey Jacobs, and Frans Sas. "Tug Stability-A Tug designer's Approach to the Harmonised Class Rules Proposal". In: *Proceedings of the 5th Tugnology Symposium, London* (2013).

[10] R.G. de Jong. "A control system model for combined DP station keeping and active roll reduction". MA thesis. 2018.

[11] Henk De Koning Gans. Private Communication. Delft, The Netherlands, 2019.

[12] E.C. Polhamus. "A concept of the vortex lift of sharp-edge delta wings based on a leading-edge-suction analogy". In: *National aeronautics and space administration* (1966).

[13] Jeffrey Falzarano, Abhilash Somayajula, and Robert Seah. "An Overview of the Prediction Methods for Roll Damping of Ships". In: *Ocean Systems Engineering* 5 (May 2015), pp. 55–76. DOI: 10.12989/ose.2015.5.2.055.

[14] T.I. Fossen. *Handbook of Marine Craft Hydrodynamics and Motion Control*. Wiley, 2011. ISBN: 9781119998686. URL: https://books.google.nl/books?id=vCAzd3DaZCgC.

[15] G.Bilici et al. "Performance Prediction for Tractor type Escort Tugs". In: *Proceedings of the 2nd International Meeting on Recent Advances in Prediction Techniques for Safe Manoeuvring of Ships and Submarines* (2016).

[16] Hoyte C. Raven. *A new correction procedure for shallow-water effects in ship speed trails*. Tech. rep. MARIN, 2016.

[17] Michael J. Hughes, Paul J. Kopp, and Ronald W. Miller. *Modelling of Hull Lift and Cross Flow Drag Forces in Large Waves in a Computationally Efficient Dynamic Stability Prediction Tool*. Ed. by Vadim L. Belenky et al. Springer International Publishing, 2019, pp. 77–90.

[18] Y. Ikeda. "Roll damping of ships". In: *Proceedings of Ship Motions, Wave Loads and Propulsive Performance in a Seaway, 1st Marine Dynamics Symposium*. The Society of Naval Architecture in Japan, 1984, pp. 241–250.

[19] IMO. *Considerations on lessons learned from the casualty during the trail of an azimuth stern drive tug*. 2019.

[20] S. Inoue, M. Hirano, and K.Kijima. "Hydrodynamic Derivatives On Ship Manoeuvring". In: *International Shipbuilding Progress* 28 (1981), pp. 112–125.

[21] S. Inoue et al. "A practical calculation method of ship maneuvering motion". In: *International Shipbuilding Progress* 28 (1981), pp. 207–222.

[22] ITTC. *Performance Prediction Method*. 1978.

[23] ITTC. *Recommended Procedures and Guidelines for Captive Model Test*. 2017.

[24] ITTC. *Recommended Procedures and Guidelines, Validation of Manoeuvring Simulation Models*. 2014.

[25] Prof. ir. J. Gerritsma. *Hydromechanica 4 - scheepsbewegingen, sturen en manoeuvreren*.

[26] J.M.J. Journee and W.W. Massie. *Offshore hydromechanics*. 2008.

[27] Donghoon Kang and Kazuhiko Hasegawa. "Prediction method of hydrodynamic forces acting on the hull of a blunt-body ship in the even keel condition". In: *Journal of Marine Science and Technology* 12 (2007), pp. 1–14. DOI: 10.1007/s00773-006-0232-7.

[28] Katsuro Kijima, Yasuaki Nakiri, and Yoshitaka Furukawa. "On a Prediction Method for Ship Manoeuvrability". In: *Proceedings of Marine Simulation and Ship Manoeuvrability Conference, Tokyo* (2001), p. 311.

[29] L. Larsson, H.C. Raven, and J.R. Paulling. *Ship Resistance and Flow*. Principles of naval architecture. Society of Naval Architects and Marine Engineers, 2010. ISBN: 9780939773763. URL: https://books.google.nl/books?id=5zi8bwAACAAJ.

[30] E.M. Lewandowski. *The Dynamics of Marine Craft: Maneuvering and Seakeeping*. Advanced series on ocean engineering. World Scientific, 2004. ISBN: 9789810247560. URL: https://books.google.nl/books?id=UbjvXKReIAUC.

[31] Edward V. Lewis. Society of Naval Architects and Marine Engineers (SNAME), 1988. ISBN: 978-0-939773-00-8. URL: https://app.knovel.com/hotlink/toc/id:kpPNASRVI3/principles-naval-architecture-4/principles-naval-architecture-4.

[32] E.V. Lewis, Society of Naval Architects, and Marine Engineers (U.S.) *Principles of Naval Architecture: Motions in waves and controllability*. Principles of Naval Architecture. Society of Naval Architects and Marine Engineers, 1988. URL: https://books.google.nl/books?id=1mwZAQAAIAAJ.

[33] Olaf Merk, Benedicte Busquet, and Raimonds Aronietis. *The Impact of Mega-Ships*. 2015.

[34] David Molyneux and Neil Bose. "Escort tug at large yaw angle: Comparison of CFD predictions with experimental data". In: 150 (Jan. 2008).

[35] Kirk Moore. *Danger lurks if tug masters don't know their own strength*. 2016. URL: https://www.workboat.com/blogs/the-noreaster/tug-masters-may-not-know-strength.

[36] Max. M. Munk. "The Aerodynamic Forces on Airship Hulls". In: (1924).

[37] John Nicholas Newman. "Some hydrodynamic aspects of ship maneuverability". In: (1966).

[38] B. Piaggio et al. "Manoeuvring model and simulation of the non-linear dynamic interaction between tethered ship and tug during escort". In: (2017).

[39] Frans Quadvlieg. *Current Status of Manoeuvring Prediction Methods, Their Mutual Pros and Cons and Ways to Quantify the Capabilities*. Tech. rep. MARIN, 2016.

[40] R.P.M. Schillings. "Quantification of Thruster Forces for Escorting Tugs". MA thesis. 2018.

[41] Henry v.Borst Sighard F. Hoerner. *Fluid Dynamic Lift*. 1985.

[42] Marco Sinibaldi and Gabriele Bulian. "Towing simulation in wind through a nonlinear 4-DOF model: Bifurcation analysis and occurrence of fishtailing". In: *Ocean Engineering* 88 (2014), pp. 366–392. ISSN: 0029-8018. DOI: https://doi.org/10.1016/j.oceaneng.2014.06.007. URL: http://www.sciencedirect.com/science/article/pii/S0029801814002200.

[43] Carl-Johan Söder, Anders Rosén, and Mikael Huss. "Ikeda revisited". In: *Journal of Marine Science and Technology* 24.1 (Mar. 2019), pp. 306–316. ISSN: 1437-8213. DOI: 10.1007/s00773-017-0497-z. URL: https://doi.org/10.1007/s00773-017-0497-z.

[44] Serge Sutulo and Carlos Guedes Soares. *Mathematical models for simulation of manoeuvring performance of ships*. Jan. 2011, pp. 661–698. ISBN: 978-0-415-69808-5. DOI: 10.13140/2.1.3538.7209.

[45] Do Thanh Sen and Tran Canh Vinh. "Determination of Added Mass and Inertia Moment of Marine Ships Moving in 6 Degrees of Freedom". In: *International Journal of Transportation Engineering and Technology* 2 (2016), pp. 8–14. DOI: 10.11648/j.ijtet.20160201.12.

[46] The Maritime Safety Committee. *Standards for ship manoeuvring*. 2002.

[47] Serge Toxopeus. "Deriving mathematical manoeuvring models for bare ship hulls using viscous flow calculations". In: *Journal of Maritime Science and Technology* (2007). DOI: 10.1007/s00773-008-0002-9.

[48] Bastiaan Alexander Vink. "A Verification Validation study on CFD Simulations for the Flow Around the RSD Tug 2513". MA thesis. 2017.

[49] Chun-lei YANG et al. "Numerical simulation of rolling for 3-D ship with forward speed and nonlinear damping analysis". In: *Journal of Hydrodynamics, Ser. B* 25.1 (2013), pp. 148–155. ISSN: 1001-6058. DOI: https://doi.org/10.1016/S1001-6058(13)60348-0. URL: http://www.sciencedirect.com/science/article/pii/S1001605813603480.

List of Figures

List of Tables

A

Dimensionless hydrodynamic derivatives

Table A.1: Dimensionless hydrodynamic derivatives

$Y'_v =$	$\frac{1}{\frac{1}{2}\rho LTU}$	$\cdot Y_v$
$Y'_r =$	$\frac{1}{\frac{1}{2}\rho L^2TU}$	$\cdot Y_r$
$Y'_{vv} =$	$\frac{1}{\frac{1}{2}\rho LT}$	$\cdot Y_{vv}$
$Y'_{rv} =$	$\frac{1}{\frac{1}{2}\rho L^2T}$	$\cdot Y_{rv}$
$Y'_{rr} =$	$\frac{1}{\frac{1}{2}\rho L^3T}$	$\cdot Y_{rr}$
$Y'_{\dot{v}} =$	$\frac{1}{\frac{1}{2}\rho L^2T}$	$\cdot Y_{\dot{v}}$
$Y'_{\dot{r}} =$	$\frac{1}{\frac{1}{2}\rho L^3T}$	$\cdot Y_{\dot{r}}$
$N'_v =$	$\frac{1}{\frac{1}{2}\rho L^2TU}$	$\cdot N_v$
$N'_r =$	$\frac{1}{\frac{1}{2}\rho L^3TU}$	$\cdot N_r$
$N'_{vv} =$	$\frac{1}{\frac{1}{2}\rho L^2T}$	$\cdot N_{vv}$
$N'_{rv} =$	$\frac{1}{\frac{1}{2}\rho L^3T}$	$\cdot N_{rv}$
$N'_{rr} =$	$\frac{1}{\frac{1}{2}\rho L^4T}$	$\cdot N_{rr}$
$N'_{\dot{v}} =$	$\frac{1}{\frac{1}{2}\rho L^3T}$	$\cdot N_{\dot{v}}$
$N'_{\dot{r}} =$	$\frac{1}{\frac{1}{2}\rho L^4T}$	$\cdot N_{\dot{r}}$
$X'_u =$	$\frac{1}{\frac{1}{2}\rho LTU}$	$\cdot X_u$
$X'_{uu} =$	$\frac{1}{\frac{1}{2}\rho LT}$	$\cdot X_{uu}$
$X'_{vv} =$	$\frac{1}{\frac{1}{2}\rho LT}$	$\cdot X_{vv}$
$X'_{vr} =$	$\frac{1}{\frac{1}{2}\rho L^2T}$	$\cdot X_{vr}$
$X'_{rr} =$	$\frac{1}{\frac{1}{2}\rho L^3T}$	$\cdot X_{rr}$
$X'_{\dot{u}}$	$\frac{1}{\frac{1}{2}\rho L^2T}$	$\cdot X_{\dot{u}}$

B
Induced drag

The following method is obtained from [11]:
Including the lift induced drag results in additional manoeuvring coefficients. The induced drag coefficient is according to Lanchester-Prandtl defined as follows:

$$c_{d_i} = C_L^2 \frac{L}{\pi T} \tag{52}$$

In which:
c_{d_i} is the drag coefficient
C_L is the lift coefficient

The lift coefficient can be calculated from the lift force:

$$C_L = \frac{L}{0.5\rho U^2 LT} \tag{53}$$

The lift for sailing vessels with a relative small drift angle ($\pm 15^\circ$) by using the linear lift coefficients is:

$$Y = Y_v v + Y_r r \tag{54}$$

The coefficients Y_v and Y_r can be calculated from the dimensionless coefficients of i.a. Kijima:

$$\begin{aligned} Y_v &= 0.5\rho L^2 U \cdot Y_v' \\ N_v &= 0.5\rho L^3 U \cdot N_v' \end{aligned} \tag{55}$$

The lift coefficient becomes now:

$$C_L = \frac{Y_v v + Y_r r}{0.5\rho U^2 LT} \tag{56}$$

When this result is put into equation 52, the induced drag becomes:

$$c_{d_i} = \frac{(Y_v v + Y_r r)^2}{0.5\rho U^2 LT} \frac{L}{\pi T} = \frac{Y_v^2 v^2 + 2Y_v Y_r vr + Y_r^2 r^2}{0.25\rho U^4 \pi L T^3} \tag{57}$$

The drag force is:

$$X = c_{d_i} \frac{-1}{2} \rho U^2 LT \tag{58}$$

Now the result of equation 57 is substituted in equation 58:

$$X = \frac{Y_v^2 v^2 + 2Y_v Y_r vr + Y_r^2 r^2}{0.25\rho U^4 \pi L T^3} \frac{1}{2} \rho U^2 LT = \frac{Y_v^2 v^2 + 2Y_v Y_r vr + Y_r^2 r^2}{0.5\rho U^2 \pi T^2} \tag{59}$$

It is common to write the X-force as an Abkowitz model. Actually the X-force is a Taylor expansion of the variables like u,v and r etc. Especially for the induced drag the following terms appear:

$$X = X_{vv} v^2 + X_{vr} vr + X_{rr} r^2 \tag{60}$$

Where the coefficients X_{vv}, X_{vr} and X_{rr} have respectively the following values:

$$\begin{aligned} X_{vv} &= -\frac{Y_v^2}{0.5\rho U^2 \pi T} \\ X_{vr} &= -\frac{2Y_v Y_r}{0.5\rho U^2 \pi T} \\ X_{rr} &= -\frac{Y_r^2}{0.5\rho U^2 \pi T} \end{aligned} \tag{61}$$

Appendices C, D, E and F are excluded in this public version of the masters thesis.